NAVAL POSTGRADUATE SCHOOL
MONTEREY, CALIFORNIA

THESIS

THE JAN MAYEN CURRENT FROM 1989 AND 1990 SUMMER DATA

by

Marla D. Stone

September, 1996

Thesis Advisors: R. G. Paquette
R. H. Bourke

Approved for public release; distribution is unlimited.

REPORT DOCUMENTATION PAGE

Form Approved OMB No. 0704-0188

1. AGENCY USE ONLY *(Leave blank)*	2. REPORT DATE	3. REPORT TYPE AND DATES COVERED
	September 1996	Master's Thesis

4. TITLE AND SUBTITLE	5. FUNDING NUMBERS
THE JAN MAYEN CURRENT FROM 1989 AND 1990 SUMMER DATA	
6. AUTHOR(S) Marla D. Stone	
7. PERFORMING ORGANIZATION NAME(S) AND ADDRESS(ES) Naval Postgraduate School Monterey CA 93943-5000	8. PERFORMING ORGANIZATION REPORT NUMBER
9. SPONSORING/MONITORING AGENCY NAME(S) AND ADDRESS(ES)	10. SPONSORING/MONITORING AGENCY REPORT NUMBER

11. SUPPLEMENTARY NOTES The views expressed in this thesis are those of the author and do not reflect the official policy or position of the Department of Defense or the U.S. Government.

12a. DISTRIBUTION/AVAILABILITY STATEMENT	12b. DISTRIBUTION CODE
Approved for public release; distribution is unlimited.	

13. ABSTRACT *(maximum 200 words)*

As part of the Greenland Sea Project, a hydrographic survey consisting of 45 CTD stations was conducted in the vicinity of the Jan Mayen Current (JMC) in August 1990 aboard the USNS BARTLETT to further characterize and quantify circulation of the JMC. Comparisons were made with a similar survey performed in September 1989. In the summer of 1990, as in 1989, the JMC appears to be both a portion of the East Greenland Current (EGC) flowing eastward to close the Greenland Sea Gyre (GSG) and an anticyclonic meander in the EGC flow north of Jan Mayen. Geostrophic velocities and transports were similar for 1990 and 1989 with typical near-surface speeds of 3 cm/s slowing to 1 cm/s at depth. The total input flow to the JMC from the EGC is estimated at 1.45 Sv for August 1990 compared to 2 Sv during September 1989. Baroclinic calculations for 1990 data indicate that the meander portion of the JMC is concentrated in the upper waters (~ 100 m) with the result that 44% of the upper layer and 25% of lower layer (~ 100 - 1000 m) flow contributes to the JMC meander. The remainder, ~ 56% from the surface and 75% from the lower layer, continues eastward as throughput to the GSG. Similarly, in 1989, it was determined that about half of the upper layer flow is involved in the meander with flow becoming more easterly with depth. In 1990, the surface was warmer and fresher, the subsurface temperature minimum was colder, and the volume of water occupied by JMC type water masses was half the amount when compared to 1989 data.

14. SUBJECT TERMS Jan Mayen Current, Greenland Sea, East Greenland Current	15. NUMBER OF PAGES 142
	16. PRICE CODE

17. SECURITY CLASSIFICATION OF REPORT	18. SECURITY CLASSIFICATION OF THIS PAGE	19. SECURITY CLASSIFICATION OF ABSTRACT	20. LIMITATION OF ABSTRACT
Unclassified	Unclassified	Unclassified	UL

NSN 7540-01-280-5500

Standard Form 298 (Rev. 2-89)
Prescribed by ANSI Std. 239-18 298-102

Approved for public release; distribution is unlimited.

THE JAN MAYEN CURRENT FROM 1989 AND 1990 SUMMER DATA

Marla D. Stone
B.S., Humboldt State University, Arcata, California, 1982
B.A., Humboldt State University, Arcata, California, 1982

Submitted in partial fulfillment
of the requirements for the degree of

MASTER OF SCIENCE IN PHYSICAL OCEANOGRAPHY

from the

NAVAL POSTGRADUATE SCHOOL
September 1996

ABSTRACT

As part of the Greenland Sea Project, a hydrographic survey consisting of 45 CTD stations was conducted in the vicinity of the Jan Mayen Current (JMC) in August 1990 aboard the USNS BARTLETT to further characterize and quantify circulation of the JMC. Comparisons were made with a similar survey performed in September 1989. In the summer of 1990, as in 1989, the JMC appears to be both a portion of the East Greenland Current (EGC) flowing eastward to close the Greenland Sea Gyre (GSG) and as an anticyclonic meander in the EGC flow north of Jan Mayen. Geostrophic velocities and transports were similar for 1990 and 1989 with typical near-surface speeds of 3 cm/s slowing to 1 cm/s at depth. The total input flow to the JMC from the EGC is estimated at 1.45 Sv for August 1990 compared to 2 Sv during September 1989. Baroclinic calculations for 1990 data indicate that the meander portion of the JMC is concentrated in the upper waters (~ 100 m) with the result that 44 % of the upper layer and 25% of the lower layer (~ 100 - 1000 m) flow contributes to the JMC meander. The remainder, ~ 56% from the surface and 75% from the lower layer, continues eastward as throughput to the GSG. Similarly, in 1989, it was determined that about half of the upper layer flow is involved in the meander with flow becoming more easterly at depth. In 1990, the surface was warmer and fresher, the subsurface temperature minimum was colder, and the volume of water occupied by JMC type water masses was half the amount when compared to 1989 data.

TABLE OF CONTENTS

LIST OF FIGURES

ACKNOWLEDGEMENTS

I wish to express my sincere appreciation to Dr. Robert G. Paquette and Dr. Robert H. Bourke for their incredible patience, inspiration and guidance throughout the course of this project. Not only is it an honor and privilege to have had such distinguished researchers as advisors, I greatly benefited from their vast experience in data analysis and scientific reasoning.

I was fortunate to be able to participate in this entire project from data collection at sea to the findings in this report. Too numerous to mention by name, I am appreciative of the excellent crew of the USNS BARTLETT and the scientific personnel that assisted with data collection during both 1989 and 1990. I would also like to thank other GSP members who made their data and cruise reports available to me.

To these and my family and friends who encouraged me to finally complete this, thank you.

I. INTRODUCTION

A. OVERVIEW

The Greenland Sea is the major connection through which the Arctic and Atlantic Oceans exchange water, salt and heat (*Carmack,* 1972). This seemingly simple statement, now well established by the scientific community, involves complicated processes for which the details are still emerging. As a center of convective activity in the Nordic Seas, the Greenland Sea Gyre (Figure 1) is an area where a large proportion of global deep waters are produced (*Jónsson,* 1989). Thereby the climatic signature of the surface waters is transmitted to the deep ocean by convective processes which form the deep and bottom water of the Nordic Seas (*Blythe,* 1990). The intermediate and upper deep waters flow southward, crossing the Denmark Strait and become the North Atlantic Deep Water which eventually surfaces in the Antarctic (*Gross,* 1977). Thus, the Greenland Sea is the conduit for a tremendous heat engine that transports cold water from north to south. The details of the processes that foster this convection are described in the works of many investigators, of which two will be cited for general orientation purposes: *Carmack and Aagaard* (1973) and *Miencke et al.* (1992).

The rate of convection is controlled by the circulation of the gyre which is, itself, affected by the variable amounts of heat and fresh water input to the current system over a full range of time scales (*GSP Group,* 1990). The Greenland Sea, therefore, has an

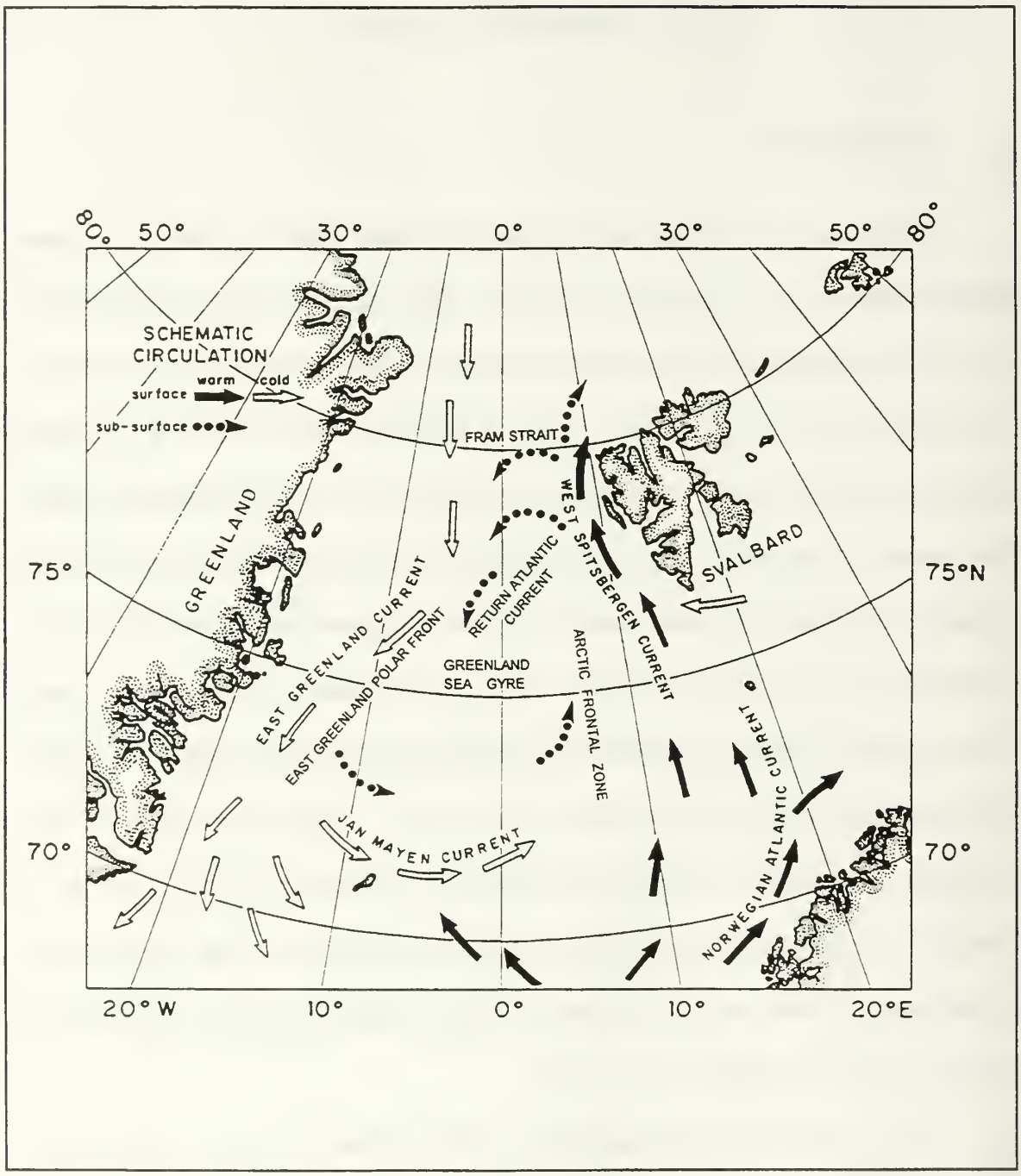

Figure 1. Schematic of the circulation in the Greenland and Norwegian Seas. The water masses composing the above currents are fully described in Chapter 3. This diagram is typical of many which do not show the JMC as partly a meander in the EGC north of Jan Mayen. The meander will be verified in this report (after *Koltermann and Lüthje,* 1989).

important role by ventilating deep oceans and affecting a large portion of the global thermohaline circulation (*McCarren,* 1991). It is increasingly clear that an understanding of the large-scale three dimensional circulation in the Greenland Sea is important to the understanding of the global impact of changes in the ventilation of deep water and the thermohaline circulation as discussed by *Rudels et al.* (1989).

In the past decade, intensive research has focused on the Nordic Seas in an effort to understand the link between climate and oceanic processes in the Nordic Seas. To this end, the Greenland Sea Project was formed.

B. THE GREENLAND SEA PROJECT

The Greenland Sea Project (GSP) (*GSP Group,* 1990) was a five year, multi-national research effort aimed at observing and modelling the atmospheric, ice, oceanic and biological processes relevant to understanding the role of the Nordic Seas in the climate system (*Meincke,* 1995). The project, as the name states, focused primarily on the Greenland Sea but included important studies in the Norwegian and Icelandic Seas.

Due to the paucity of data in this region, an important outcome of the project was the collection of data sets which covered a wide range of temporal and spatial scales. Each contributor was assigned a specific aspect or region of the general circulation to study in detail. The Naval Postgraduate School (NPS) conducted two cruises to investigate the circulation and water mass characteristics of the Jan Mayen Current (JMC) during 1989 and 1990.

To ensure that CTD data were comparable to a high degree of accuracy, all

participants agreed to perform an *in situ* calibration cast at the designated inter-calibration site in the deep Lofoten Basin. Additionally, a group of census hydrographic stations were selected. Investigators agreed to orient cruise tracks to sample a maximum number of the census stations in order to achieve as many repeat samplings of the water column as possible during the project. To better determine interannual fluctuations, two intense field phases for the GSP were devised which covered the periods 1987-1989 and 1993 with lesser sampling between these periods (*GSP Group,* 1990).

C. GENERAL CIRCULATION

Any discussion of circulation in the Greenland Sea must include a description of the bathymetry that separates it from the other Nordic Seas. The topography serves as a barrier to limit the exchange of water between the regions and directs the geostrophic currents to flow along contours of (f/H), where f is the Coriolis parameter and H is the water depth. For these reasons, the circulation is highly affected by the bathymetry (*Jónsson,* 1989).

The Greenland Sea is separated from the Norwegian Sea by the Mohn Ridge, an extension of the mid-Atlantic Ridge, as is shown in Figure 2. The Greenland Fracture Zone divides the Greenland Sea into two basins, the Boreas Basin to the north and the Greenland Basin to the south. Similarly, the Jan Mayen Fracture Zone divides the Norwegian Sea into two basins, the Lofoten Basin to the north and the Norwegian Basin

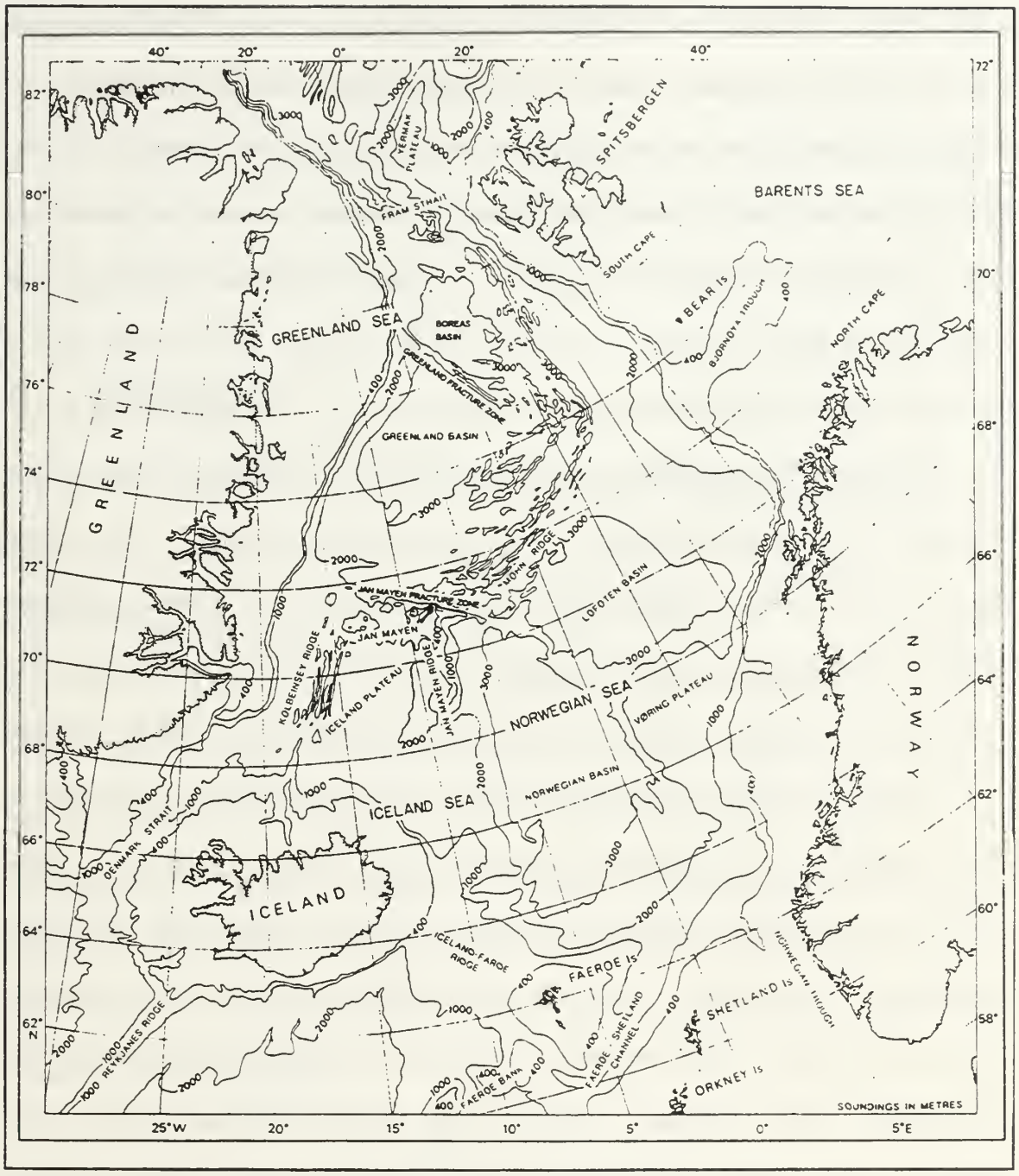

Figure 2. The bathymetry of the major features of the Nordic Seas. Depth contours are in meters on a polar stereographic projection (after *Hopkins,* 1988).

to the south. The Jan Mayen Fracture Zone extends to the west of Jan Mayen and separates the Greenland and Iceland Seas. The Iceland Sea is further separated from the Norwegian Sea by the Jan Mayen Ridge which extends due south of Jan Mayen. To the far north, the Fram Strait, between Greenland and Spitsbergen, connects the Nordic Seas to the Arctic Ocean. Thus, the Greenland Sea is a semi-enclosed sea with depths over 3000 m in both basins, bounded by the Fram Strait to the north, the Greenland coast to the west, the Jan Mayen Fracture Zone to the south, and the Mohn Ridge to the east.

The large-scale circulation in the Greenland Sea is dominated by the cyclonic rotation of the Greenland Sea Gyre (GSG) as was stylized in Figure 1. The eastern branch of the Norwegian Atlantic Current (NAC) and the West Spitsbergen Current (WSC) flow northward carrying warm, saline Atlantic Water (AtW) along the eastern side of the gyre. The western branch of the NAC has a less clear role that will be discussed later. The Arctic Frontal Zone, previously termed the Polar Ocean Front by *Johannessen* (1986), separates the AtW from the cooler, fresher GSG water (*van Aken et al.*, 1995). The WSC flows along the Svalbard coast passing through the eastern side of the Fram Strait into the Arctic Ocean. A portion of the WSC turns westward and submerges between 78°N and 81°N, then continues southward as the Return Atlantic Current (*Bourke et al.*, 1988). On the west side of the Fram Strait, the East Greenland Current (EGC) transports colder, fresher Polar Water (PW) southward following the Greenland continental slope and forms the western boundary of the GSG. The recirculation of the warm AtW forms the East Greenland Polar Front (EGPF) which separates the PW of the EGC from the Return Atlantic Current (RAC). The core of the RAC is beneath and

seaward of the PW of the EGC (*Paquette et al.,* 1985). The Jan Mayen Current (JMC) is usually described as forming the southern limb of the GSG; however, the real situation is more complex. The JMC consists of surface polar waters and Atlantic intermediate waters which appear to be both a portion of the EGC flowing eastward to close the GSG and as a meander in the EGC flow north of Jan Mayen (*Bourke et al.,* 1992).

D. OBJECTIVES

The purpose of this study is to determine specific features of the circulation and water mass characteristics of the Jan Mayen Current based on high-quality CTD data collected during the August 1990 cruise of the USNS BARTLETT. As part of the GSP, this cruise was a follow-up to a similar survey aboard the BARTLETT in September 1989. The 1989 CTD data have been analyzed in detail by *Blythe* (1990) and are the topic of a published paper (*Bourke et al.*, 1992). This report will serve to verify the 1989 findings and allow interannual comparisons between the two data sets. Any phenomenon observed in 1989 which changed in 1990 will be discussed. The objectives of this study, partly based on the BARTLETT 1990 data report of *Paquette et al.* (1991) with extensions, are listed below:

- quantify features of the JMC including speed, volume transport and fresh water contributions based on geostrophic calculations,
- verify the meander-like nature of the upper waters of the JMC seen in 1989,
- determine the volume of the JMC which contributes to the meander in the EGC and compare to 1989, and

- describe water mass properties of the JMC in 1990 and compare to 1989.

In the following chapters, the BARTLETT 1990 data are analyzed and compared to BARTLETT 1989 data to achieve the above objectives. Supplemental data, such as hydrographic survey results and Lagrangian drifter tracks, are used to support the analysis. This study will focus on the upper water column (0-1000 m). The deep water CTD data (1000-3500 m) collected during both cruises have already been examined to determine deep and bottom water characteristics of the Greenland Sea and are the subject of a separate paper (*Bourke et al.*, 1993).

II. GENERAL

A. CRUISE SUMMARY

During the month of August 1990, a hydrographic cruise was conducted on board the USNS BARTLETT (T-AGOR-13) by personnel from the Naval Postgraduate School (NPS) and the University of Paris. The scientific party embarked at Tromsø, Norway on 1 August and disembarked at Trondheim on 24 August. The survey track consisted of five southwest-northeast tending legs from 71°N to 76°N which were expected to pass through the anticipated course of the JMC and to transect the southern and central Greenland Basin. The BARTLETT 90 data set consists of conductivity, temperature, and pressure measurements collected using a Neil Brown Instrument Systems Mark III CTD. The unit was calibrated before and after the cruise at the NPS calibration facility and by water samples taken with a rosette sampler. A total of 45 high-quality CTD stations were occupied to depths of 1000 m with 21 sites extended to near bottom at depths of 2200 to 3500 m (Figure 3). Of the 45 stations, 30 were repeats of the BARTLETT 89 stations. The ice edge rapidly encroached eastward during the western transect which forced proposed stations to be eliminated and new stations to be added farther east. In addition to CTD measurements, four autonomous listening array moorings were recovered one year after deployment on the BARTLETT 89 cruise. These moorings were used to track SOFAR floats which will be discussed later.

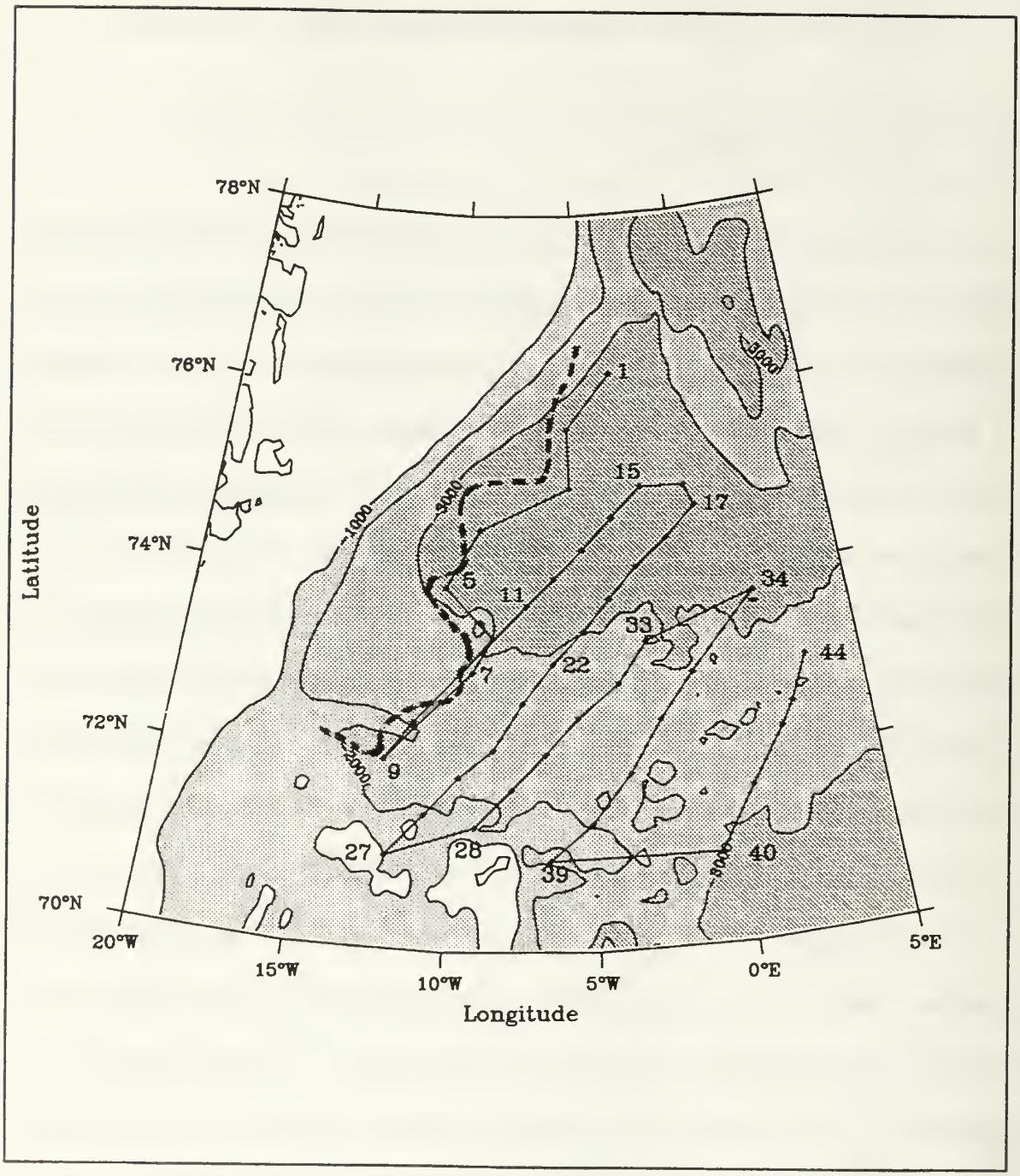

Figure 3. USNS BARTLETT station positions of August 1990. A total of 45 CTD casts were made to 1000 m. The mean ice edge position is shown as a dashed line. The bottom bathymetry in 1000 m intervals is shown by various grey shades.

Navigation was accomplished via the ship's satellite navigation system which provided better than 0.5 km accuracy. Refer to Appendix A for details of instrumentation and data processing.

B. ADDITIONAL DATA SOURCES

This study is largely a comparison between the BARTLETT 1990 and 1989 CTD data; thus, the primary additional data source is the BARTLETT 89 data set. Several additional sources of data have greatly assisted in verifying the characteristics of the Jan Mayen Current.

The results of the BARTLETT 89 data analysis by *Blythe* (1990) and the subsequent journal article by *Bourke et al.* (1992) were critical to an interannual comparison with the BARTLETT 90 data. The BARTLETT 89 station plan is shown in Figure 4. For lack of more recent data, *Blythe* (1990) made seasonal and historical comparisons with the late winter and summer surveys of the JOHAN HJORT and POLJARNIK during 1958, which are shown in the *Dietrich* (1969) atlas. The summer surveys of the JOHAN HJORT (1958) are also compared to the BARTLETT 90 data to note changes or similarities.

Other GSP consortium members have kindly supplied data or information to assist in this study. CTD data results from the summer cruises of the POLARSTERN during 1989 and 1990 have been published by *Budéus et al.* (1993). The data of the summer CTD surveys of the BJARNI SÆMUNDSSON during 1987 to 1990 were provided by *J.*

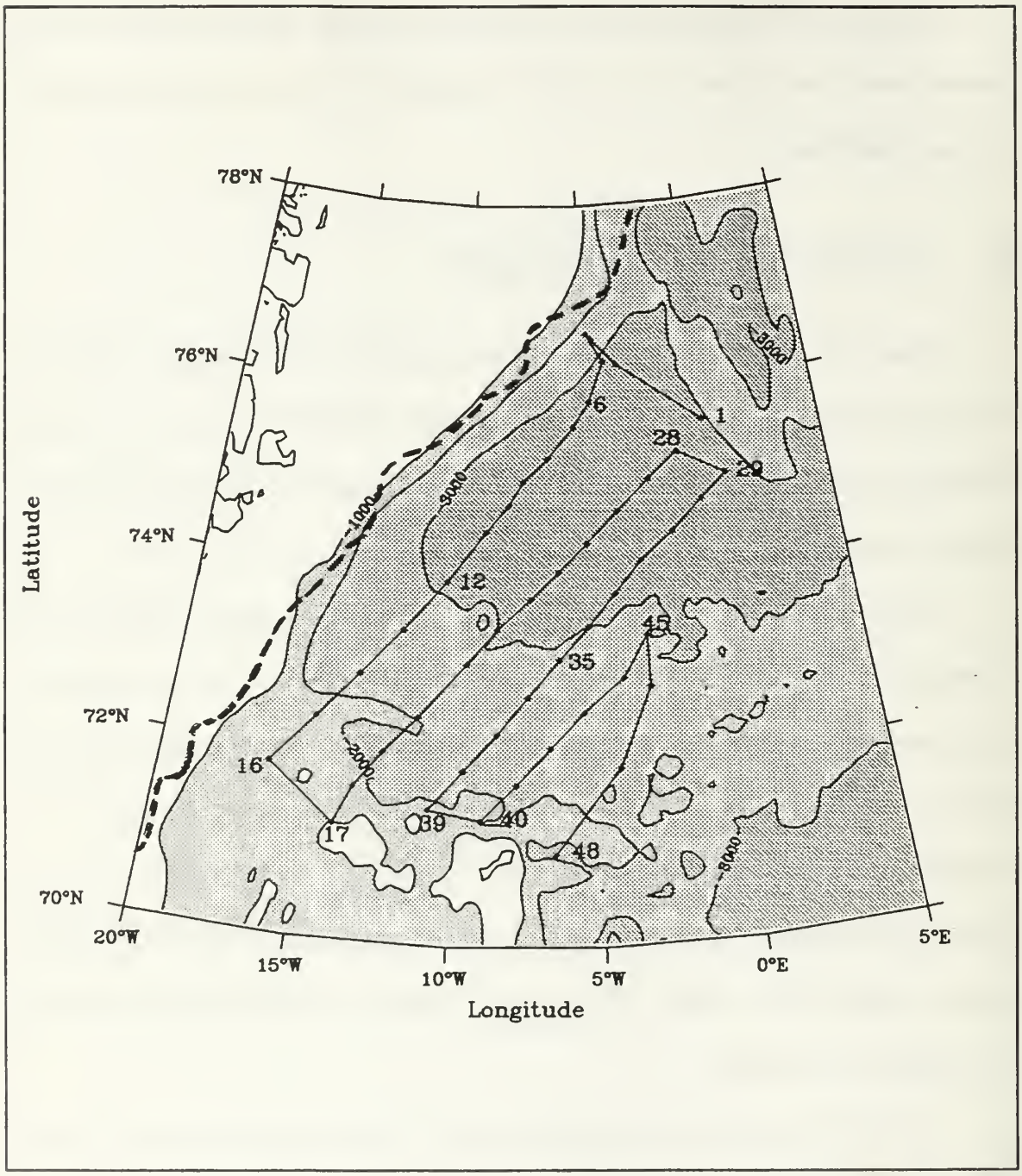

Figure 4. USNS BARTLETT station positions of September 1989. A total of 48 CTD casts were made to 1000 m. The mean ice edge position is shown as a dashed line. The bottom bathymetry in 1000 m intervals is shown by various grey shades.

Mortensen (*personal communication*, 1991). While these surveys had only minor overlap with the BARTLETT 90 station plan, they still provide helpful information concerning surrounding water masses.

The previously mentioned network of Autonomous Listening Stations (ALS) was placed in the Fram Strait in 1988 with a second network deployed in the southern Greenland Sea in 1989 and recovered in 1990 by the BARTLETT cruises (*Richez et al.*, 1995). These devices record acoustic signals received from Lagrangian drifting floats which are set to drift at a constant depth. The analysis of the drifting SOund Fixing And Ranging (SOFAR) buoys in the Greenland Sea during 1989 to 1990 by *McCarren* (1991) provides important information about the circulation in the vicinity of the Jan Mayen Current. The positions of the 1989 ALS and SOFAR buoy launch sites are shown in Figure 5. The near-surface circulation has been mapped with Lagrangian drifters by *Poulain et al.* (1996) who have generously made their results available. Additionally, *W. Maslowski* (*personal communication*, 1996) has kindly provided the results from a recent high-resolution modeling study for the Nordic Seas and Arctic Ocean further aiding in determining circulation in the JMC region.

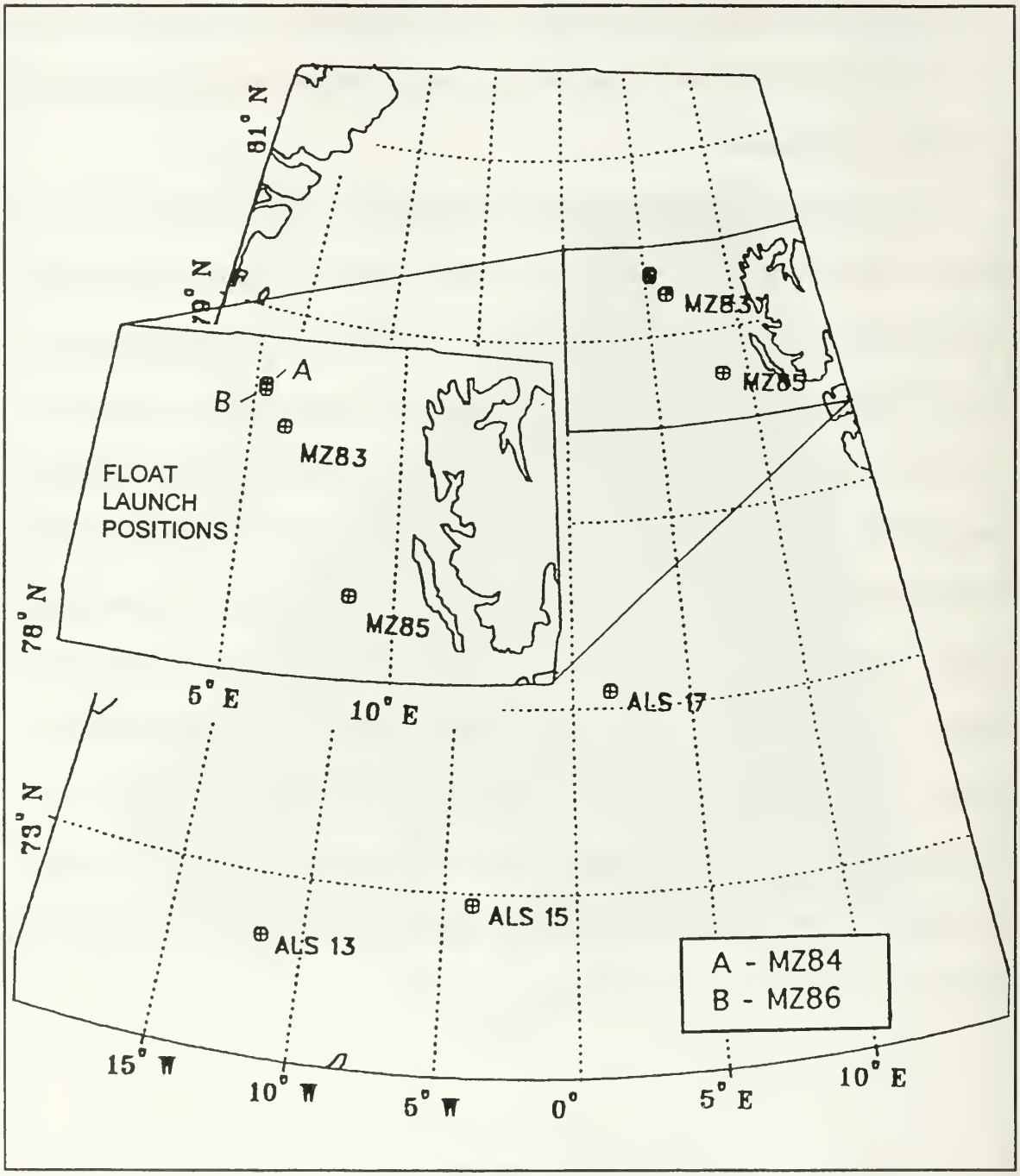

Figure 5. Autonomous Listening Station (ALS) and SOFAR float deployment locations. The four floats are labeled MZ83 to MZ86 (from *McCarren,* 1991).

III. DESCRIPTIVE OCEANOGRAPHY

The Jan Mayen Current (JMC) is important to both the circulation and water mass characteristics of the waters circulating in the Greenland Basin. At least episodically, it brings cold, fresh surface water and warm, saline intermediate water from the East Greenland Current (EGC) into the southern part of the Greenland Sea Gyre (GSG) (*van Aken et al.,*1991; *Carmack and Aagaard,*1973; *Hopkins,* 1988). The fresh water input to the GSG from the JMC is important to the generation of deep and bottom water by vertical convection and serves as the principal source of stratification in the convective region of the Greenland Sea (*Aagaard and Carmack,* 1989). The JMC is generally considered to be the southern limb of the GSG but a portion, as much as half in 1989, of the upper layer baroclinic flow is a wide meander in the EGC north of Jan Mayen (*Blythe,* 1990; *Bourke et al.,* 1992). The meander feature is in contrast to the traditional concept, shown in many circulation diagrams, that the JMC is solely the southern boundary of the GSG. In further discussion, the water going eastward to complete the GSG will be called "throughput" as opposed to the meander which returns to the channel between Jan Mayen and Greenland.

This chapter describes the classical water masses and circulation in the Greenland Sea. The next chapter details the structure of the JMC and the southern GSG in August 1990 and compares the findings to the September 1989 characteristics. The comparison will serve to verify the 1989 data analysis results and further clarify water mass properties of the JMC. In the following chapter, the effects of the JMC on circulation in the GSG

and the transports associated with the JMC flow are discussed. The 1990 CTD data analysis generally support the findings by *Blythe* (1990) in his study of the 1989 observations though some inter-annual differences will be noted.

A. WATER MASS DEFINITIONS

The water mass definitions are adapted from *Hopkins* (1988) with some modifications based on BARTLETT 89 and 90 observations. The deeper waters (over 1000 m) will not be discussed in detail as they are the focus of a separate analysis (*Bourke et al.*, 1992).

Three broad categories of water exist in the Greenland Basin:

- Polar Water (PW) is a cold, fresh surface water usually of Arctic Ocean origin and transported into the region by the EGC. PW is typically found within 100 meters of the surface.
- Atlantic Water (AtW) is a warm, saline surface or intermediate water initially transported into the area as a surface water of the Norwegian Atlantic Current (NAC). Surface AtW is usually found in the upper 200 m of the water column, whereas intermediate AtW typically occurs between 100-400 m.
- Arctic Water (ArW) is a generic term for the characteristic surface and intermediate waters formed in the Nordic Seas, usually a mixture of the previous two water masses. Surface ArW usually occurs within 100 m of the surface and intermediate ArW completes the water column between the surface layer and the deep waters at depths exceeding 1000 m.

The details of the further subdivisions of these broad categories are shown in Figure 6 and Table 1 (adapted from *Hopkins*, 1988).

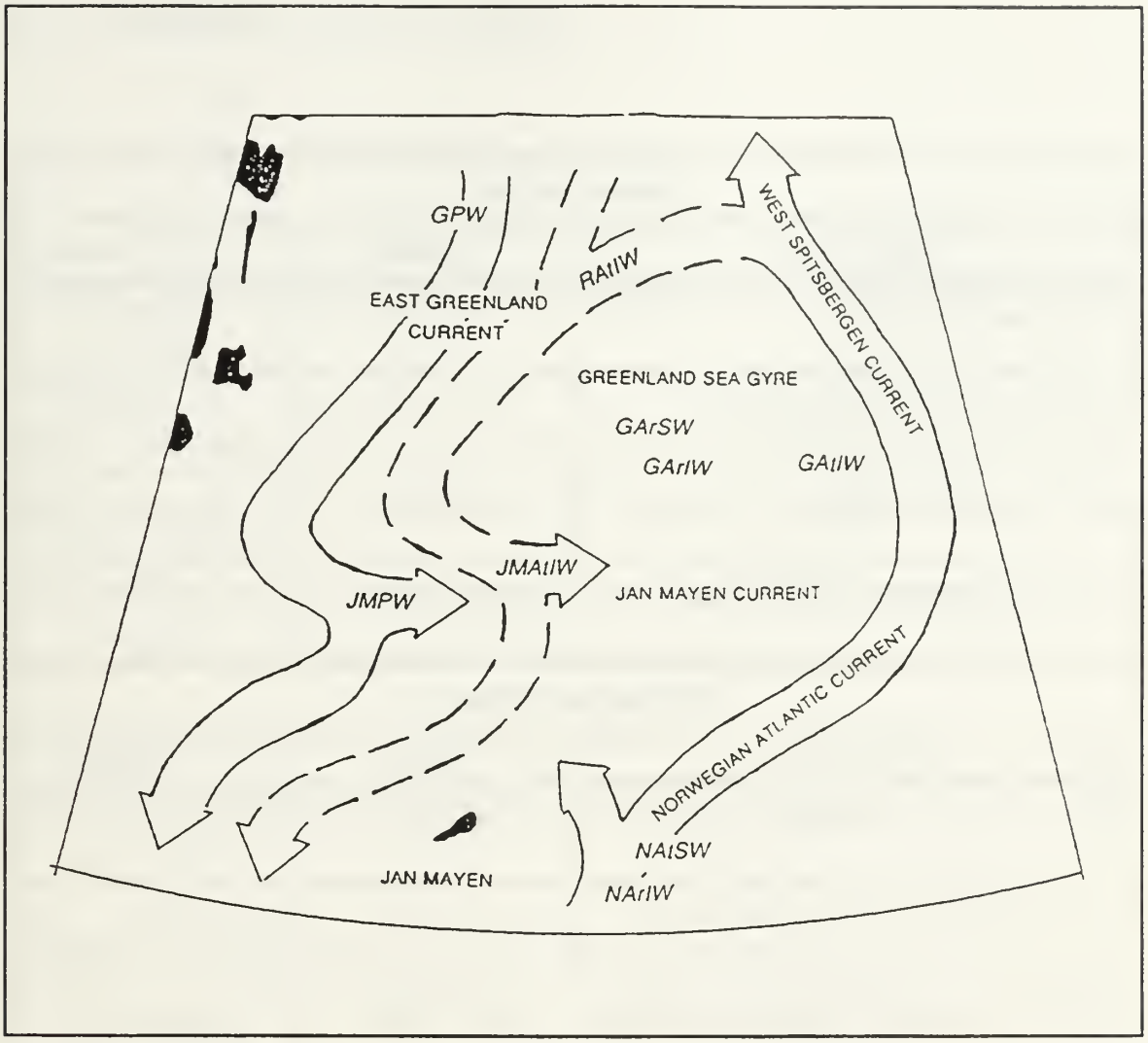

Figure 6. Greenland-Norwegian Sea surface and intermediate water mass circulation schematic. In the north, the East Greenland Current (EGC) carries surface Greenland Polar Water (GPW) from the Arctic Ocean in to the region; similarly in the south, the Norwegian Atlantic Current (NAC) carries in Norwegian Atlantic Surface Water (NAtSW) and Norwegian Arctic Intermediate Water (NArIW). NAtSW sinks isopycnally in the West Spitsbergen Current (WSC) to supply intermediate water to the Arctic Ocean via Fram Strait, the EGC as Return Atlantic Intermediate Water (RAtIW), and directly to the Greenland Sea from the east as Greenland Atlantic Intermediate Water (GAtIW). The Jan Mayen Current (JMC) contains not only throughput to the east but also a large meander in the EGC. The cyclonic Greenland Sea Gyre (GSG) consists of a mixture of waters from the surrounding circulations. Refer to Table 1 for complete water mass descriptions (from *Blythe,* 1990).

Surface Waters		
Water Mass	Symbol	T - S Range
Greenland Polar Water	(GPW)	T < 5°C S < 34.0
Greenland Arctic Surface Water	(GArSW)	T: 0 to 5°C S: 34.0 - 34.7
Jan Mayen Polar Water	(JMPW)	T: -1.5 to 0°C S: 34.0 - 34.7
Norwegian Atlantic Surface Water	(NAtSW)	T > 2°C S > 35.0
Intermediate Waters		
Water Mass	Symbol	T - S Range
Return Atlantic Intermediate Water	(RAtIW)	T: 0 to 3°C S: 34.9 - 35.0
Greenland Arctic Intermediate Water	(GArIW)	T < 2°C S: 34.7 - 34.88
Jan Mayen Atlantic Intermediate Water	(JMAtIW)	T: 0 to 1.5°C S: 34.7 - 35.0
Norwegian Arctic Intermediate Water	(NArIW)	T ~ 0.5°C S ~ 34.88

Table 1. Surface and Intermediate Water Masses of the Greenland Basin (after *Hopkins,* 1988). The temperature and salinity ranges of JMPW and JMAtIW are broadened from the values given in *Hopkins* (1988) based on BARTLETT 89 and 90 observations; similarly those of RAtIW are broadened based on observations of *Bourke et al.* (1987). The temperature and salinity ranges of GPW, GArSW and GArIW have additionally been adjusted to reflect BARTLETT 90 observations (adapted from *Blythe,* 1990).

B. GENERAL CIRCULATION

1. Surface Water Masses

Three major surface water masses are found within the Greenland Basin. The first is a cold, relatively fresh surface PW with origins in the Arctic Ocean which is transported to the western periphery of the Greenland Basin via the EGC (*Bourke et al.,* 1987). As the surface water of the EGC, this PW is termed Greenland Polar Water (GPW). The second water mass has its origin in the North Atlantic. This warm, saline surface AtW, termed Norwegian Atlantic Surface Water (NAtSW), is transported into the region by the NAC and found on the eastern side of the Greenland Basin. The NAC can be divided into two parts, the western and eastern branches. The bifurcation is assumed to be a result of the bathymetry when the current passes Vøring Plateau (*Hopkins,* 1988). The western portion branches to the west near the latitude of Jan Mayen then veers northeastward on encountering the Mohn Ridge, converging with the JMC until it rejoins the eastern branch of the NAC. The eastern branch becomes the West Spitsbergen Current (WSC) as it passes Svalbard. Near Fram Strait, the NAtSW sinks along isopycnals under the less dense PW and becomes intermediate AtW which supplies both the Eurasian Basin and the seaward side of the EGC. Both of these surface water masses are dynamically constrained to remain on the periphery of the Greenland Basin, GPW on the west and NAtSW on the east.

The third major water mass is a surface ArW which results from a mixture of GPW and NAtSW exposed to atmospheric exchanges. This water mass, termed

Greenland Arctic Surface Water (GArSW) is the surface water of the GSG. Secondary to the three major surface waters is the Jan Mayen Polar Water (JMPW), a slightly denser, near-surface water within the JMC that results from a mixture of GPW and GArSW. JMPW consists of a core of cold, moderately saline water at ~ 50 m depth. The surface signature of the JMC is a tongue of cold, fresh GPW penetrating into the GArSW of the southern Greenland Sea Gyre.

2. Intermediate Water Masses

There are three major intermediate water masses in the Greenland Basin. The first is termed Return Atlantic Intermediate Water (RAtIW) and represents that portion of submerged NAtSW which branches cyclonically to the west from the WSC to merge with the EGC south of Fram Strait (*Bourke et al.,* 1988). The warm, saline core of RAtIW lies within the EGC to the seaward side and beneath the East Greenland Polar Front (EGPF) at depths of 100 to 400 m (*Bourke et al.,* 1987). The second intermediate water mass, Norwegian Arctic Intermediate Water (NArIW), occurs in a layer about 200 m thick between the NAtSW and the deep waters of the NAC. The third major intermediate water is Greenland Arctic Intermediate Water (GArIW) which forms a layer between GArSW and the deep GSG waters. It is formed during winter from the GArSW and underlying intermediate waters so that its amount and water type characteristics are variable. One source of underlying intermediate waters is Greenland Atlantic Intermediate Water (GAtIW) which is found on the east side of the basin. It is thought to be a westward subsurface extension of NAtSW origin (*Hopkins,* 1988). It was not encountered

in the BARTLETT surveys.

Jan Mayen Atlantic Intermediate Water (JMAtIW) is formed by the dilution of RAtIW with GArIW as it travels eastward into the Greenland Sea. This water, secondary to the three major types, is the intermediate water of the JMC and occurs in a warm, saline core between 50 and 400 m, typically at ~ 100 m, along the southern periphery of the Greenland Basin.

IV. RESULTS

A. DYNAMIC HEIGHTS

The direction of geostrophic flow can be inferred from the contours of dynamic topography with flow moving parallel to the isopleths in a direction to the right of the "downhill" slope of isolines in the Northern Hemisphere. A historical example of dynamic topography over the Greenland Sea is shown in Figure 7 (*Gladfelter,* 1964). The purpose for including this figure, based on data collected during the cruise of the USS ATKA from 9 August to 4 September, 1962, is its depiction of cyclonic flow over the GSG including the EGC to the west and a branch of the NAC from the south forming the eastern boundary of the GSG, regions the BARTLETT cruises were unable to sample completely. The JMC is shown primarily as a meander in the EGC protruding eastward at about 73°N. In Figure 7, the highest baroclinic speeds in the southeast are about 20 cm/s and those near the isopleth numbering in the northwest are approximately 10 cm/s.

The 1990 summer dynamic heights at the surface (10 m) relative to 1000 m are shown in Figure 8. In this and all subsequent 1990 plan views, the BARTLETT 90 data, collected from 1 to 24 August, has also been combined with a portion of the CTD data from the joint Danish/Icelandic cruise of the BJARNI SÆMUNDSSON collected from 10 to 20 September, 1990 (*J. Mortensen, personal communication*). The Danish/Icelandic CTD data covers the important region between East Greenland and Jan Mayen which the BARTLETT was unable to reach. Although these data are non-synoptic with the

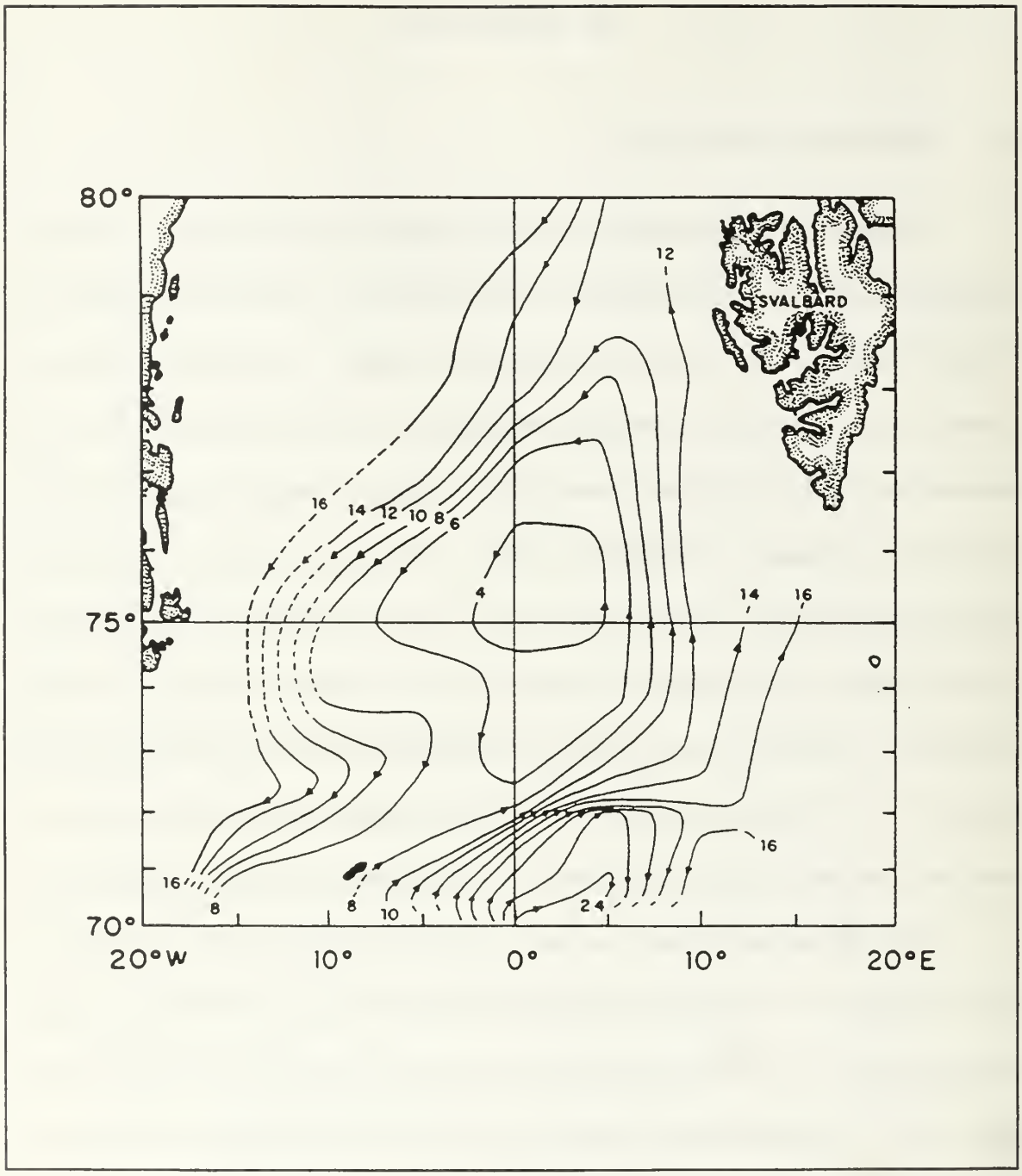

Figure 7. Dynamic topography at the surface relative to 1000 dbar (dyn cm) from the cruise of the USS ATKA, 9 August to 4 September, 1962. This historical example of dynamic topography depicts the flow over an area much larger than the BARTLETT was able to sample (adapted from *Gladfelter,* 1964).

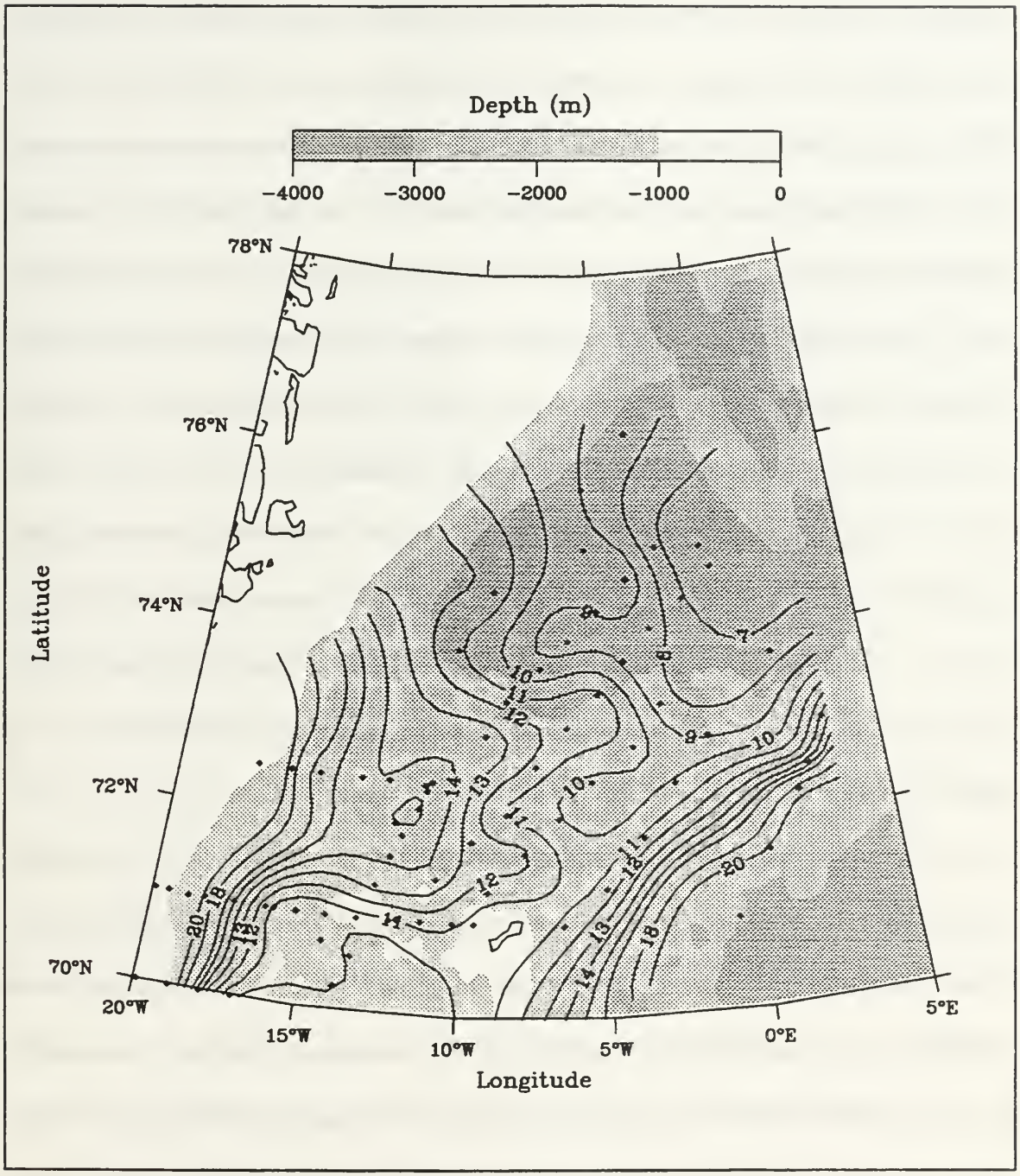

Figure 8. BARTLETT and BJARNI SÆMUNDSSON 90 dynamic height at the surface (10 m) referenced to 1000 dbar (dyn cm). The surface expression of the JMC branches eastward from the EGC between 74°N and 75°N, partially forming an anticyclonic meander in the flow that extends to 5°W.

BARTLETT data by 17 to 50 days, they greatly improve understanding of the processes and conditions in the extreme southwest part of the survey area. The Danish/Icelandic station plan for 1990 is shown in Appendix B, Figure 1. To permit the reader to assess any possible distortions from combining the data sets, the BARTLETT 90 dynamic heights are shown in Appendix B, Figure 3 without the addition of the Danish/Icelandic data. It is believed that the combined data in Figure 8 more realistically represents the circulation in the southwestern part of the area. Similar pairs of figures will be presented for other parameters discussed later. It is evident in Figure 8 that the lack of data in the ice-covered areas north of the Danish/Icelandic data has obscured the presence of the strong East Greenland Current that is evident in Figure 7. The extension of contour lines outside the station grid, particularly obvious in the northwest and northeast regions shown in Figure 8, are an unfortunate artifact of the plotting program. Similar remarks will apply to others of the horizontal diagrams.

In Figure 8, the dynamic heights at the surface (10 m) for 1990 clearly portray the northeastward flowing NAC on the southeastern side of the region and the southward flow of the EGC on the southwestern side. Centered at about 73°N, the surface expression of the JMC branches eastward from the EGC, partially forming an anticyclonic meander in the flow that extends to 5°W. The eastward flow of the surface GPW at 73.5°N, seen best in the 10 to 12 dyn cm contours, has a maximum geostrophic velocity on the order of 3 cm/sec. At 5°W, the meander turns southwest with flow becoming westward at 71°N where the current is again incorporated into the EGC completely at about 17°W. The overall eastward protruding meander of the JMC is distorted at about 72°N,

evidenced by the 11 dyn cm contour. The eddy-like structure at 72°N, 12°W could be due to a lack of synopticity in Danish/Icelandic data or to greater density of information in this area. However, another perturbation of smooth flow may be seen at 72°N, 5°W that suggests the variability in 1990 is distinctly greater than the condition in 1989 which will be discussed in the following description of 1989 dynamic heights. Further, it appears that only a portion of the surface JMC flow, represented by the 8 to 10 dyn cm contours, enters the GSG circulation or joins the western branch of the NAC. About half of the surface flow is involved in the meander. The center of the Greenland Gyre is not demonstrated in Figure 8 due to a lack of stations east of 0°E in the region from 74°N to 76°N. The cruise of the USS ATKA in 1962 (Figure 7) shows the apparent center of the GSG at the classical location, 75.5°N, 2°E.

Inasmuch as there is a rough separation of the surface and intermediate waters at 100 m, it is interesting to examine the dynamic heights at the 100 dbar surface similarly. In Figure 9, the meander is much less prominent than at the surface and a greater fraction of the flow north of Jan Mayen continues eastward to complete the GSG. A quantitative estimate of the transports will be given in Chapter V. There it will be shown that the surface waters are 44 % meander with 56 % throughput to the GSG. The water column beneath the surface layer is divided as 25 % meander and 75 % throughput.

Figure 10 shows the dynamic heights at the surface (10m) for the 1989 summer data. As was done with the 1990 data, the BARTLETT 89 data, collected from 6 to 23 September, has been combined with a portion of the CTD data from the joint Danish/Icelandic cruise of the BJARNI SÆMUNDSSON collected from 11 to 19

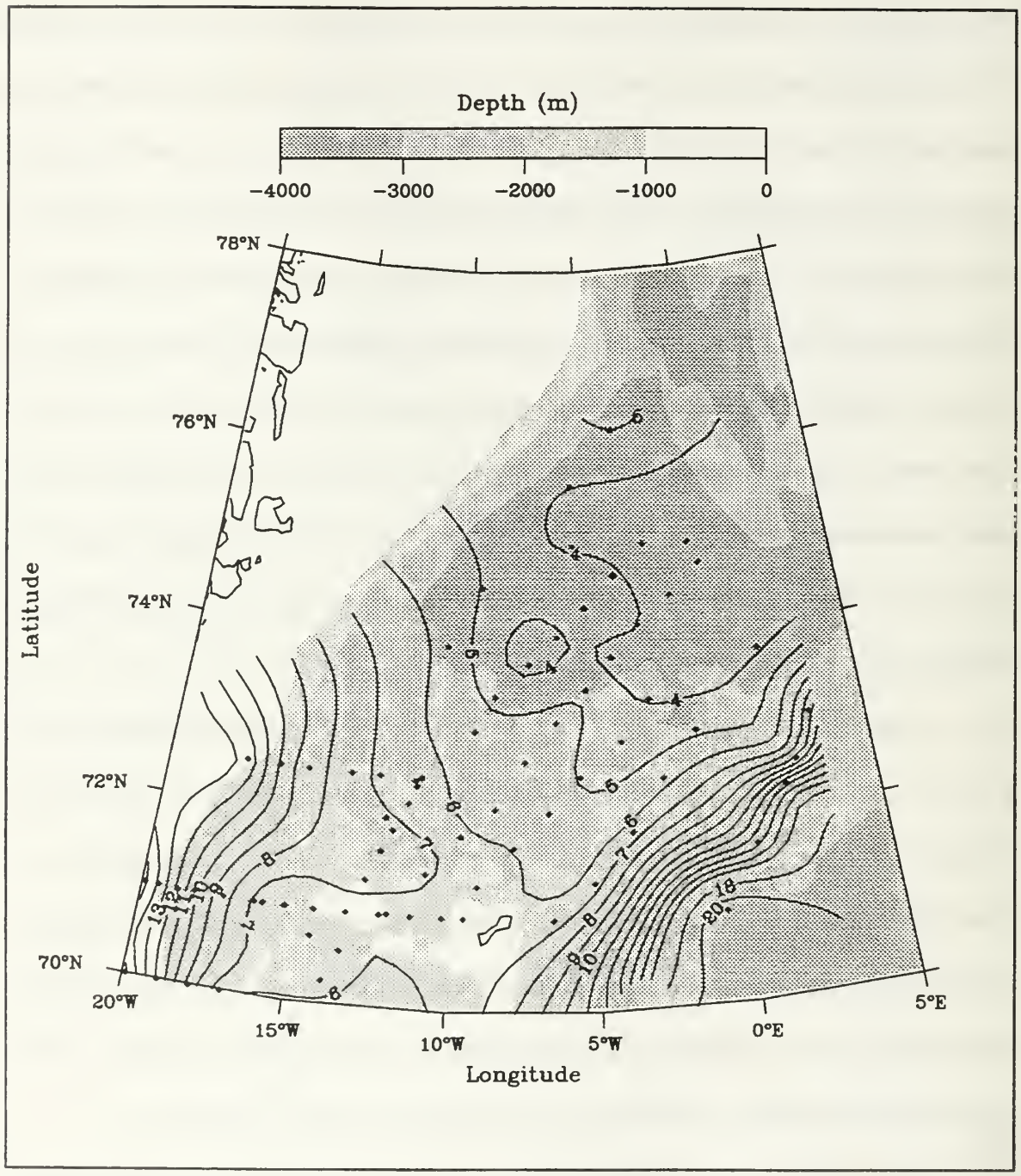

Figure 9. BARTLETT and BJARNI SÆMUNDSSON 90 dynamic height at 100 dbar referenced to 1000 dbar (dyn cm). The JMC meander is less prominent than at the surface and a greater fraction of the flow north of Jan Mayen at this level continues eastward as evidenced by the 5 and 6 dyn cm contour lines.

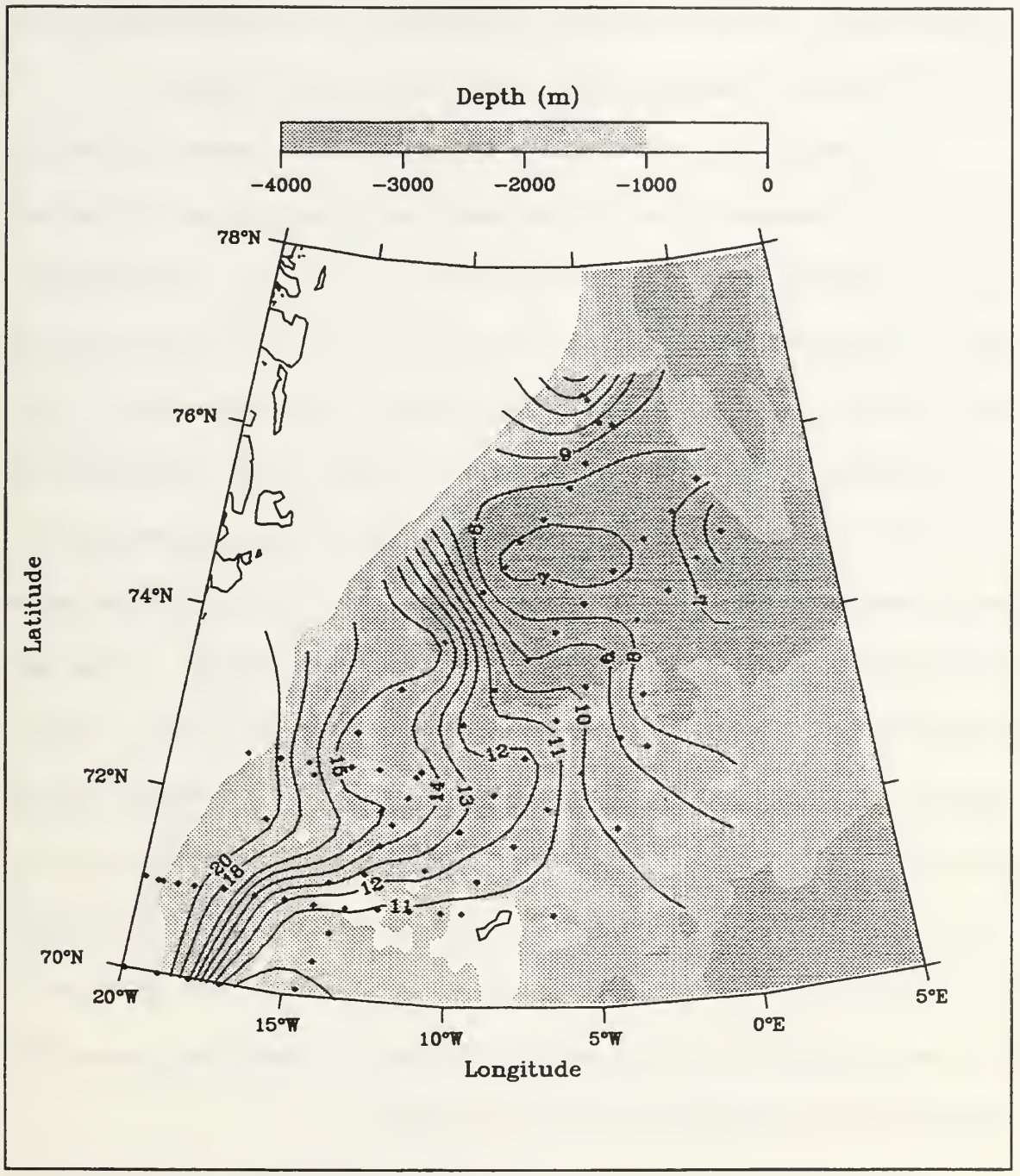

Figure 10. BARTLETT and BJARNI SÆMUNDSSON 89 dynamic height at the surface (10 m) referenced to 1000 dbar (dyn cm). The dynamic height values for 1989 are similar to 1990 but with a higher gradient where the JMC branches from the EGC at 74°N. This equates to a geostrophic velocity of ~ 7 cm/s, over twice the speed found in 1990.

September, 1989 (*J. Mortensen, personal communication*). The Danish/Icelandic station plan for 1989, which is similar to 1990, is shown in Appendix B, Figure 2.

As in 1990, the surface of the JMC is seen as an eastward meander of GPW from the EGC plus a southeasterly throughput presumably turning northward into the Greenland Gyre east of the most easterly station lines. The NAC does not show in the diagram in 1989. The values of dynamic heights are much the same over the region for the two years. However, the gradient of dynamic heights, about 7 dyn cm over 100 km, results in a maximum geostrophic velocity of about 7 cm/sec where the JMC branches from the EGC at 74°N, over twice the speed found in 1990. This difference may be due to the seasonal westward retreat of the ice edge in September 1989 which permitted the ship to sample the EGC and the EGPF region with its expected higher velocities. The eastward extent of the ice in August 1990 prevented the ship from sampling near the continental slope and EGPF. Using a figure similar to Figure 10, *Blythe* (1990) concluded that half of the flow lines form an anticyclonic meander in the EGC while the other half enter the GSG circulation or join the NAC to the east. Apparent in a comparison of Figures 8 and 10 is the less convoluted path of the large-scale surface meander in 1989. In Figure 11, the dynamic heights of the 100 dbar surface in 1989 show even more clearly than in 1990 the large fraction of throughput as compared to meander.

North to south and east to west vertical sections of temperature and salinity that also help to characterize the area are more appropriately associated with a description of intermediate water and will be discussed in Section C of this chapter.

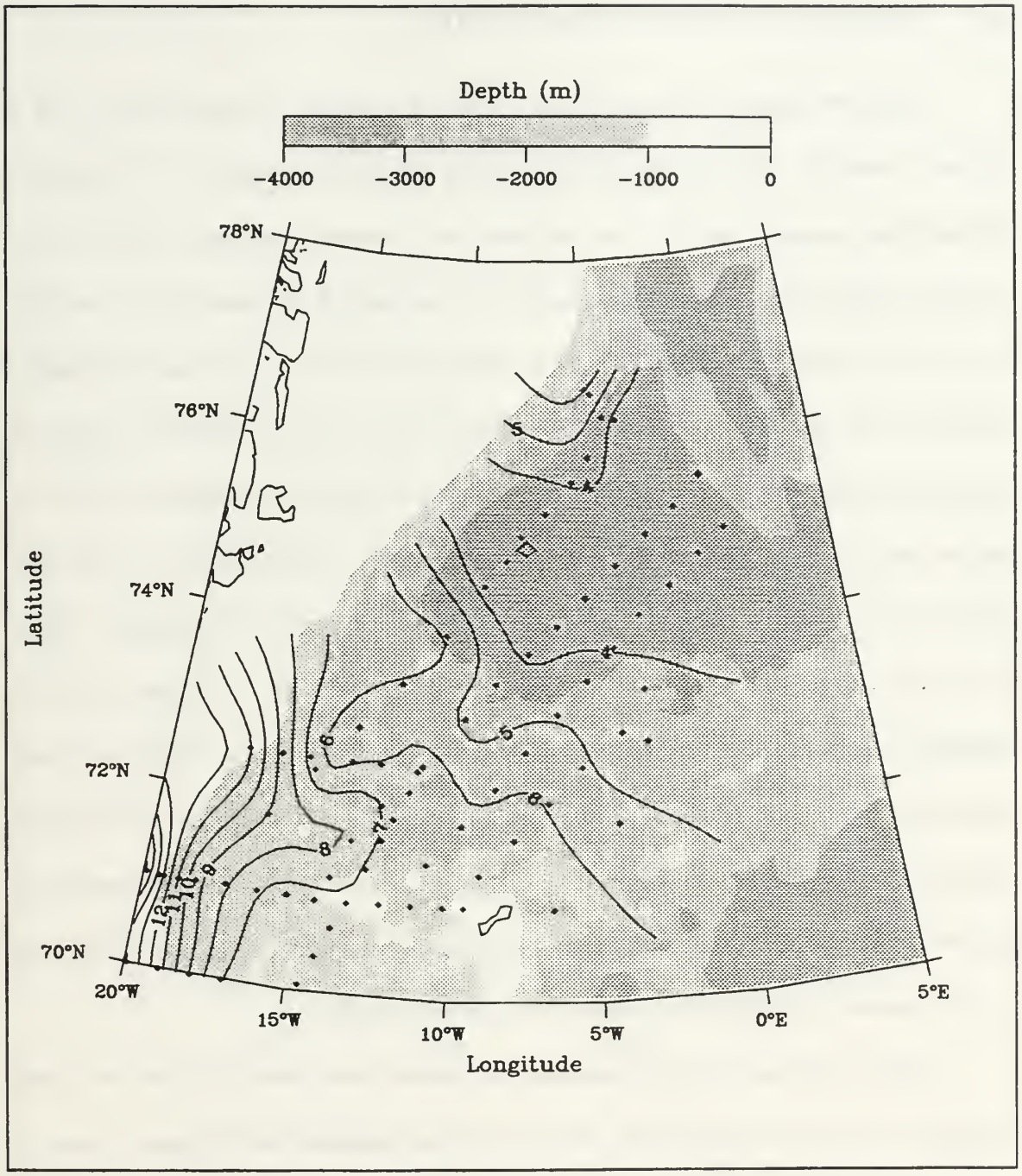

Figure 11. BARTLETT and BJARNI SÆMUNDSSON 89 dynamic height at 100 dbar referenced to 1000 dbar (dyn cm). More clearly than in 1990, the larger fraction of throughput compared to meander is seen in the 4 to 6 dyn cm contours.

B. SURFACE WATER PROPERTIES

The 1990 summer surface (10 m) temperature pattern is shown in plan view in Figure 12 with the corresponding surface salinity contours in Figure 13. In Figure 12, the isotherms increase from 1°C over the lower east Greenland continental slope to 10°C over the Lofoten Basin where the warm NAC is encountered. At about 73°N, the colder (1°C to 5°C) isotherms bow eastward at the 3000 m isobath which delineates the base of the slope of the Jan Mayen Fracture Zone (JMFZ) to the south. Similarly, in Figure 13, the relatively fresh GPW from the EGC forms an obvious meander centered at 73°N. The surface salinity varies from 30 PSU in the west, nearest the EGC, to over 35 PSU near the Mohn Ridge where the saline NAtSW of the NAC is located. The meander can be seen in the general bulging of the isotherms between 71° and 73°N. The position of the throughput shown in the dynamic heights (Figure 8) is reflected in a secondary bulge along the 3000 m isobath. A somewhat more pronounced pattern is seen in the surface salinities compared to temperatures. The relationship between flow and bathymetry will be noted in Section C. Surface temperature and salinity contours for BARTLETT 90 data only are shown in Appendix B, Figures 4 and 5, respectively.

The sea surface (10 m) temperature and salinity plan views for 1989 are shown in Figures 14 and 15, respectively. These are to be compared with Figures 12 and 13, respectively, for 1990. The temperatures were generally colder by 1 to 3°C in summer 1989 compared to 1990. In a comparison of BARTLETT 89 with JOHAN HJORT 1958 summer data, *Blythe* (1990) found a similar condition in which the 1989 surface

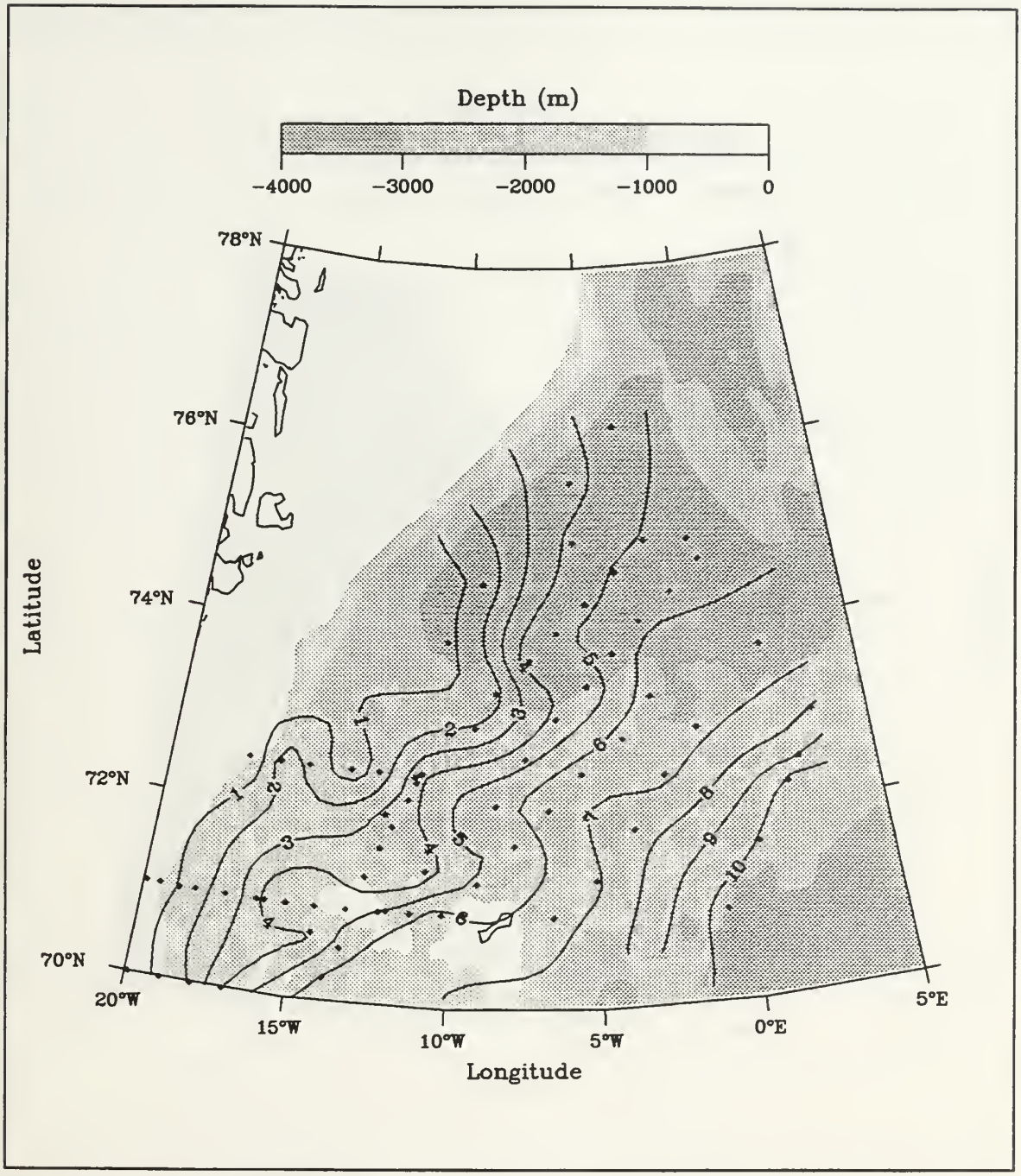

Figure 12. BARTLETT and BJARNI SÆMUNDSSON 90 surface (10 m) temperature (°C). The colder (1°C to 5°C) isotherms bow eastward at about 73°N along the 3000 m isobath which coincides with the base of the slope of the Jan Mayen Fracture Zone (JMFZ) to the south. Temperatures to 10°C occur over the Lofoten Basin where the warm NAtSW of the NAC is encountered.

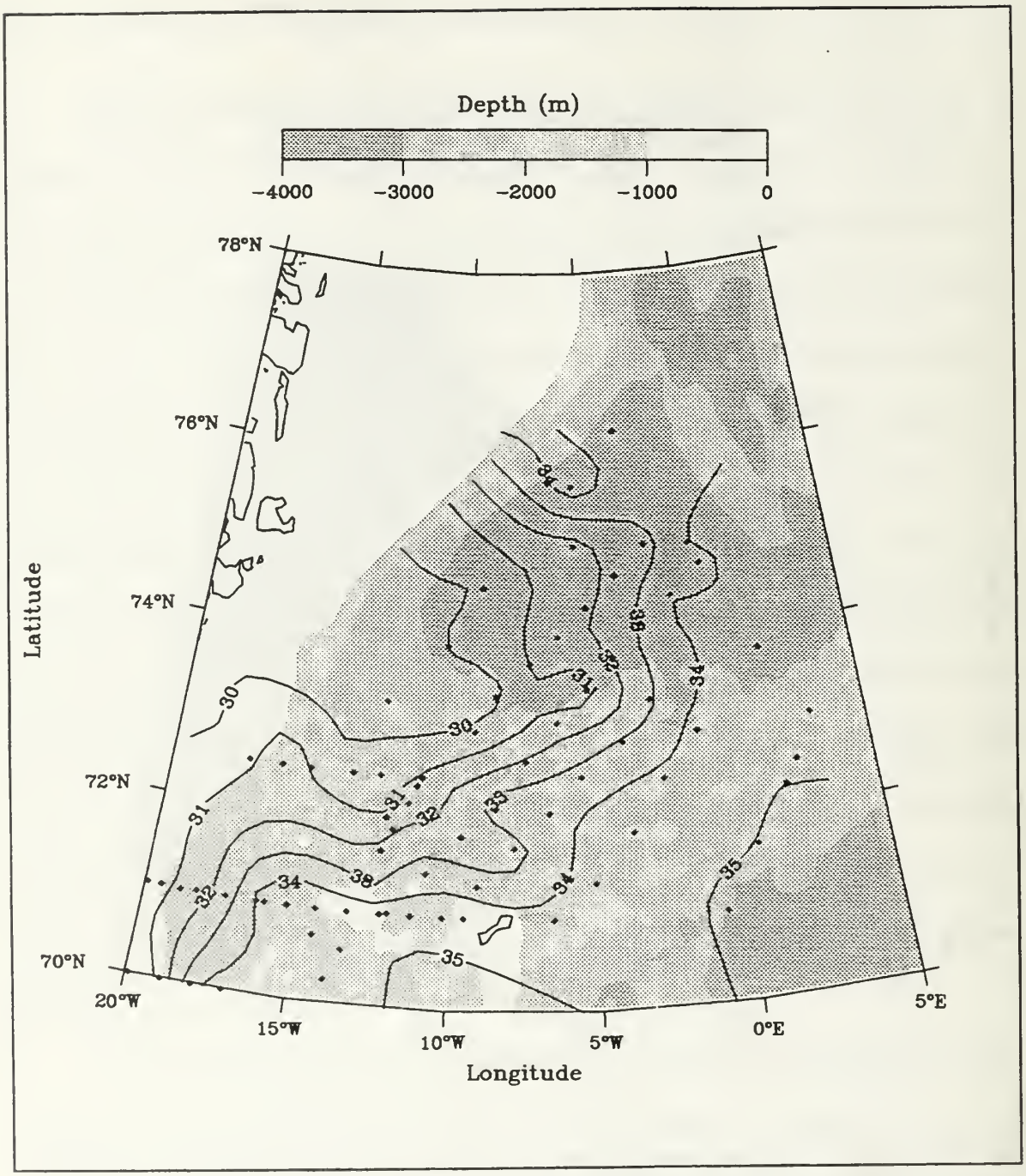

Figure 13. BARTLETT and BJARNI SÆMUNDSSON 90 surface (10 m) salinity (PSU). Similar to the surface temperature pattern, the relatively fresh GPW from the EGC forms an obvious meander at 73°N. The salinities vary from 30 PSU nearest the EGC to over 35 PSU near the Mohn Ridge where the saline NAtSW is located.

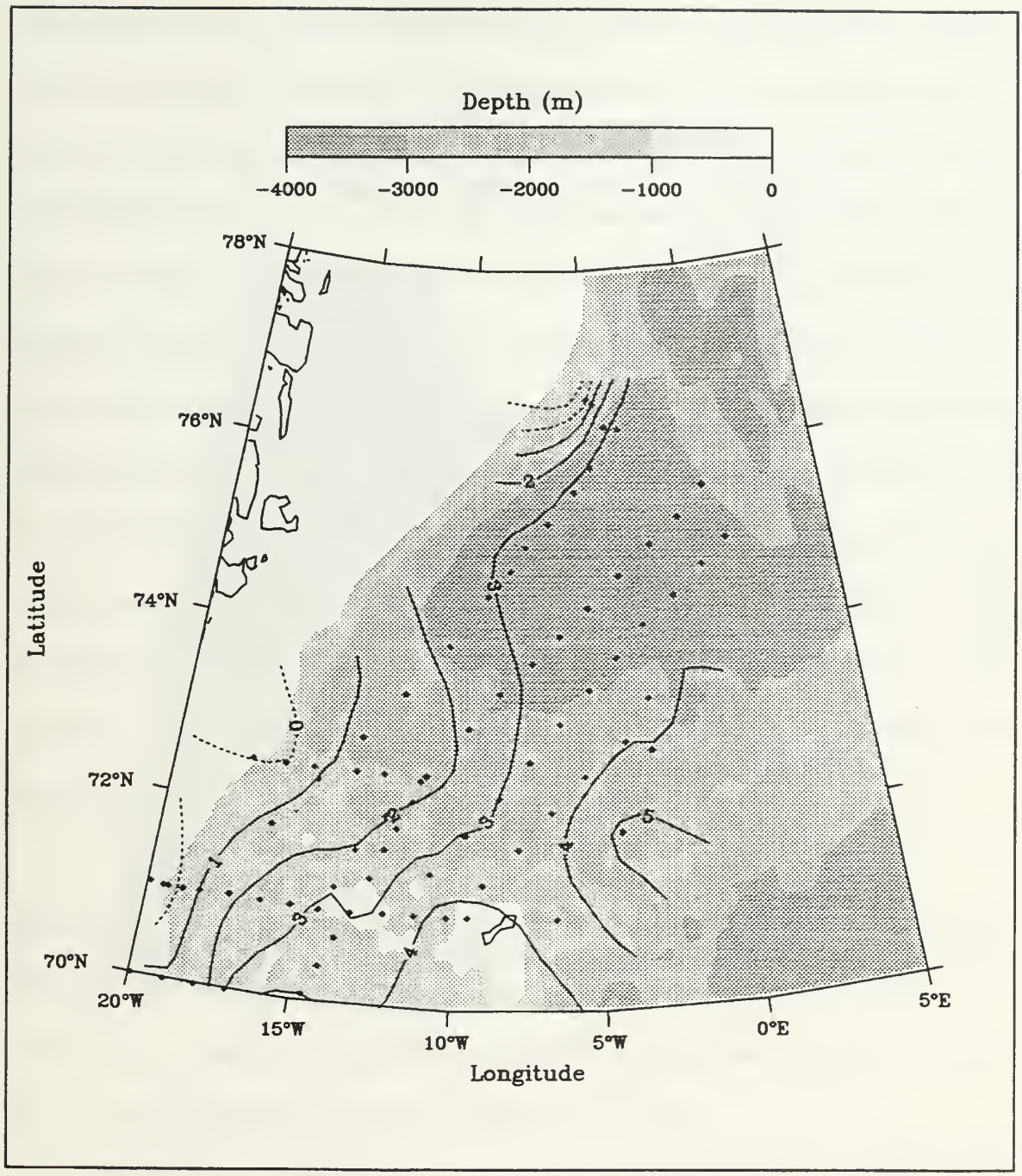

Figure 14. BARTLETT and BJARNI SÆMUNDSSON 89 surface (10 m) temperature (°C). Temperatures are colder at the surface by 1°C to 3°C compared to 1990.

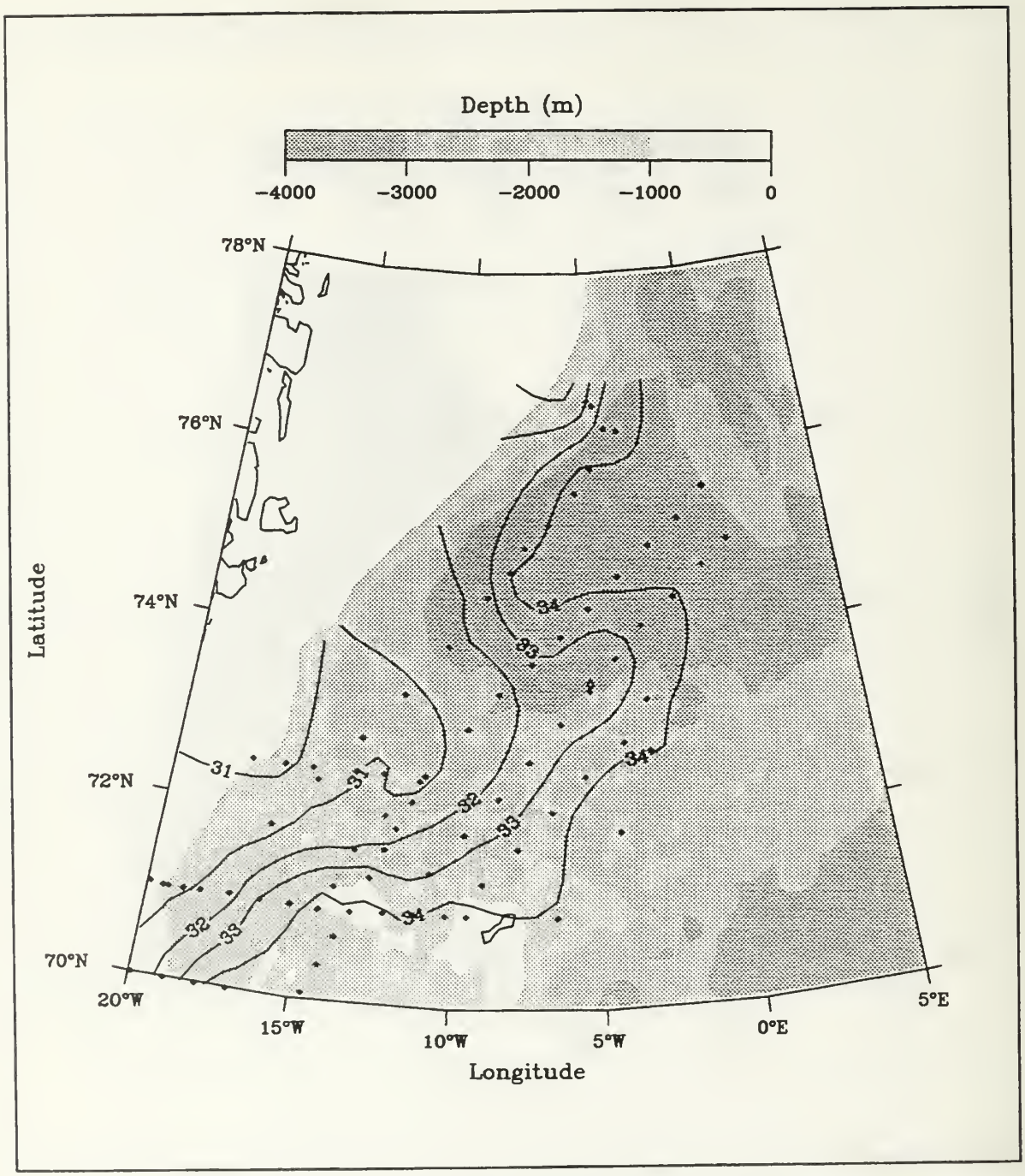

Figure 15. BARTLETT and BJARNI SÆMUNDSSON 89 surface (10 m) salinity (PSU). Salinities are higher by 1 to 2 PSU in the meander region compared to 1990. The 1989 contours, more markedly than 1990, show the separation of the effects of meander and of throughput into the GSG.

temperatures were 2°C colder than in 1958 and the 1989 axis of the meander was located 120 km south of the 1958 position. In a comparison of CTD data collected along two west-east transects at 74°45' N and 78°N during June 1989 and July 1990 aboard the POLARSTERN, *Budéus et al.* (1993) also found the Greenland Basin was significantly colder in 1989 than in 1990. The surface (10 m) salinity contours for 1989 (Figure 15) much more markedly show the separation of the effects of meander and of throughput into the GSG. However, salinities are higher by 1 to 2 PSU in the meander region compared to 1990 even though the 1989 survey was able to extend farther west toward the EGC. The 34 PSU isohaline, as an approximation of the eastern edge of the JMC surface meander, is similar to the 1990 position except over the central GSG. In 1989, the GSG displays a salinity range of 32 PSU to over 34 PSU. In 1990, evidence of the gyre is not reflected in the temperatures because the gyre center was well east of the station grid.

The JOHAN HJORT 1958 surface salinity data, analyzed by *Blythe* (1990), indicates salinities were higher by up to 3 PSU in 1958 compared to 1989 in both the JMC and GSG. Values ranged from 34 PSU just west of the EGC to over 35 PSU in the NAC region. *Blythe* (1990) attributes the increase in surface salinity in 1958 to a reduced flow of cold, fresh GPW in the EGC compared with 1989.

The warmer, fresher surface conditions in August 1990, as compared with September 1989, could be due to seasonal and/or interannual changes. According to *Pawlowicz* (1995), July and August are the months of greatest surface heating and most rapid melting of ice. He notes that June, representing the end of the spring season, and

September, the beginning of fall, exhibit cooler temperatures than mid-summer with a lesser rate of inflow of fresh water to the GSG. This agrees with observations from the BARTLETT: August 1990 daily air temperatures were, on average, 3°C higher than during September 1989. This also coincides well with the July 1990 POLARSTERN and August 1990 BARTLETT cruises which exhibit warmer, slightly fresher surface conditions than the June 1989 POLARSTERN and September 1989 BARTLETT cruises. According to *Gloersen et al.*(1992), who analyzed ice records from 1978 to 1987, the maximum melt-back of sea ice occurs in September. Thus, normal seasonal effects are in the correct sense to account for the higher temperatures in August 1990.

What should be the seasonal effect on the surface salinity is not so clear. Although an appreciable amount of fresh water is present in the area in September, it will not necessarily be recognizable in the surface because wave activity in the open water will have had time to mix it downward to varying degrees. From theory, it cannot be certified that the surface in August 1990 should be fresher. However, the mixing hypothesis can be tested. The surface salinity and the fresh water content in the upper 100 m of three BARTLETT transects, tending north to south between about 73.5°N to 71.5°N, with identical station positions for 1990 and 1989, were compared. The average salinity in the surface in August 1990 was 0.84 PSU fresher than in 1989. Likewise, the integrated fresh water content of the upper 100 m of the water column contained an average 170 kg/m^2 more fresh water in 1990 than in 1989. Additionally, as expected, the surface salinity increased and the integrated fresh water content decreased with distance from the ice edge for both years.

It should also be noted that the surface salinity and temperature fields for the two surveys are related to the fact that the ice edge continually recedes in summer, reaching a minimum in September. Hence, more fresh water was present in August 1990 when the ice edge was about 100 km seaward of its position in September 1989. This is in agreement with the investigation by *Pawlowicz* (1995) showing conditions in July and August are warm and fresh due to maximum solar heating and a much broader ice area in the process of melting.

C. INTERMEDIATE WATER PROPERTIES

1. Temperature Maximum Layer

The warm saline RAtIW flowing southward as part of the EGC system, just to the east of the EGPF, is distinguishable by a temperature maximum, which according to *Hopkins* (1988), is often as warm as 2°C with a salinity between 34.9 and 35.0 PSU and typically occupies a depth range from about 150 to 800 m. Surveys by *Bourke et al.* (1987) from 1981, 1984, and 1985, conducted after the *Hopkins* data sets, indicate RAtIW temperatures in the EGC can be 3°C or warmer. At about 73°N, a portion of this RAtIW turns eastward into the Greenland Sea, becomes diluted by GArIW, and is referred to as JMAtIW. The sharp temperature maximum associated with RAtIW, although now slightly moderated, remains prominent in JMAtIW in contrast to the colder GArIW so contours of the intermediate water temperature maximum (Tmax) are a useful guide in locating the JMC in both its meander and throughput manifestations.

A map of the temperature at Tmax for 1990, shown as Figure 16, clearly shows the meander centered at about 72.5°N and the throughput at about 73.5°N. The Tmax values in the region of the Greenland Gyre (< -0.5°C) near 74.5°N, 0°E do not mark JMAtIW, as will be seen later. The warm intermediate water meander is similar in shape and location to the surface GPW meander seen in Figure 12. Both features are affected by underlying bathymetry as evidenced by turning at the 3000 m isobath. *Blythe* (1990) states the flow of the water column is coordinated between the surface and intermediate levels and that this, together with a distinct and coordinated response to the bathymetry at both levels, suggests the flow is significantly barotropic as is expected in the region. The salinity at Tmax, Figure 17, mimics the temperature to some extent. Because salinity is more conservative than temperature, it conforms better to the dynamic heights patterns previously discussed in reference to Figure 8. The depth of Tmax in 1990 is shown in Figure 18. There is a poorly defined tendency for the Tmax to be lower where the depth of Tmax is greater. The contours of temperature, salinity and depth at Tmax for BARTLETT 90 data only are shown in Appendix B, Figures 6, 7 and 8, respectively, and would lead to no changes in the conclusions. A similar triplet of diagrams for the 1989 data in Figures 19, 20 and 21, respectively, exhibit much the same relationships. The 1989 intermediate water temperature maximum contours, shown in Figure 19, exhibit the expected eastward protrusion of warm JMAtIW. The warmer water was found at the eastern edge of the cruise track (3°W between 72 to 74°N) and may have extended farther, had sampling been possible. In Figure 20, any patterns of JMAtIW are masked by the natural variability of the salinity at Tmax. There is a notable lack of mesoscale

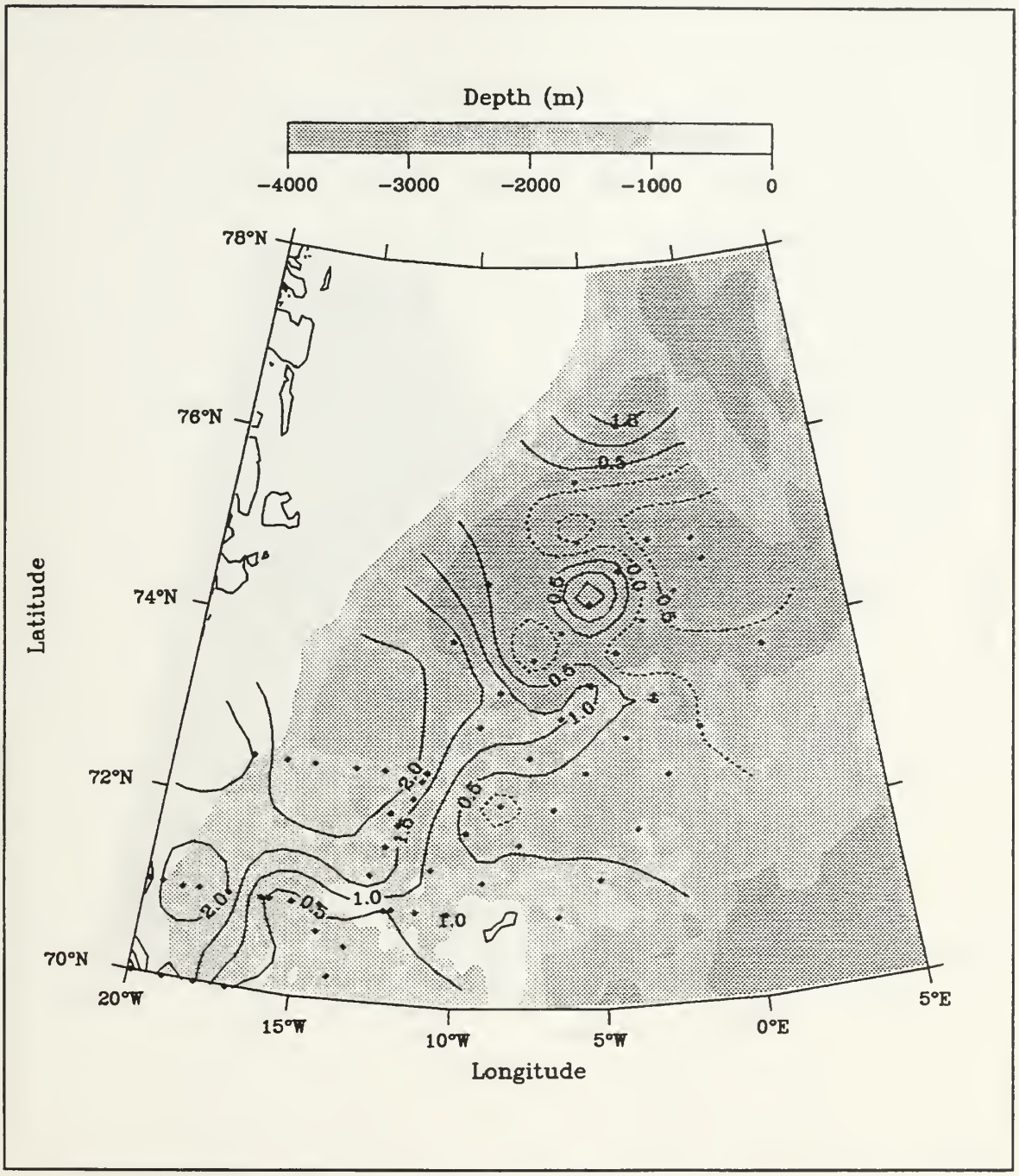

Figure 16. BARTLETT and BJARNI SÆMUNDSSON 90 contours of intermediate temperature maximum (Tmax) (°C). Tmax is associated with the JMAtIW of the JMC. The meander, seen in the 0.5°C to 2.0°C isotherms, is similar in shape and location to the surface, both features being affected by the bathymetry. Likewise, the JMC throughput to the GSG is centered at 73°N, best seen in the 0.5°C to 1.5°C isotherms.

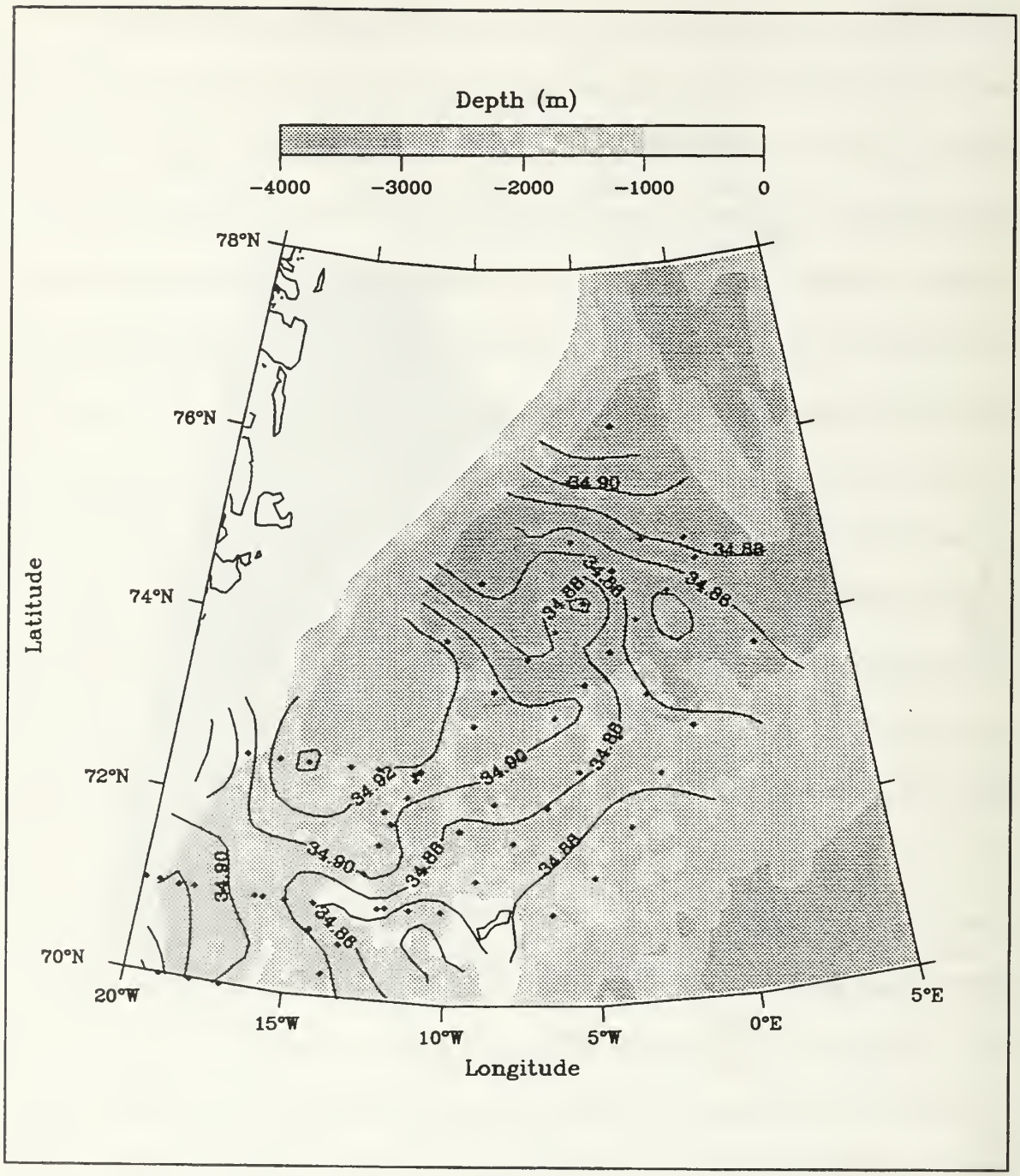

Figure 17. BARTLETT and BJARNI SÆMUNDSSON 90 salinity at the intermediate temperature maximum (Tmax) (PSU). The salinity contours mimic the patterns seen in Tmax.

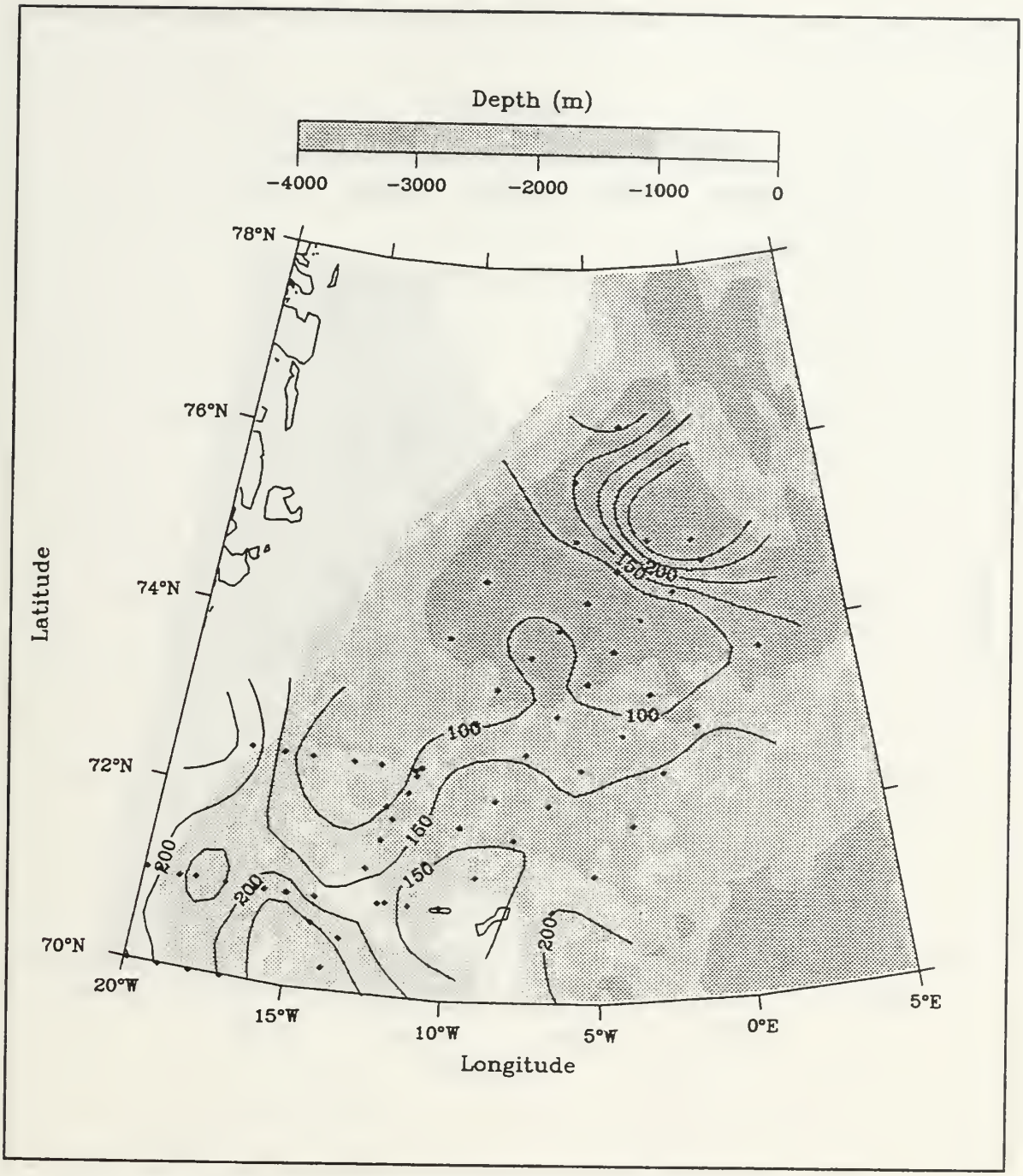

Figure 18. BARTLETT and BJARNI SÆMUNDSSON 90 depth of the intermediate temperature maximum (Tmax) (m). The depth of Tmax, typically 100 m in the JMC, deepens to the east. Tmax occurs at depths over 200 m in the GArIW of the GSG.

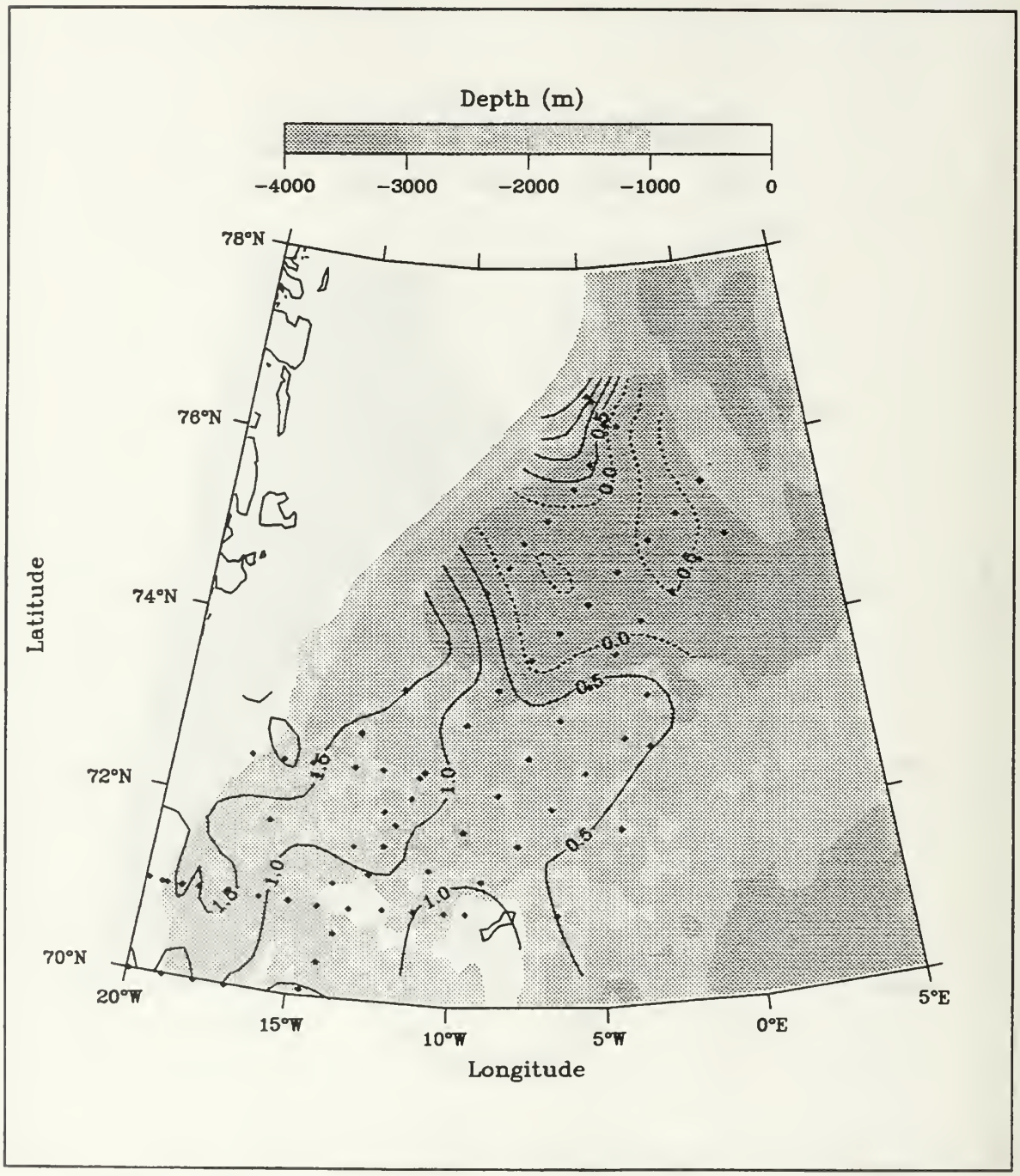

Figure 19. BARTLETT and BJARNI SÆMUNDSSON 89 contours of intermediate temperature maximum (Tmax) (°C). Similar to 1990, the JMC is evident in the eastward protrusion of the 0.5°C isotherm. There is a lack of eddy-like features compared to 1990.

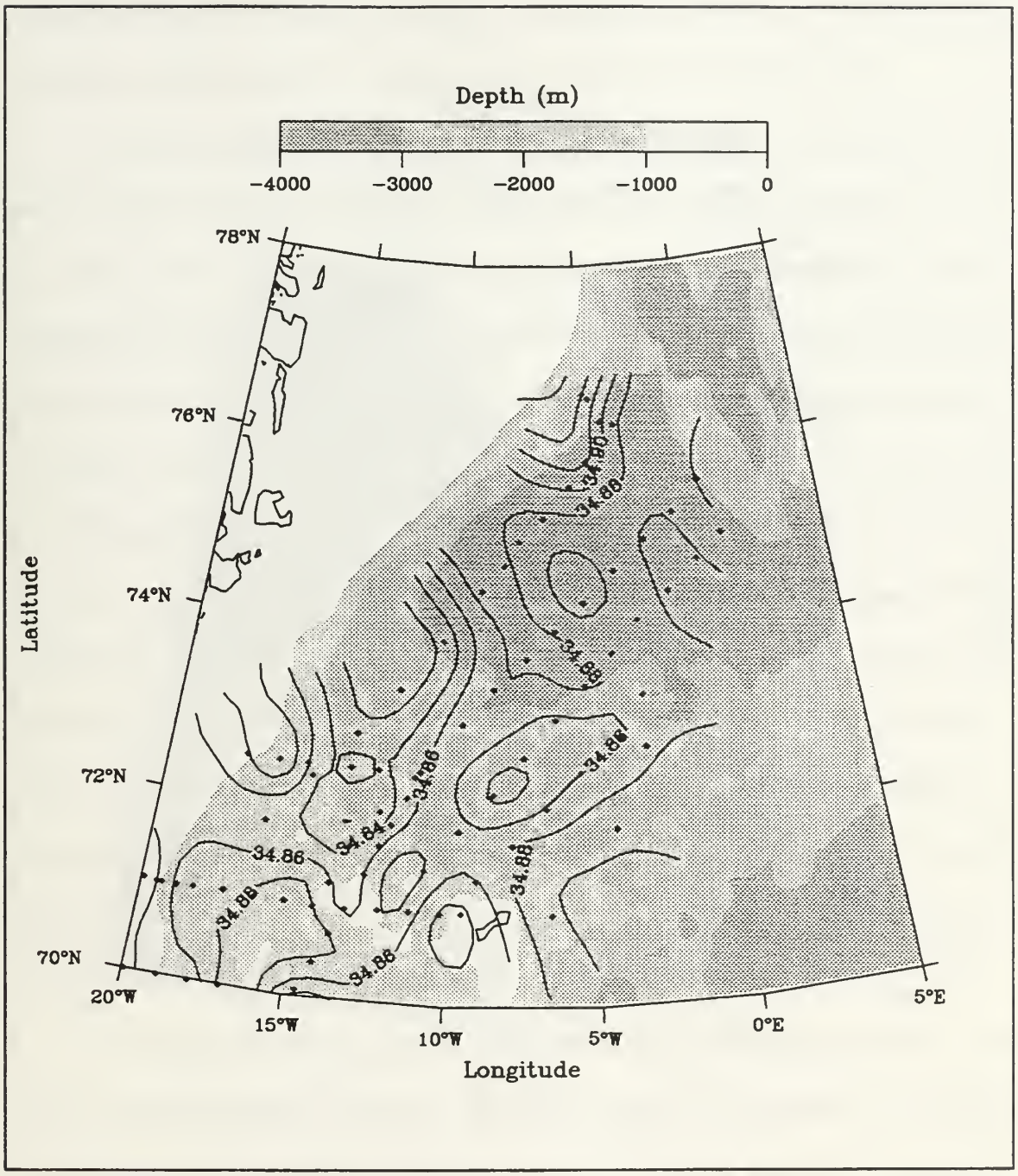

Figure 20. BARTLETT and BJARNI SÆMUNDSSON 89 salinity at the intermediate temperature maximum (Tmax) (PSU). Any patterns of JMAtIW are masked by the natural variability of the salinity at Tmax.

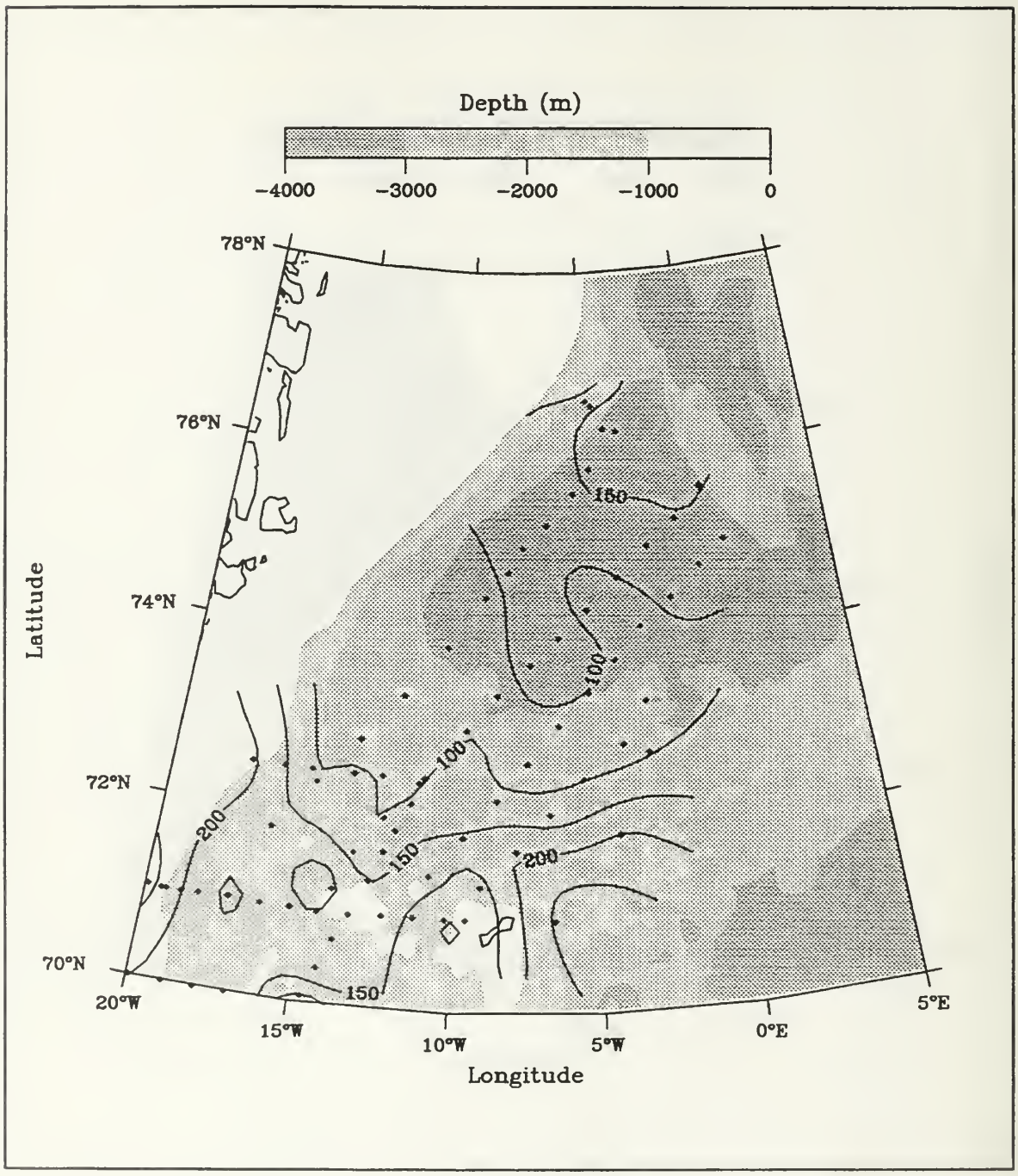

Figure 21. BARTLETT and BJARNI SÆMUNDSSON 89 depth of the intermediate temperature maximum (Tmax) (m). Similar to 1990, JMAtIW occurs at ~ 100 m.

eddy features in 1989 compared to 1990. A detached eddy, typical of flows exhibiting a strong baroclinic shear, was present in 1990 centered at 74°N (Figure 16).

Several diagrams will be presented to help clarify the nature of the waters in the survey area; the BARTLETT 90 station sequences used are shown in Figure 22. Along the course of the throughput, the portion of the JMAtIW that continues eastward to complete its rotation around the Greenland Gyre, Tmax may be seen in the set of temperature-salinity correlations in Figure 23. The stations used in Figure 23 are those of Transect D shown in Figure 22 with the deletion of Stations 5 and 21 for clarity and the addition of Station 44 (see Figure 3) at the extreme eastern end of the T-S section as the nearest example of water beneath the NAC. The data in Figure 23, block-averaged every 20 m, reveal Tmax becomes distinctly colder with distance from the source and with time, although the depth of Tmax changes little. Tmax changes from 0.6°C (#6) to -0.5°C (#34) over a distance of 300 km but the change is decidedly non-isopycnal, i.e., the mixing of JMAtIW with GArIW is not along isopycnals. JMAtIW is not notably different in composition from the deeper parts of the NAC (Station 44) at a depth of about 400 m and a potential density anomaly of about 28.02.

An analysis of T-S diagrams and temperature-depth curves (not shown) for each station reveals that nearly all stations have some amount of finestructure. In general, finestructure is present wherever there are notable horizontal gradients in properties. Interleaving of large elements, typical of frontal boundaries, is most marked near the ice margin and the junction of JMAtIW with the NAC. Interleaving is least common in the GSG and the NAC. There are almost no step-like structures.

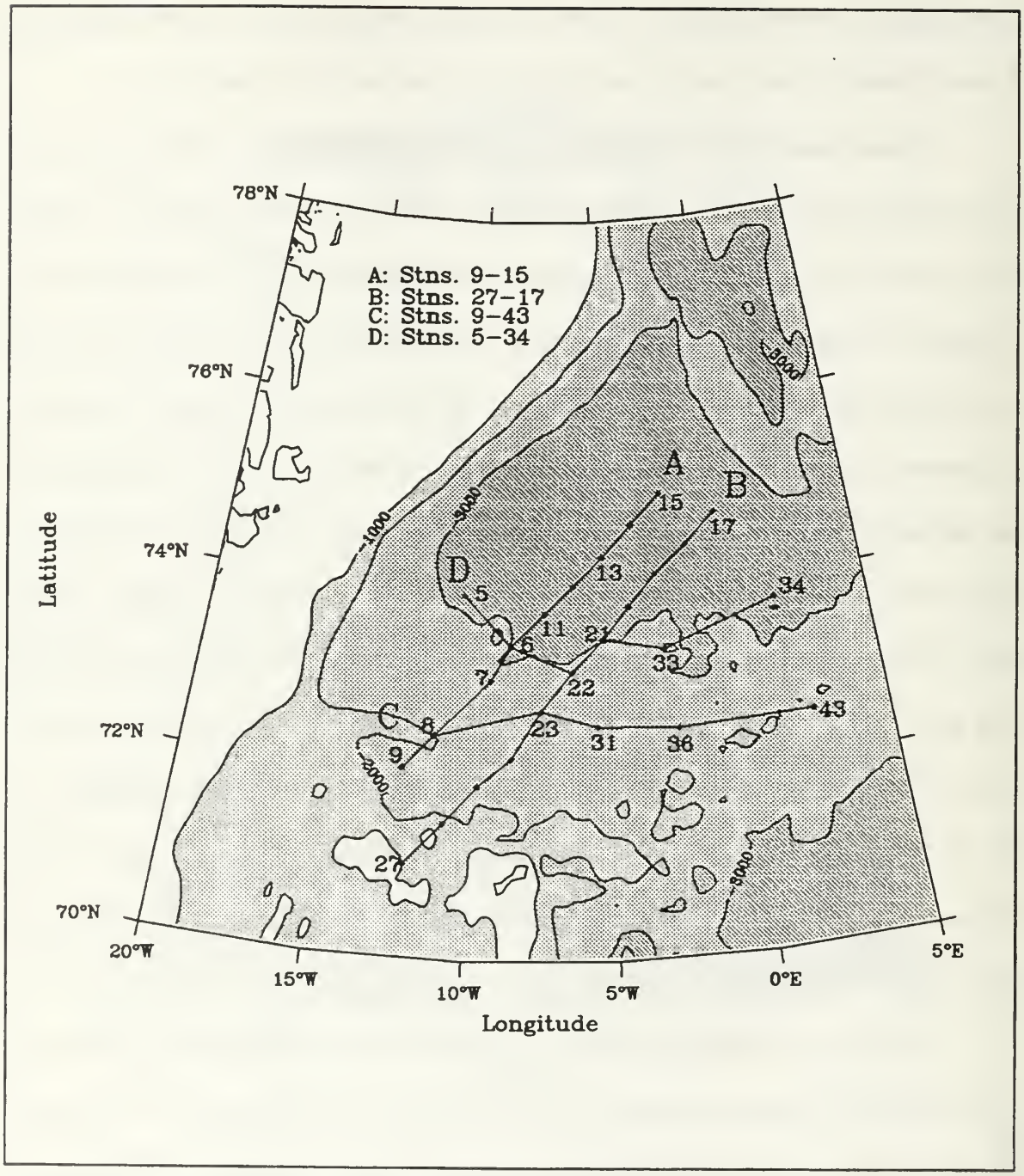

Figure 22. Location of BARTLETT 90 Transects A - D. The temperature and salinity for these sets of stations will be presented in vertical cross-section.

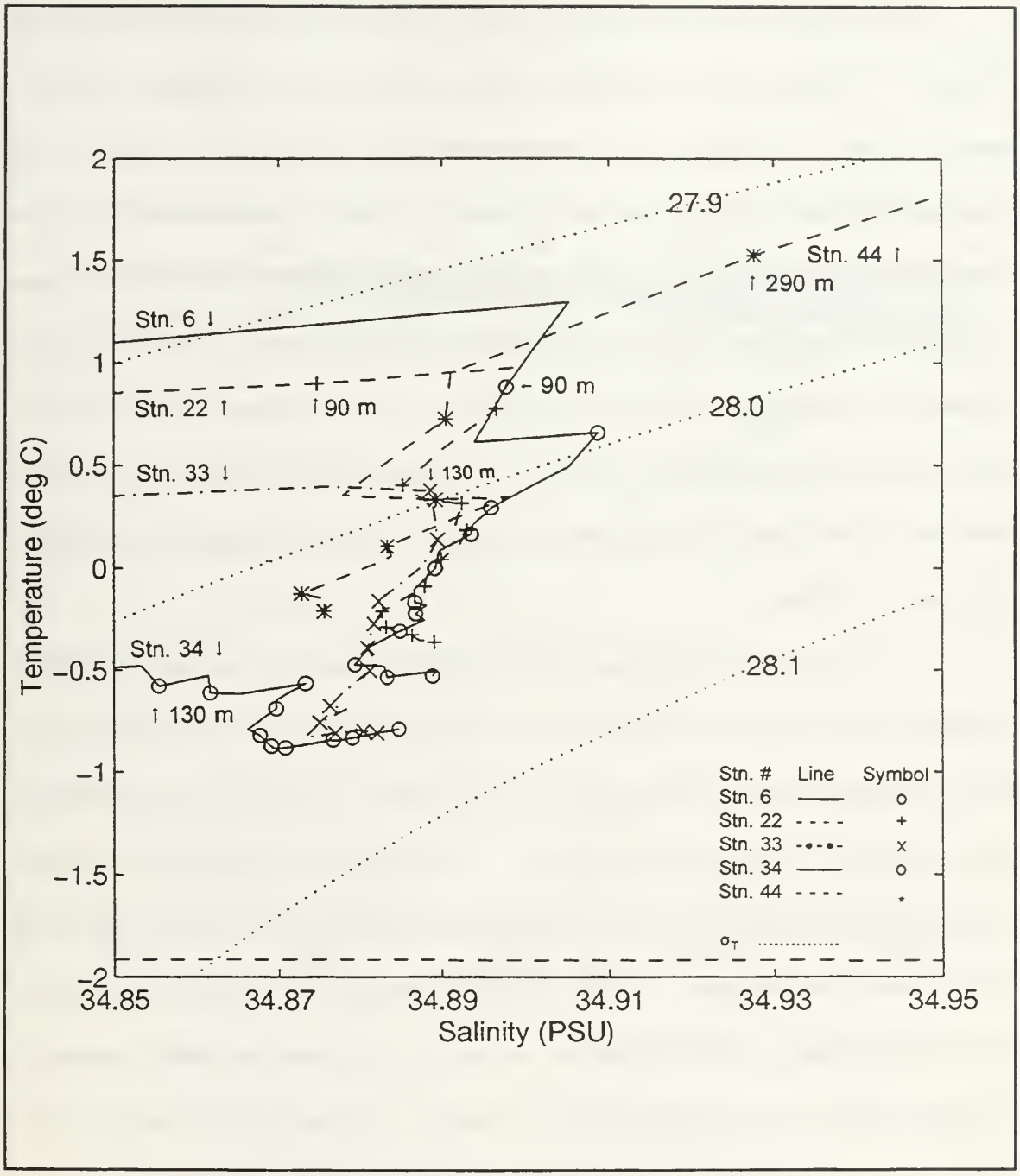

Figure 23. T-S correlations along Transect D showing the progression of Tmax associated with JMAtIW from west to east. Stations 5 and 21 are deleted for clarity. Station 44 is included as an example of water beneath the NAC. Data are block-averaged every 20 m with symbols placed every 40 m. Depth of the first symbol is labeled.

The course of the JMAtIW may be seen in the vertical-section format in Figures 24 and 25. (In these and all subsequent vertical sections, data are plotted to 500 m for better resolution of features.) The temperatures along Transect D in Figure 24 are consistent with the comments accorded to Figure 23. Tmax is found close to 100 m and deepens slightly to the east. JMAtIW, bounded at depth by the 0° C isotherm, appears to ride up over the colder GArIW on the eastern side of the transect. The doming of the isotherms has repeatedly been identified with the cyclonic rotation of the GSG. The associated salinities are shown in Figure 25. A weak correlation of Tmax with a salinity maximum slightly deeper and a general progression toward higher upper layer salinities to the east is evident.

In 1989, the section of stations representing the greatest throughput of JMAtIW, as determined by *Blythe* (1990), is Transect D shown in Figure 26. The vertical sections for the temperature and salinity along the 1989 Transect D are shown in Figures 27 and 28, respectively. Compared to Figure 24 for 1990, the intermediate waters greater than 0°C, representing JMAtIW, encompass a larger area in 1989 as seen in Figure 27 though Tmax is again centered close to 100 m. The underlying GArIW is much less prominent in the east compared to 1990. Likewise, the region of an associated salinity maximum is larger in 1989 when comparing Figures 25 and 28. A quantitative comparison of the volume of JMAtIW present in 1989 and 1990 will be discussed in Chapter V.

There are instances of a temperature maximum not associated with JMAtIW or RAtIW. These are illustrated in the temperature-salinity diagram of Figure 29 along Transect B in Figure 22 for 1990. In Figure 29, Stations 22 and 26, which are more

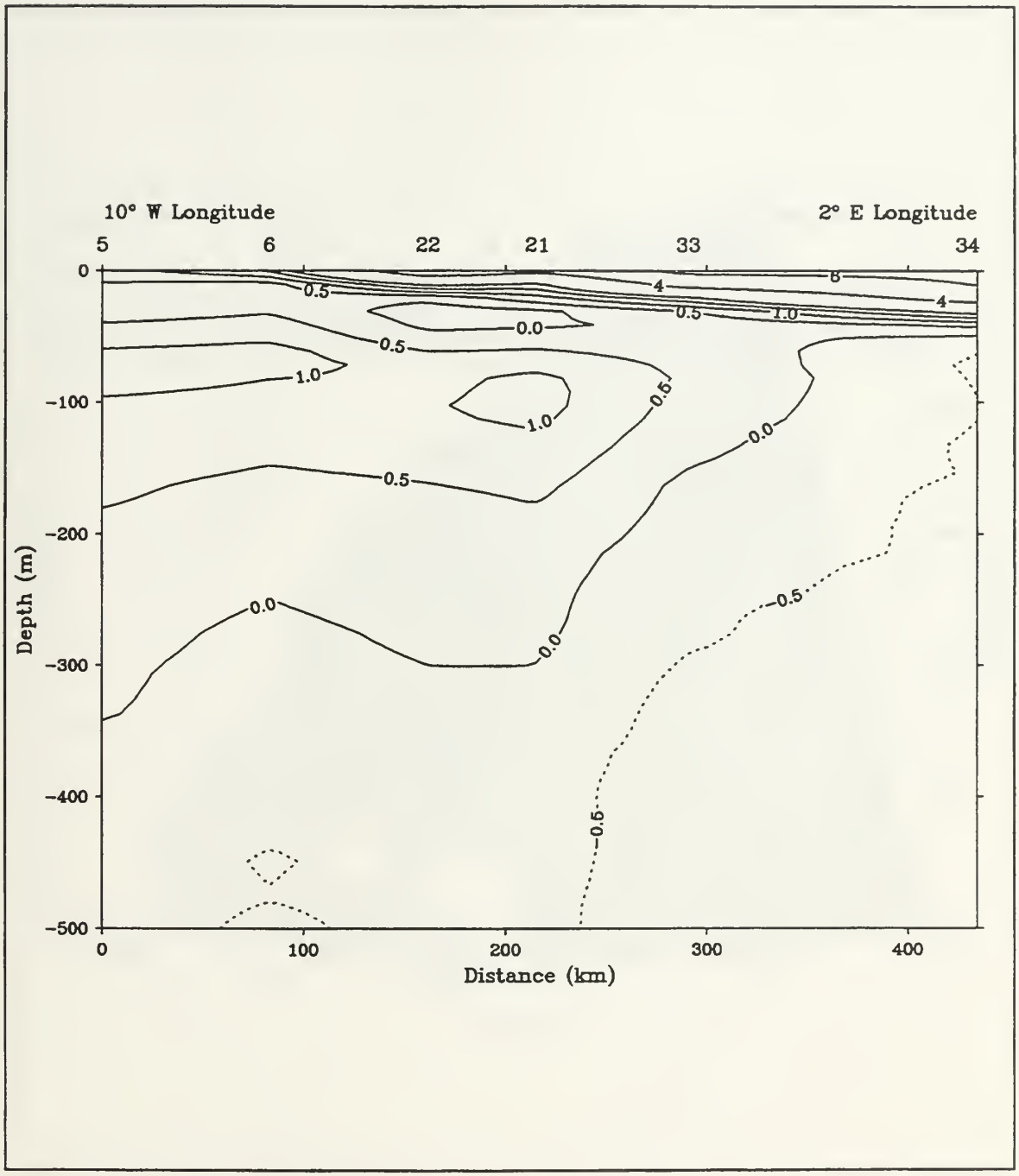

Figure 24. BARTLETT 90 temperature along Transect D (°C). This west to east section shows the course of JMAtIW as it moves eastward across the southern portion of the GSG. Tmax is found close to 100 m and deepens to the east. JMAtIW, bounded by the 0°C isotherm, rides up over the colder GArIW to the east. This doming is associated with the cyclonic rotation of the GSG.

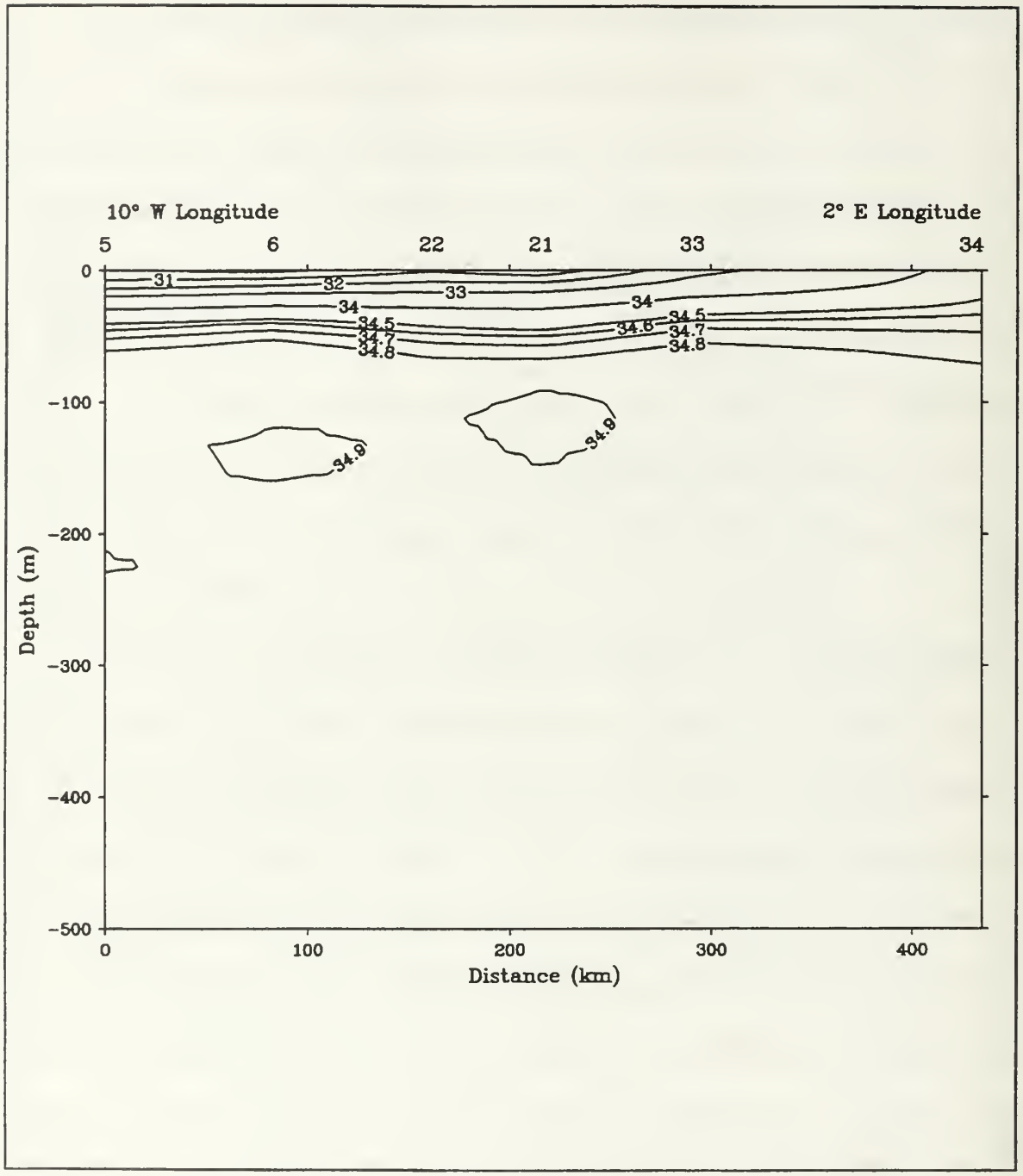

Figure 25. BARTLETT 90 salinity along Transect D (PSU). A weak correlation of Tmax with a salinity maximum slightly deeper is evident. There is a general progression toward higher upper layer salinities to the east as distance from the EGC increases.

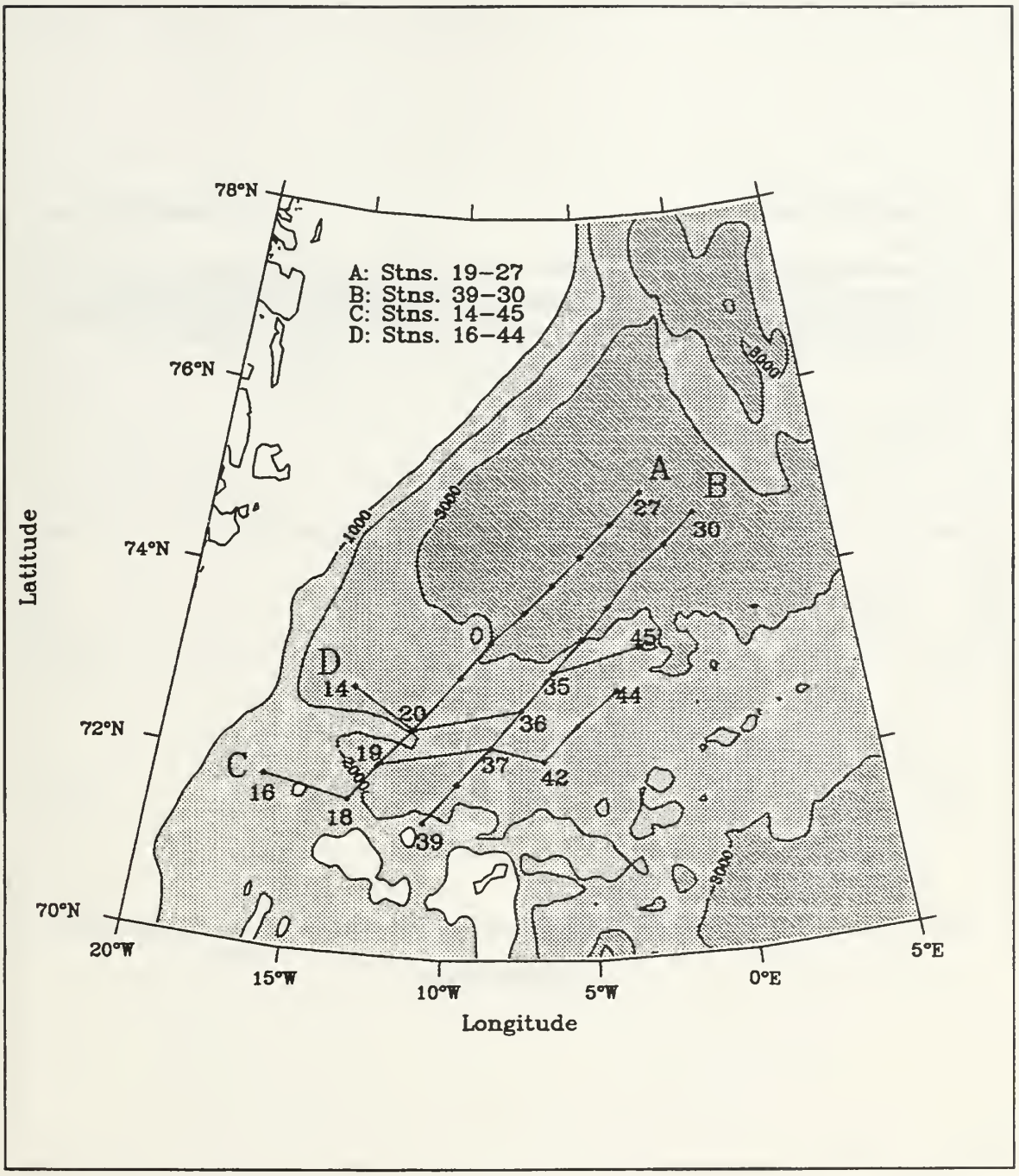

Figure 26. Location of BARTLETT 89 Transects A - D. The temperature and salinity for these sets of stations will be presented in vertical cross-section for comparison with BARTLETT 90 Transects A - D.

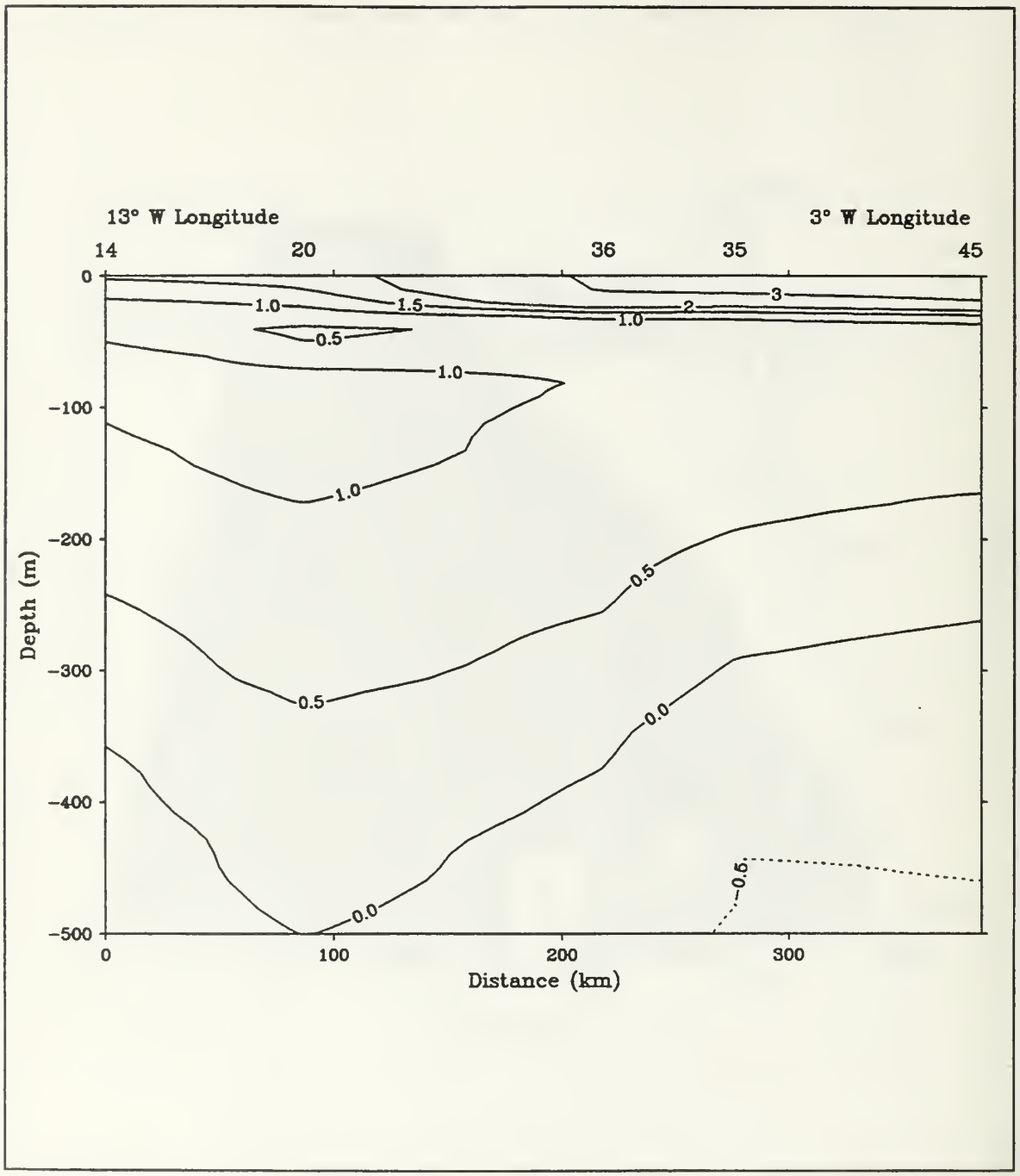

Figure 27. BARTLETT 89 temperature along Transect D (°C). This west to east section represents the region of greatest throughput of JMAtIW eastward during 1989 and is south of the 1990 position by about 100 km. JMAtIW, bounded by the 0°C isotherm, encompasses a larger area compared to 1990. As is typical, Tmax is centered at 100 m.

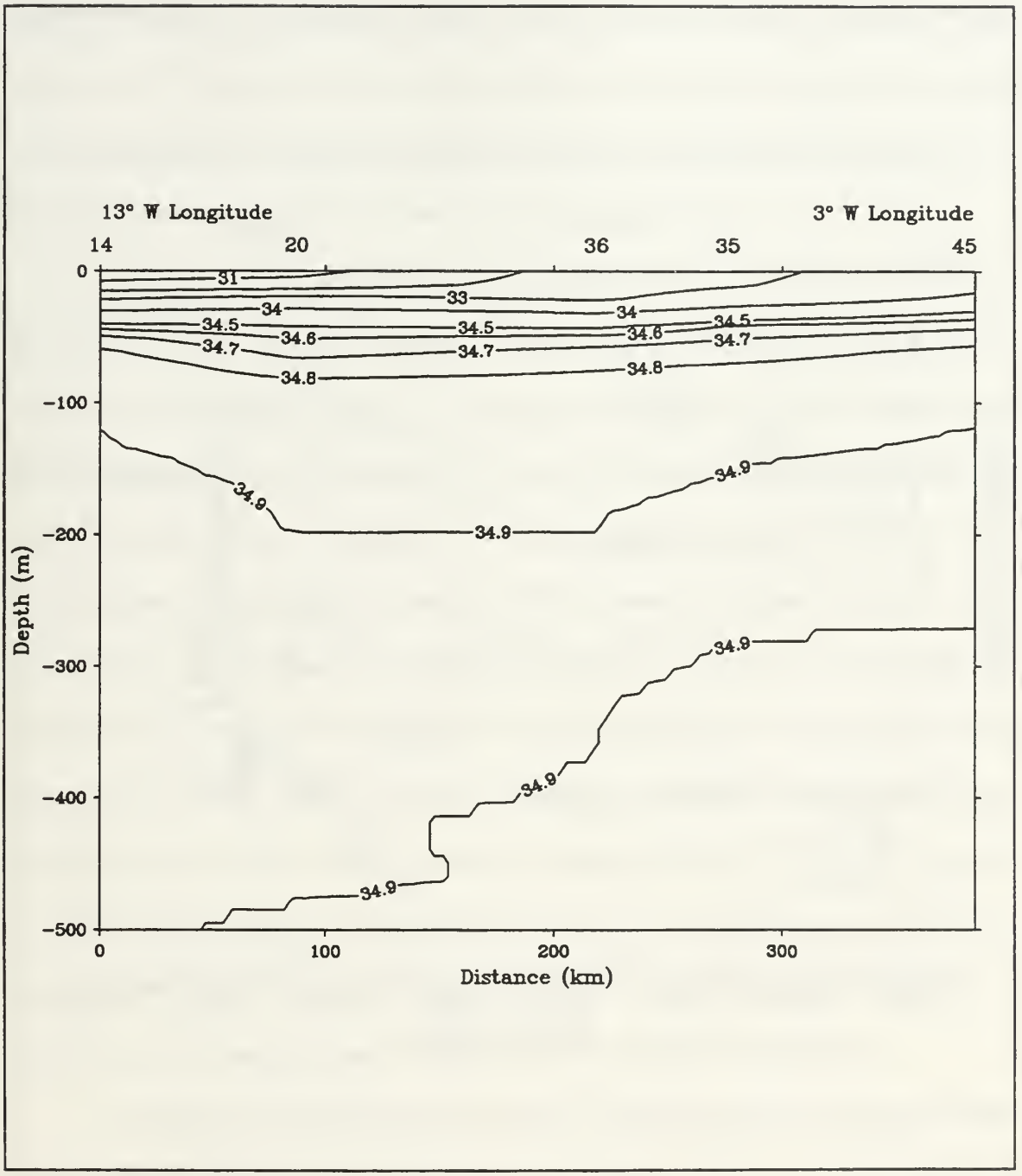

Figure 28. BARTLETT 89 salinity along Transect D (PSU). As in temperature, the region of an associated salinity maximum is larger in 1989 compared to 1990. The underlying GArIW is less prominent in the east relative to 1990.

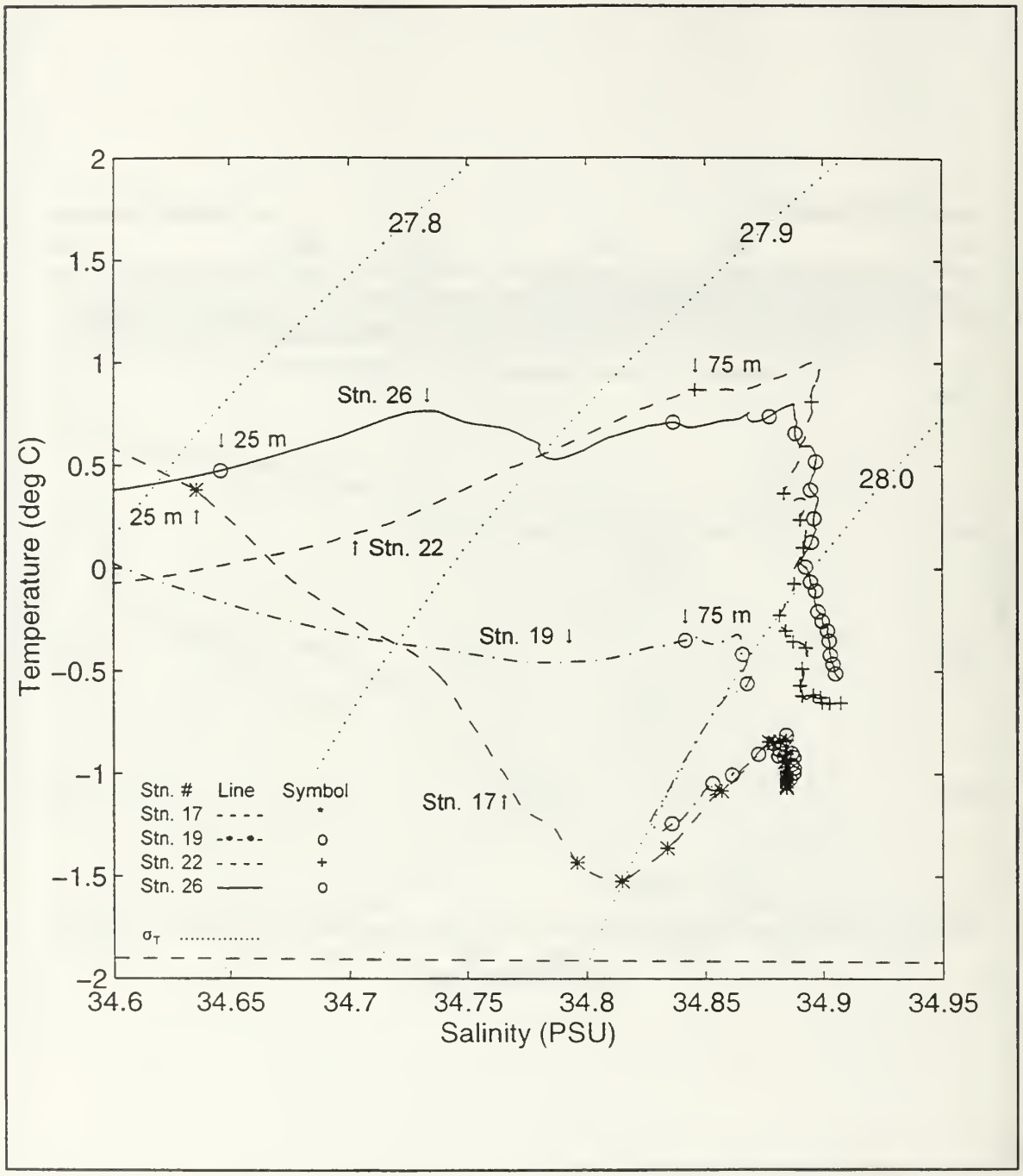

Figure 29. T-S correlations showing Tmax behavior along four stations from Transect B 1990. Two regimes are evident with Stations 22 and 26 representing JMC type waters with a Tmax above 0°C. Stations 17 and 19, at the north end of Transect B, exhibit a Tmax with lower temperatures (< 0°C) and do not mark JMAtIW. Data is running-averaged with symbols placed every 50 m. The depth of the first symbol is labeled.

southerly, have a T-S relationship typical of JMC type waters with a prominent Tmax well above 0°C. Stations 17 and 19, at the north end of Transect B, exhibit a Tmax that is associated with lower temperatures and greater depths and thus does not mark JMAtIW. The Tmax structure at Stations 17 and 19 is typical of GArIW.

A vertical section of temperature along Transect B for 1990 is shown in Figure 30. The core of the JMAtIW throughput is seen centered at Station 21 at about 100 m, close to the cold water of the GSG. The nose of the meander is seen at Station 26 and distinctly separated from the throughput. The corresponding salinities, Figure 31, again show the core of JMAtIW at Station 21. The lower salinities associated with the water in the meander are present to the south. In 1989, Transect B (Figure 26) is identical in location to the 1990 Transect B. The vertical sections of temperature and salinity for Transect B in 1989 are shown in Figures 32 and 33, respectively. The temperature along Transect B in 1989 is similar to 1990 but without the separation of the throughput and meander evident in 1990. Both sections show a sharp boundary at about 73.5°N, north of which are the colder waters of the GSG (< 0°C), in association with the 3000 m isobath where the JMC turns eastward from the EGC. Similar comments apply to a comparison of the salinity along Transect B in 1989 with the 1990 section.

To complete the characterization of the area, vertical sections of temperature and salinity along Transect A for 1990 are shown in Figures 34 and 35. The throughput of JMAtIW is seen at 75 m at Station 6 with the waters of the meander to the south in Figure 34. The cold waters of the GSG north of Station 11 are interrupted by a pronounced eddy feature at Station 13 (radius perhaps exaggerated by station spacing).

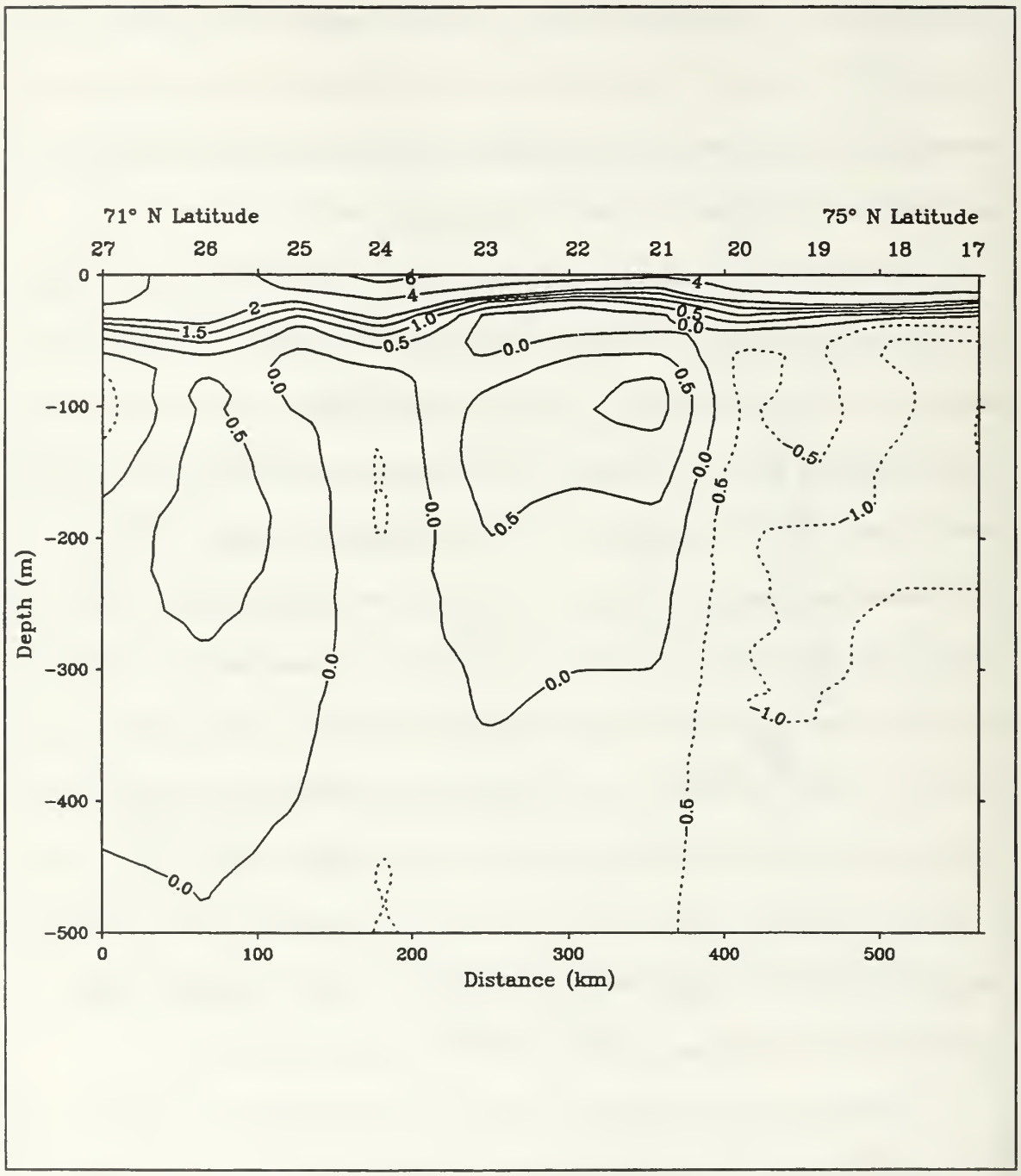

Figure 30. BARTLETT 90 temperature along Transect B (°C). This south to north section shows the core of JMAtIW centered at Station 21 at about 100 m. The meander is seen at Station 26 distinctly separated from the throughput by an intrusion of colder water at Station 24. North of Station 21 are the colder waters of the GSG.

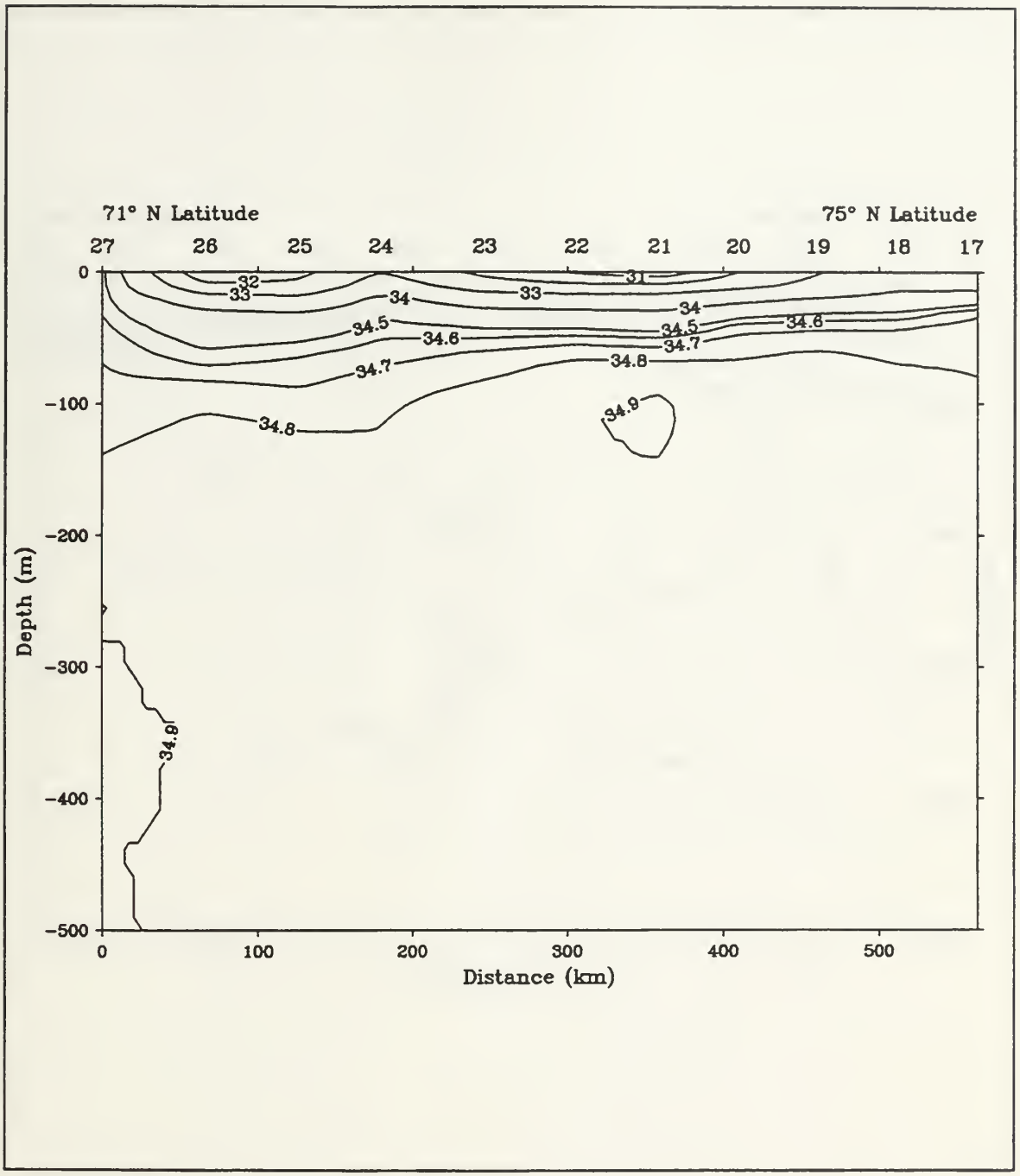

Figure 31. BARTLETT 90 salinity along Transect B (PSU). The core of JMAtIW is again seen at Station 21. Salinities corresponding to JMAtIW typically exceed 34.9 PSU. The lower salinities associated with the meander are present to the south.

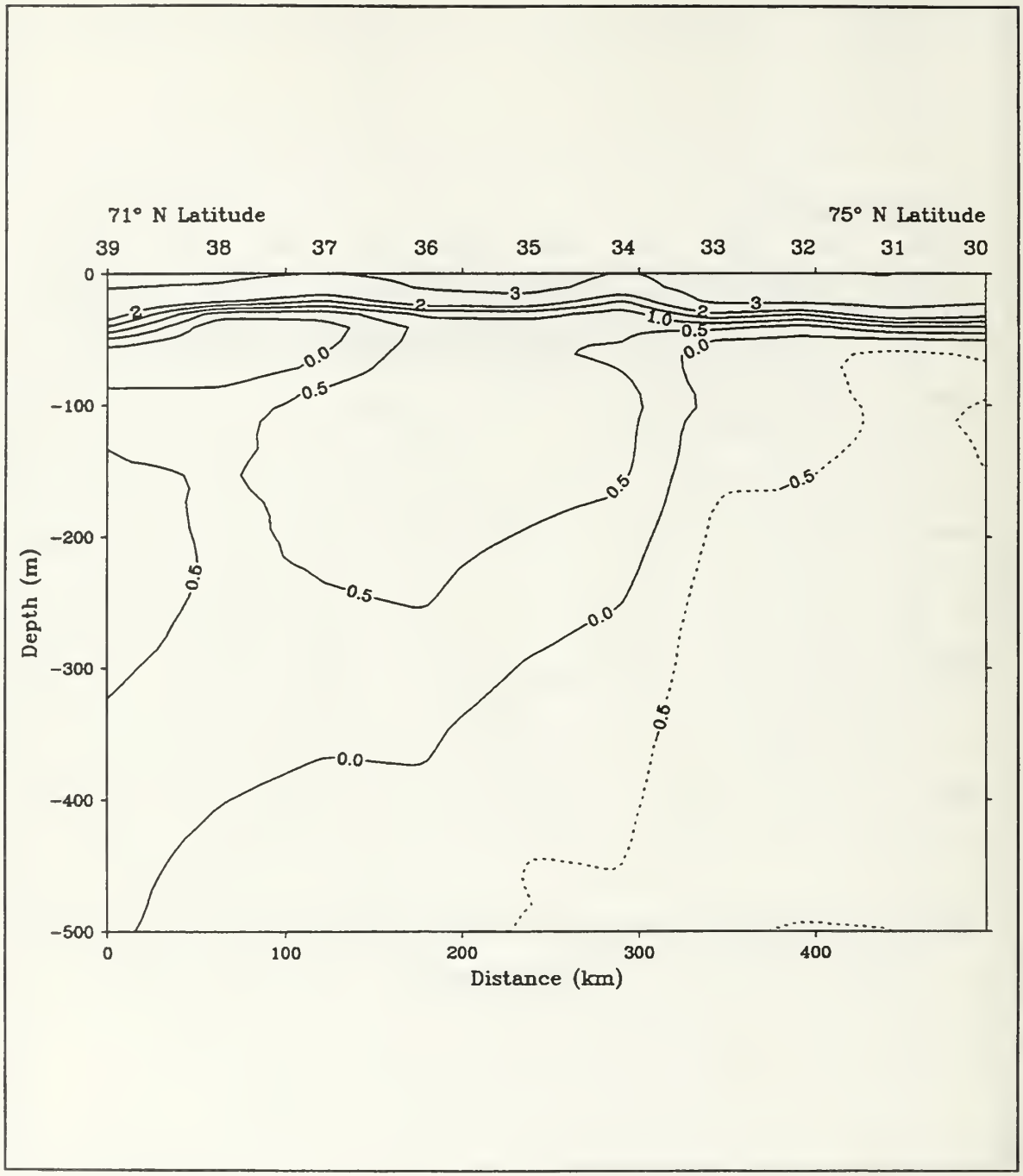

Figure 32. BARTLETT 89 temperature along Transect B (°C). This south to north section, identical in position to 1990 Transect B, is similar to 1990. In both years, a sharp boundary exists at about 73.5°N between the JMC and GSG in association with the 3000 m isobath where the JMC turns eastward from the EGC.

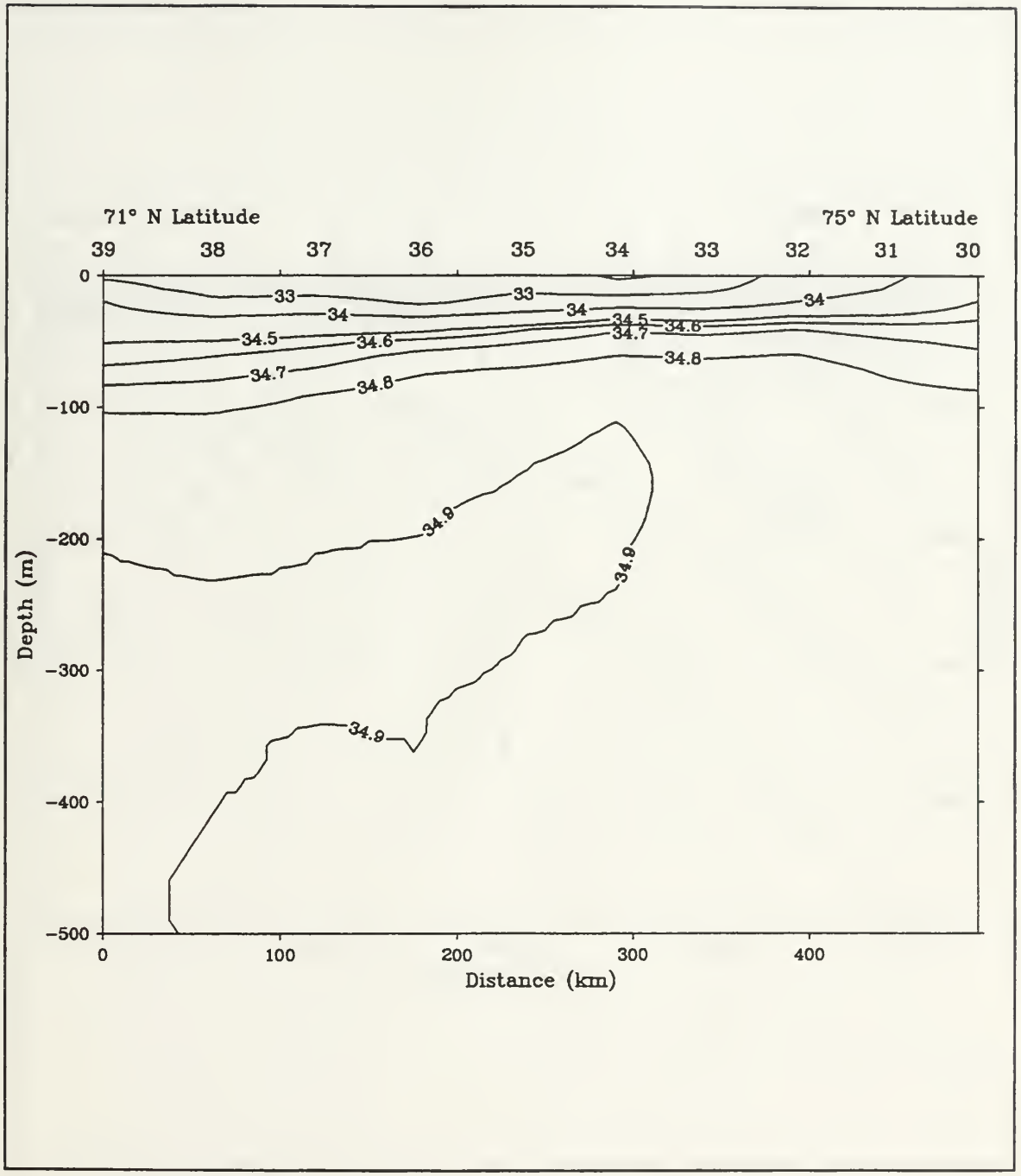

Figure 33. BARTLETT 89 salinity along Transect B (PSU). Similar to 1990 but without the separation of meander and throughput.

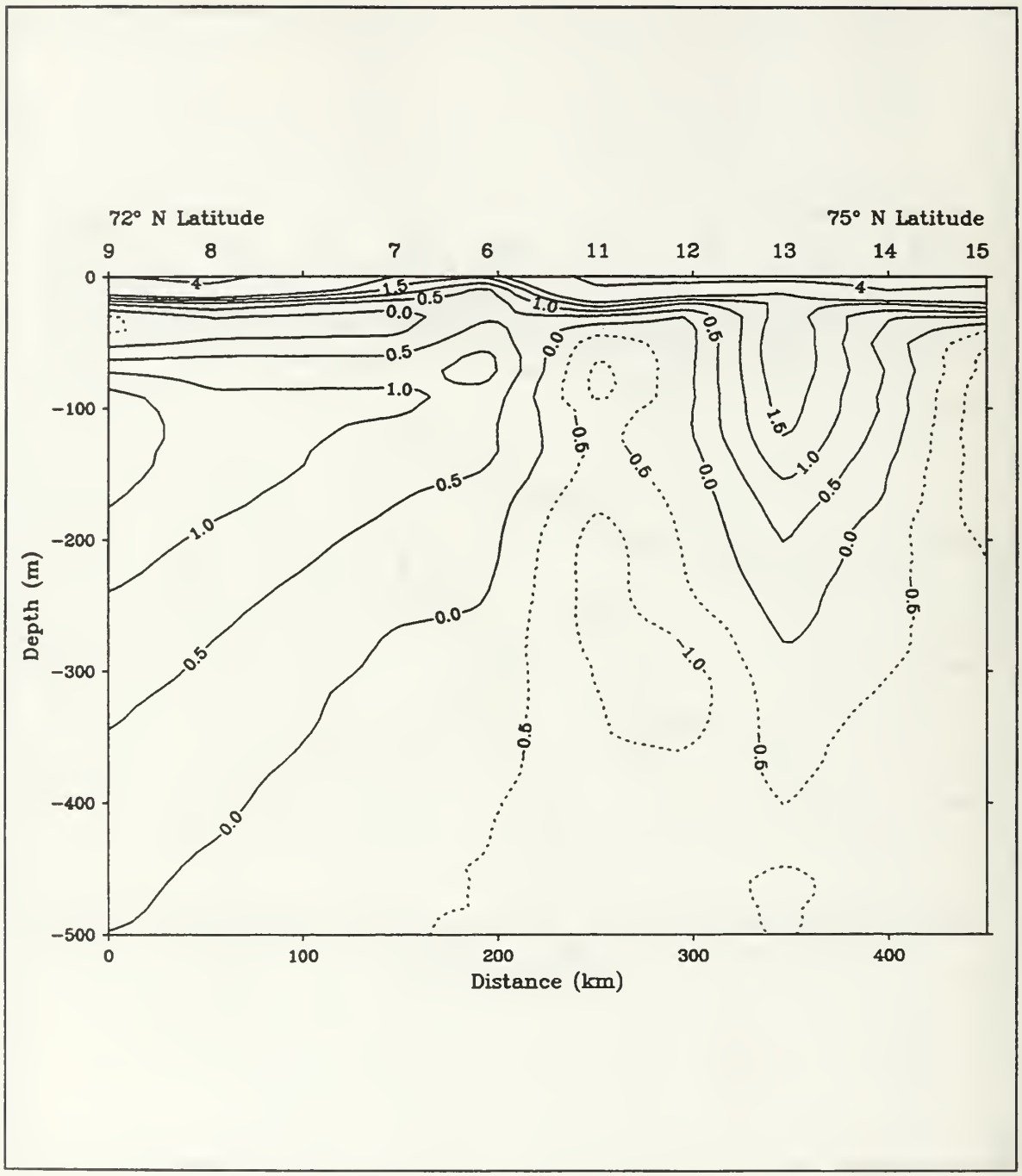

Figure 34. BARTLETT 90 temperature along Transect A (°C). This south to north section, closer to the EGC than Transect B, shows JMAtIW at 75 m at Station 6 with meander waters to the south. Colder waters of the GSG are located north of Station 11 but are interrupted by a pronounced eddy feature at Station 13. This warm-core eddy has likely been shed from the JMAtIW based on T-S characteristics.

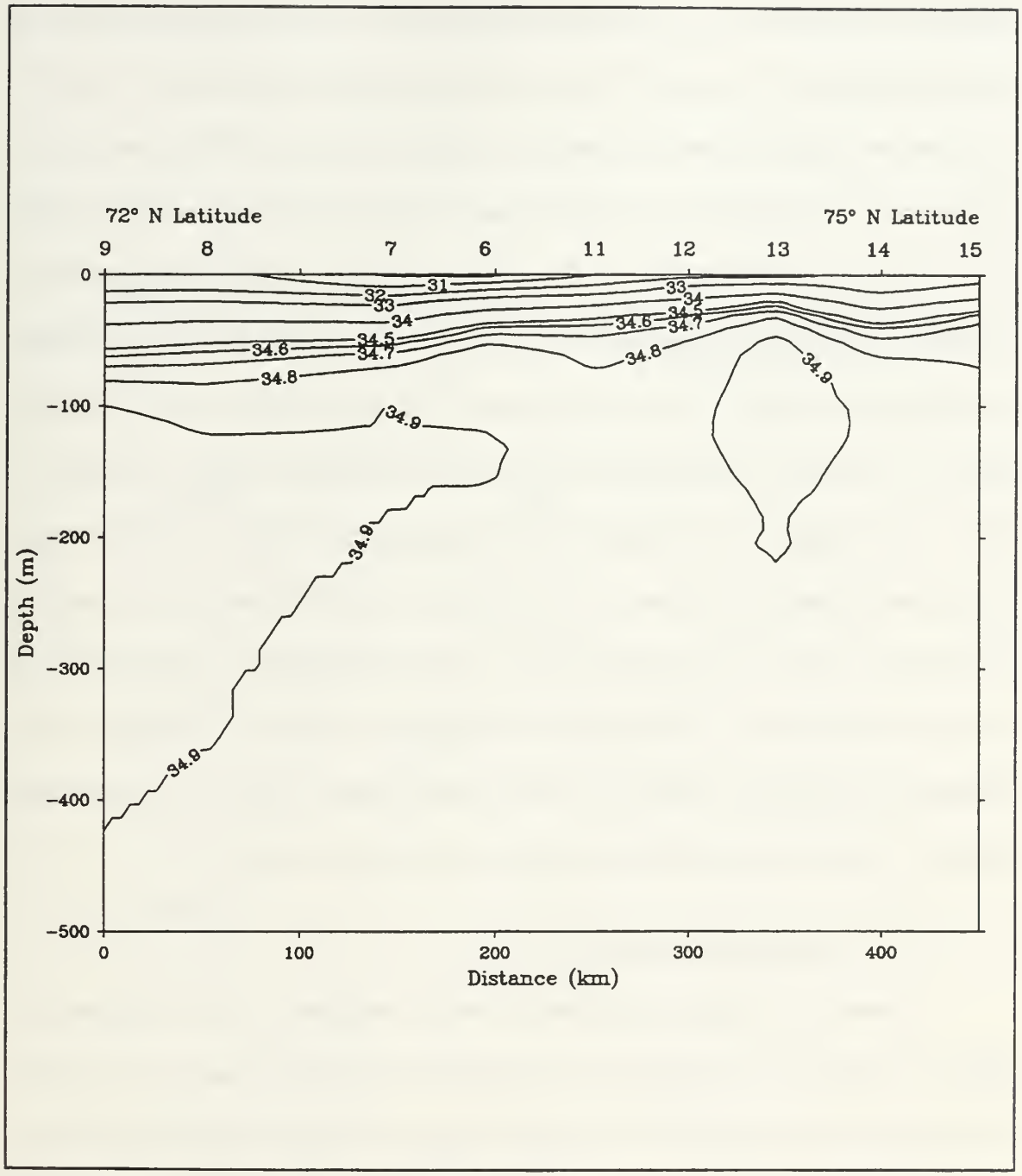

Figure 35. BARTLETT 90 salinity along Transect A (PSU). As in Transect B, salinities exceeding 34.9 PSU indicate JMAtIW from Station 6 southward. A similar salinity is present in the eddy at Station 13.

Based on a comparison of T-S characteristics at the eddy site with stations located in the throughput region, it is postulated that this warm-core eddy has been shed or "pinched off" from the JMAtIW. The eddy could also possibly indicate RAtIW advected into the region; however, the latter seems unlikely based on the distance from the EGC. Eddies are commonly found associated with the Arctic Frontal Zone (AFZ) to the east but no evidence presently exists for penetration of eddies of AFZ origin far into the GSG interior (*van Aken et al.*, 1995). The salinities associated with Transect A in 1990 are shown in Figure 35. Similar to Transect B, the salinities corresponding to JMAtIW exceed 34.9 PSU. The throughput is not distinctly visible. The eddy is clearly marked by a region of high salinity centered at about 120 m at Station 13. In 1989, Transect A (Figure 26) is identical in location to the 1990 Transect A. The vertical sections of temperature and salinity for Transect A in 1989 are shown in Figures 36 and 37, respectively. The temperature and salinity sections in 1989 are quite similar to the 1990 section along Transect A with the exception of the previously mentioned eddy in 1990.

2. Temperature Minimum Layer

In summer, a minimum temperature layer is established in the Greenland Sea region as a result of the warming of a nearly uniform winter PW surface layer from above by atmospheric heat input and to a slight degree from below by heat flux from the underlying warmer intermediate water (*Aagaard and Coachman,* 1968). In general, the temperature minimum, Tmin, is either at or near the bottom of the previous winter's depth of isothermal/haline penetrative convection, i.e., that convection driven by brine rejection

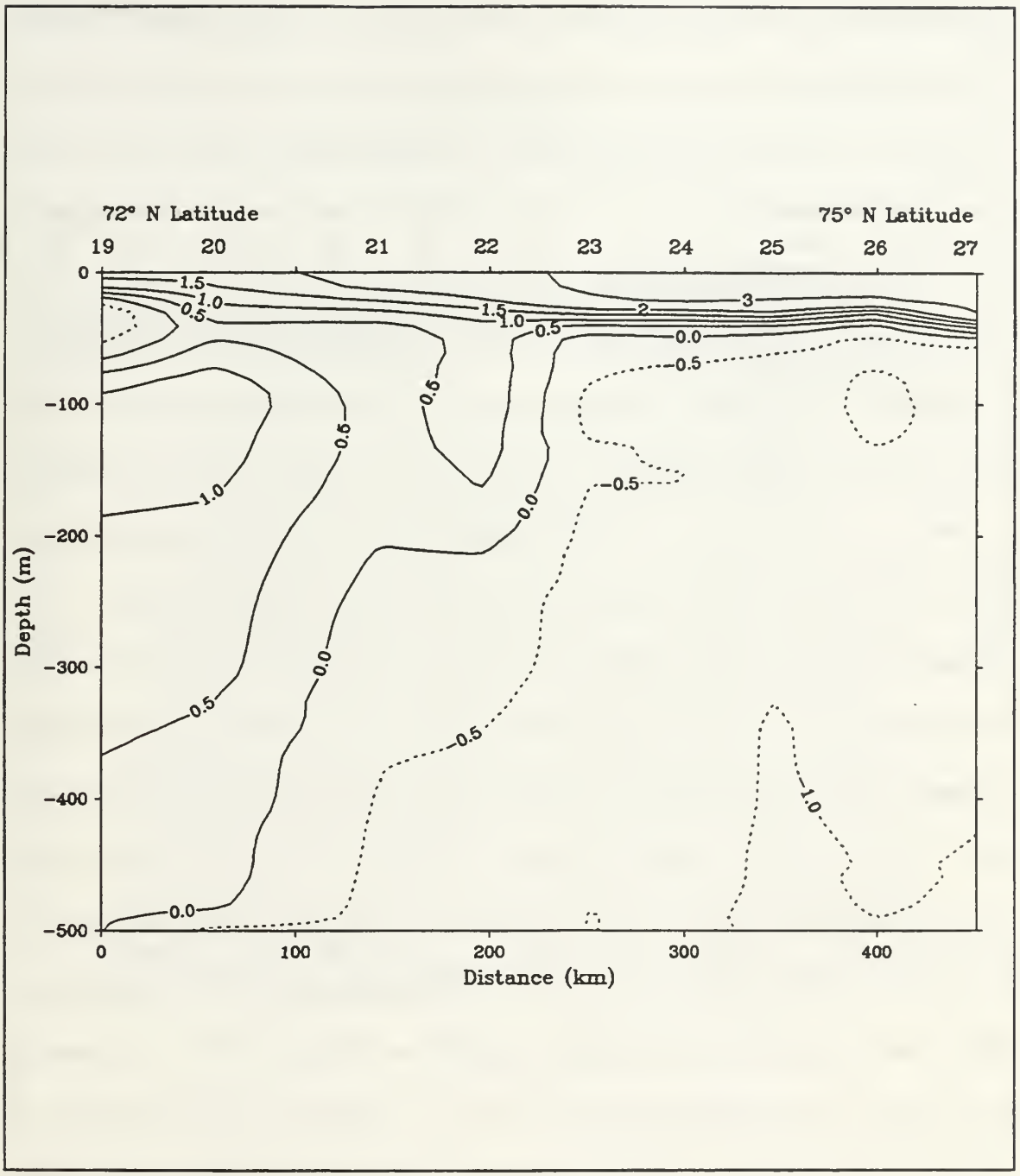

Figure 36. BARTLETT 89 temperature along Transect A (°C). Identical in position to 1990 Transect A, the JMC is seen south of Station 23 with colder waters of the GSG to the north. Except for the eddy, the section is quite similar to 1990.

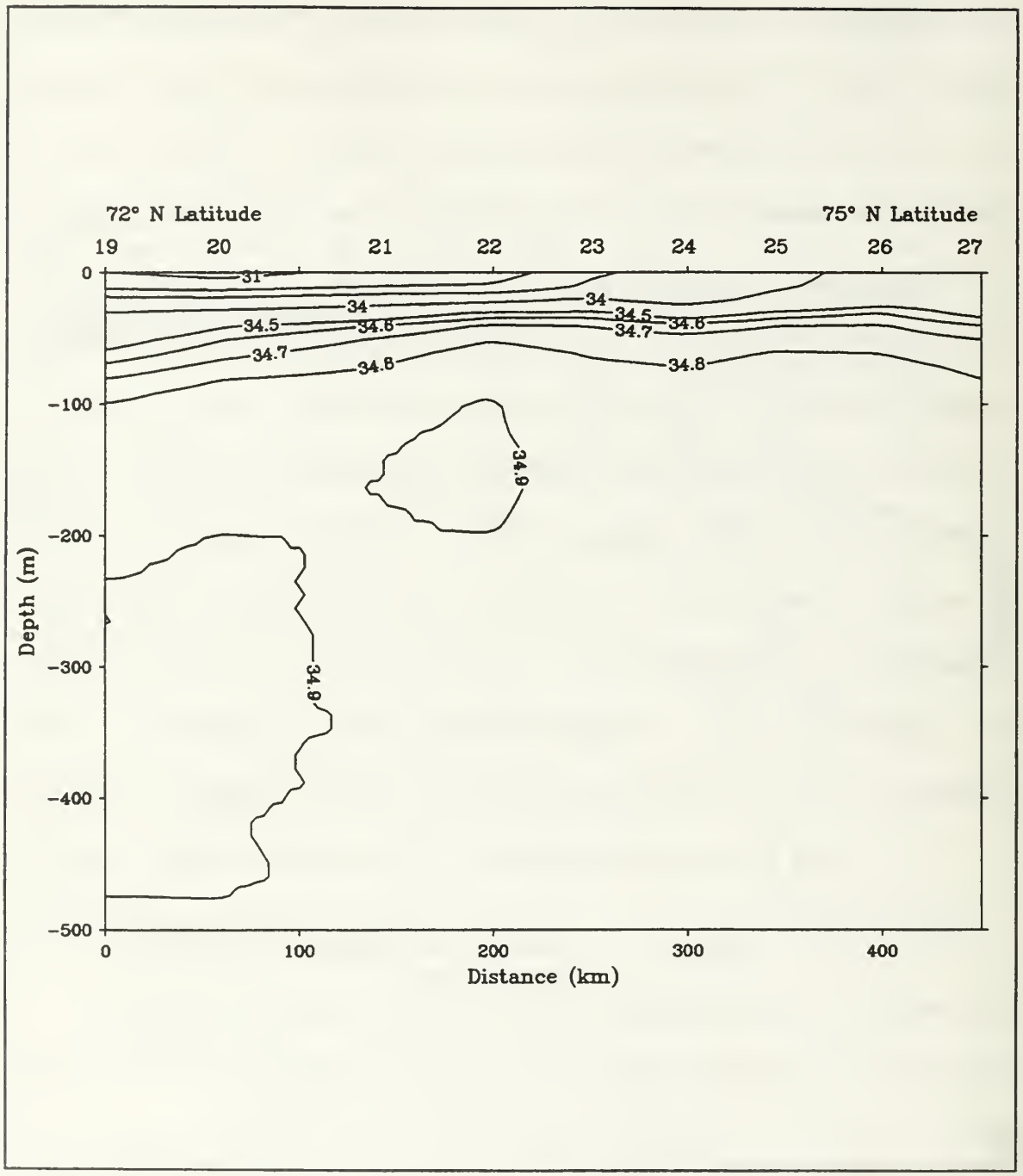

Figure 37. BARTLETT 89 salinity along Transect A (PSU). Similar to 1990 with JMAtIW salinities over 34.9 PSU south of Station 23.

from the freezing of sea ice. With the onset of melting, the surface warms, especially if it is ice free and exposed to the sun, thus leaving a temperature minimum between the surface and the warm water beneath the maximum depth of convection. The depth of Tmin is positively correlated with distance from the ice edge. Water beneath the ice canopy of the EGC holds the most fresh water and has the highest stability at the onset of freezing. Therefore, the depth of convective penetration is shallow. Water well out into the GSG has little fresh water content and has a relatively low stability, thus, convection is deeper, salinity is higher, and the temperature slightly lower due to the decreased freezing point of the higher-salinity water.

The 1990 summer expression of the above described processes can be seen in Figures 38 and 39. In Figure 38, the subsurface minimum temperature, shown in plan view, ranges from 0.5°C to -1.5°C with most values from 0°C to -0.6°C, now appreciably warmed since the freezing temperatures of winter. Extending eastward from the EGC, in the region from 71.5°N to 73.5°N, is a layer with a typical Tmin near -0.5°C which is termed Jan Mayen Polar Water (JMPW), a mixture of GPW and GArSW, and which represents the subsurface component of the JMC (*Blythe,* 1990). JMPW mixes with the warmer (1°C - 1.5°C) JMAtIW underlying it resulting in a comparatively warm Tmin. At about 75°N, Tmin in the GSG is -1.0°C or less due to mixing with the colder (0°C or less) GArIW beneath the Tmin level. The depth of Tmin for summer 1990 is shown in Figure 39. The 25 m and 50 m contour lines, extending east from the EGC, mark the general region where the majority of JMPW is encountered. The water in this region comes from under the ice; hence, Tmin is relatively shallow. The depth of Tmin is

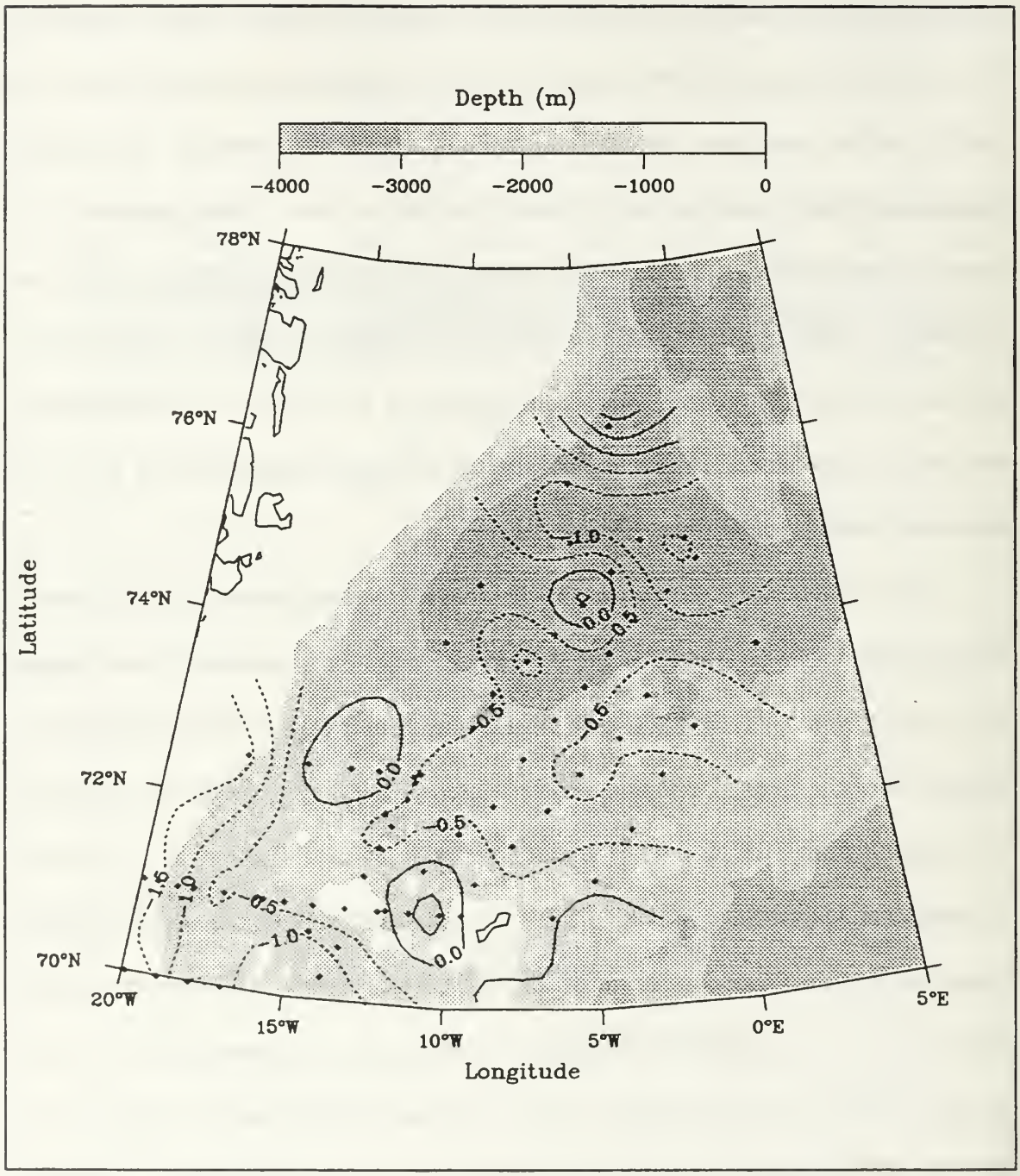

Figure 38. BARTLETT and BJARNI SÆMUNDSSON 90 contours of subsurface temperature minimum (Tmin) (°C). A subsurface temperature minimum occurs between the surface, warmed by insolation and intermediate waters. In the JMC region, Tmin occurs within a shallow subsurface layer of modified GPW termed Jan Mayen Polar Water (JMPW) having a typical Tmin value near -0.5°C.

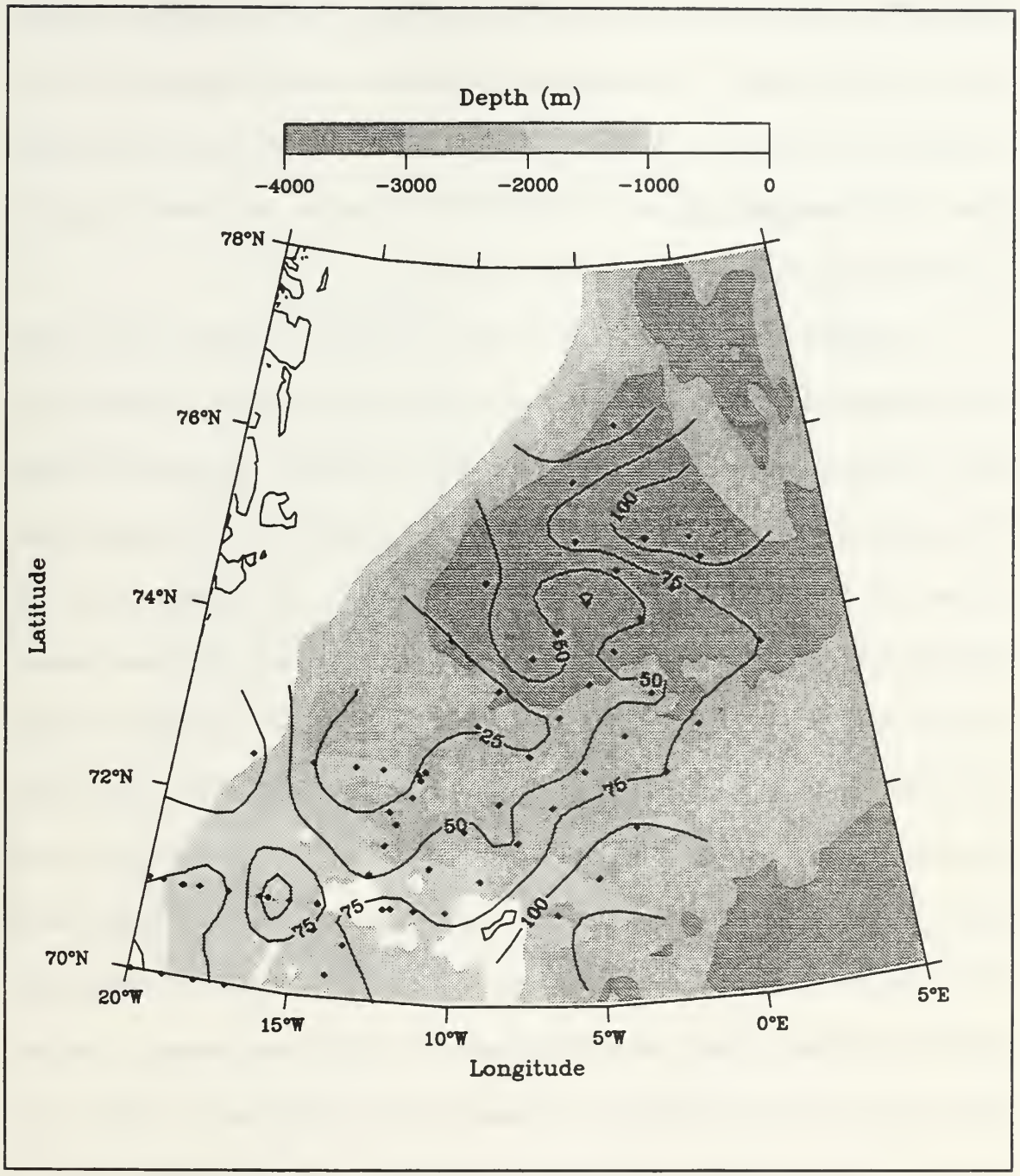

Figure 39. BARTLETT and BJARNI SÆMUNDSSON 90 depth of subsurface temperature minimum (Tmin) (m). The 25 and 50 m contour lines, extending east from the EGC, mark the region where the majority of JMPW is encountered. Tmin deepens to the east and north.

greatest in the north as the water of the GSG is more saline, has lower stability, and thus, deeper convection depths. Tmin deepens toward the east, centered along about 73°N, as this region is receiving a maximum of GSG water with the circulation of the throughput water. The corresponding figures for BARTLETT 90 data only are shown in Appendix B, Figures 9 and 10, and give much the same results.

In summer 1989, the Tmin values, shown in Figure 40, reveal a similar pattern when compared to Figure 38 for 1990. However, as expected due to the additional 30 days of insolation, the September 1989 Tmin values are slightly higher than in August 1990, commonly up to 0.5°C warmer in the waters north of 72.5°N. Likewise, the depth of Tmin for 1989, seen in Figure 41, is slightly deeper in the vicinity of the JMC compared to Figure 39 for 1990 but shallower elsewhere. The notable difference between 1989 and 1990 is the region of shallower Tmin represented by the 25 m contour in Figure 39 for 1990. *Budéus et al.* (1993) also noted the colder Tmin values in 1990 when comparing the July 1990 and June 1989 surveys of the POLARSTERN along a west to east transect at 74°45' N. They attribute the colder temperatures in the Tmin layer in the GSG during 1990 to a lack of deep convection during winter 1989-1990. This reduced depth of convection is likely due to an increase in the fresh water content of the near surface waters in winter 1989-90, i.e., increased stability (*Meincke et al.,* 1992). In the absence of deep convection, the negative atmospheric heat input during winter is distributed over only a small volume resulting in very cold temperatures in the Tmin layer. The reduced convection also reduces the amount of warm intermediate water entrained into the surface layer thus maintaining the relatively cold condition. The extent

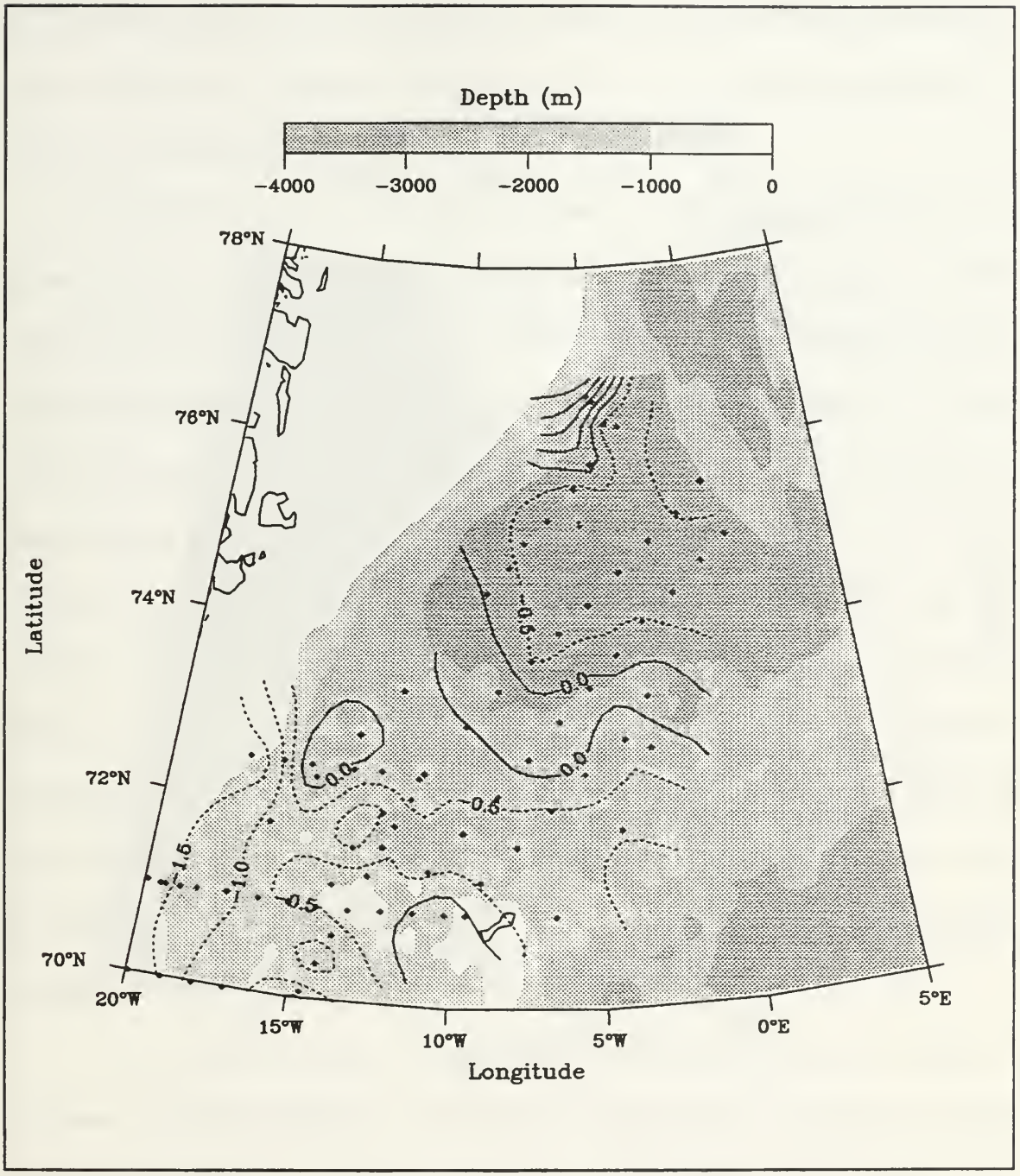

Figure 40. BARTLETT and BJARNI SÆMUNDSSON 89 contours of subsurface temperature minimum (Tmin) (°C). The Tmin contour patterns are similar to 1990 but values are generally higher by 0.5°C in the region north of 72.5°N due to a longer period of insolation by September compared to August.

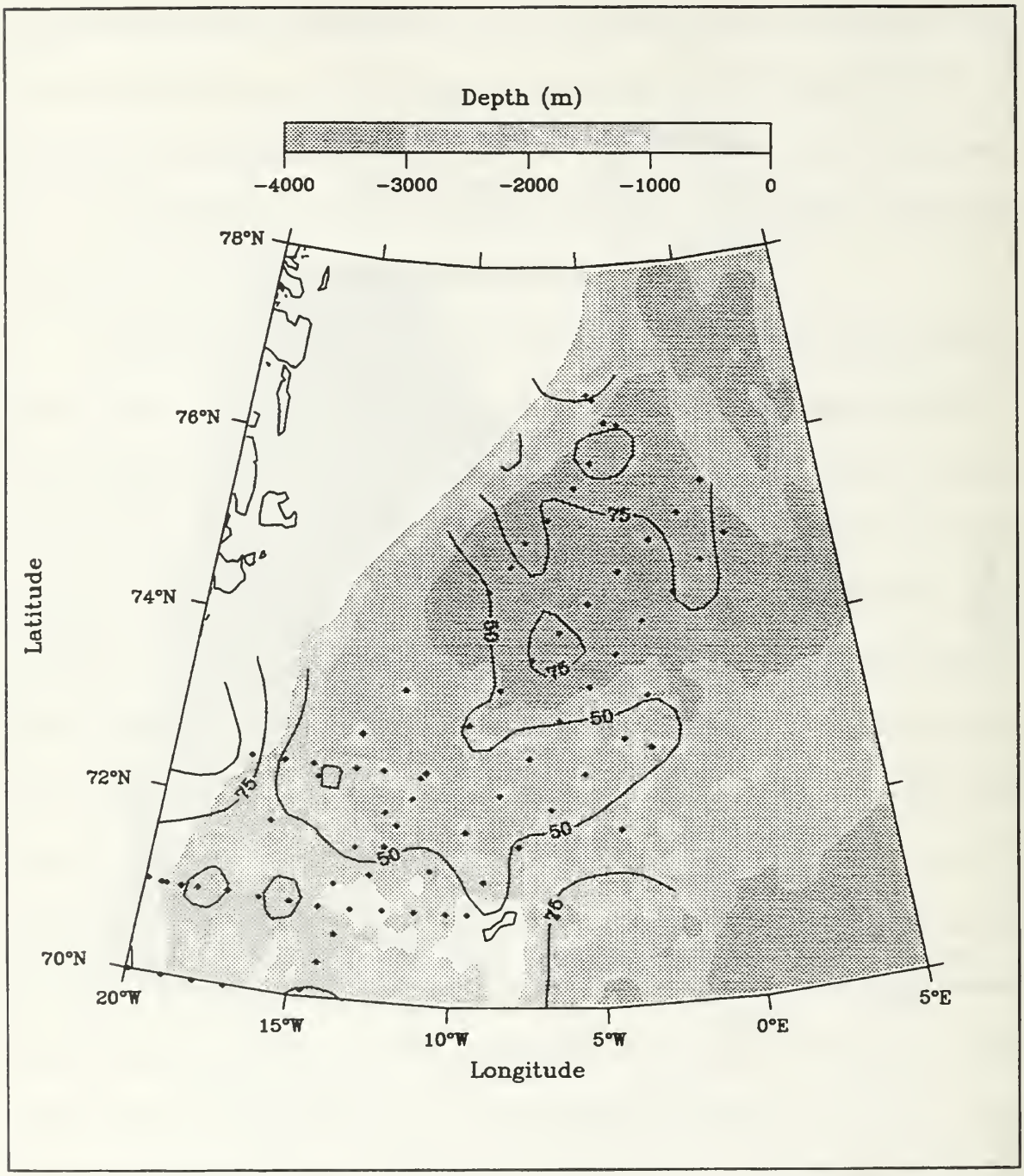

Figure 41. BARTLETT and BJARNI SÆMUNDSSON 89 depth of subsurface temperature minimum (Tmin) (m). The depth of Tmin for 1989 is slightly deeper in the vicinity of the JMC compared to 1990.

of this layer indicates the area excluded from deeper convection during the previous winter. *Budéus et al.* (1993) conclude that the depth of convection was approximately 250 m in 1990 and about 2200 m in 1989.

The Tmin values, seen in Figures 38 and 40, do not present the JMPW clearly; however, it can be seen in an analysis of temperature and salinity cross-sections which reveals a region of maximum expression of JMPW at about 72°N for 1990 with the cold Tmin layer gradually reverting to background properties from west to east. Vertical sections of temperature and salinity along Transect C (Figure 22) for 1990 are shown in Figures 42 and 43. In Figure 42, the subsurface layer of JMPW (< 0°C) is seen at 50 m at Station 9 in the west, deepening to the east as GSG water is encountered. Figure 43 shows the salinity along Transect C for 1990. While JMPW is not easily discerned in salinity (range: 34 to 34.7 PSU), Figure 43 reveals a pattern of higher surface salinity, decreased stability (lowered salinity gradient) with a subsurface deepening of isohalines toward the east. In both Figures 42 and 43, it is interesting to note the possible descent of JMAtIW into the mid-depths of the NAC at Station 43 with evidence of interleaving, indicative of mixing.

For 1989, the vertical sections of temperature and salinity for the region of maximum expression of JMPW, as determined by *Blythe* (1990), along Transect C (Figure 26) are shown in Figures 44 and 45, respectively. The temperature and salinity sections in 1989 are quite similar to the corresponding 1990 sections in Figures 42 and 43. JMPW is again centered in a shallow layer at about 50 m, shown in Figure 44. In 1989, Transect C, which is displaced to the west relative to Transect C for 1990, showed colder

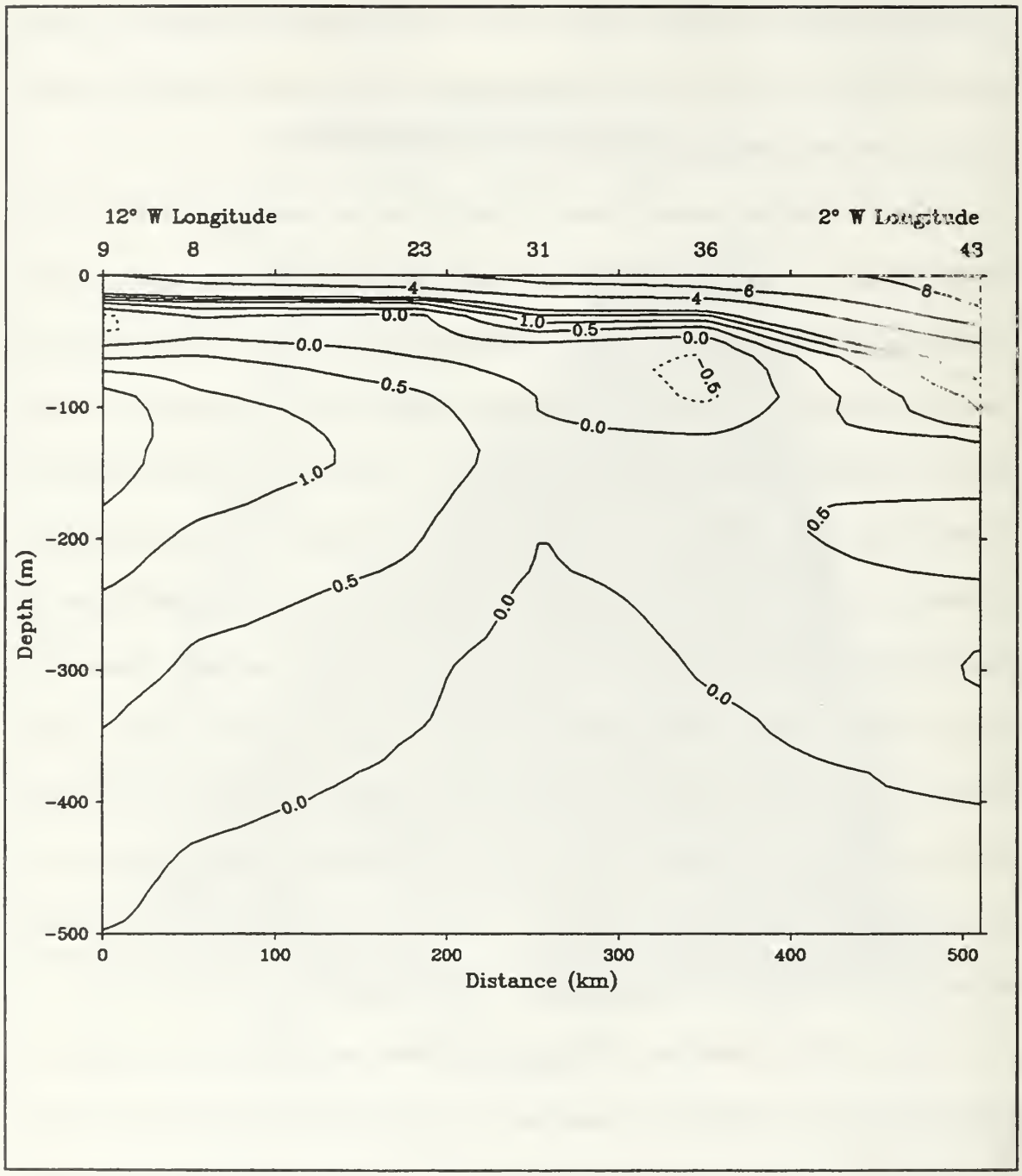

Figure 42. BARTLETT 90 temperature along Transect C (°C). This west to east tending section at about 72°N shows the maximum expression of JMPW for 1990 in a subsurface layer from 50 to 75 m with temperatures less than 0°C. JMPW deepens to the east as GSG is encountered.

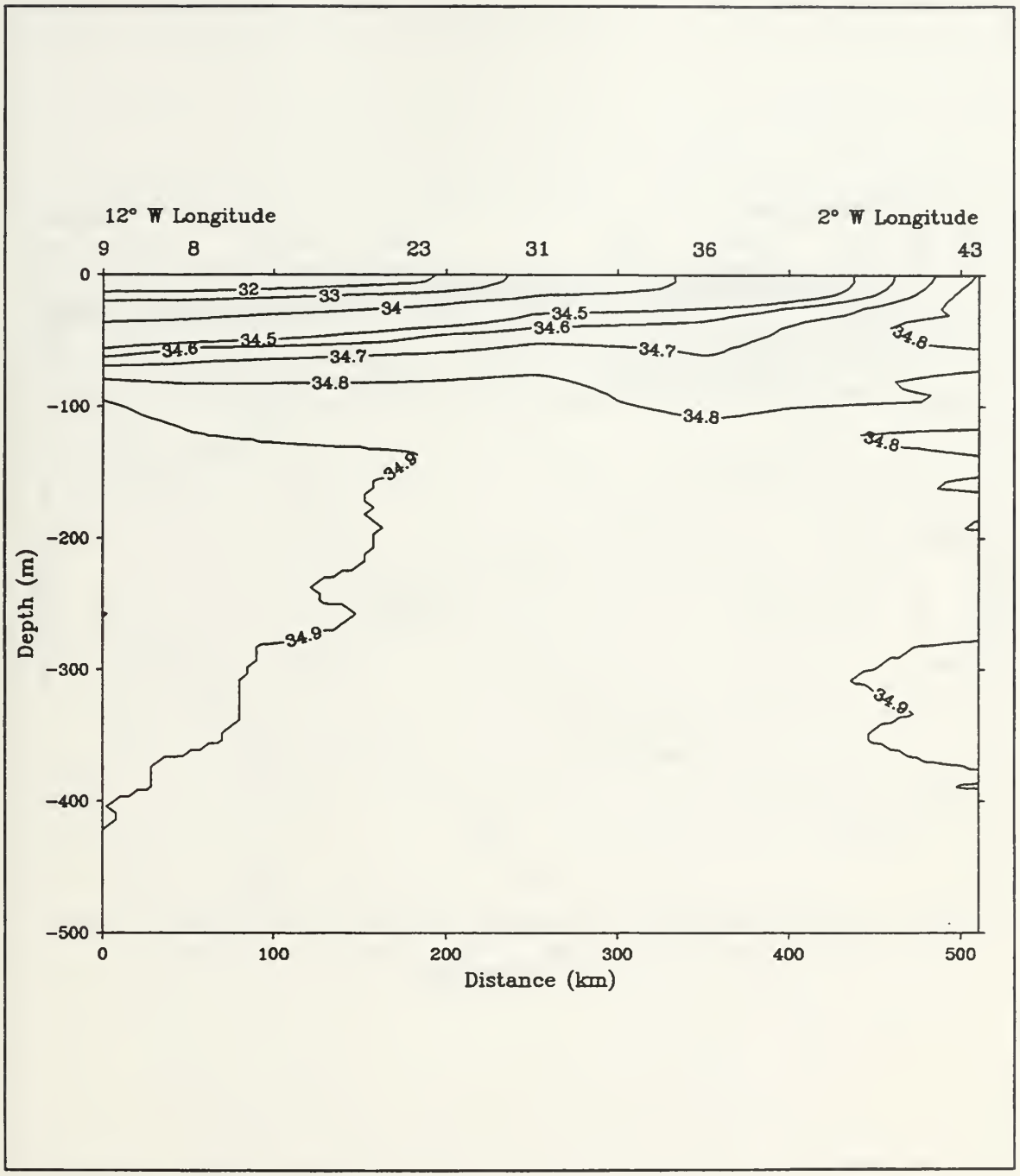

Figure 43. BARTLETT 90 salinity along Transect C (PSU). JMPW, with a salinity range from 34 to 34.7 PSU, is not readily apparent in a salinity section compared to temperature. There is a pattern of higher surface salinities and a subsurface deepening of isohalines toward the east. It is worth noting the possible descent of JMAtIW into the mid-depths of the NAC at Station 43 seen in this section.

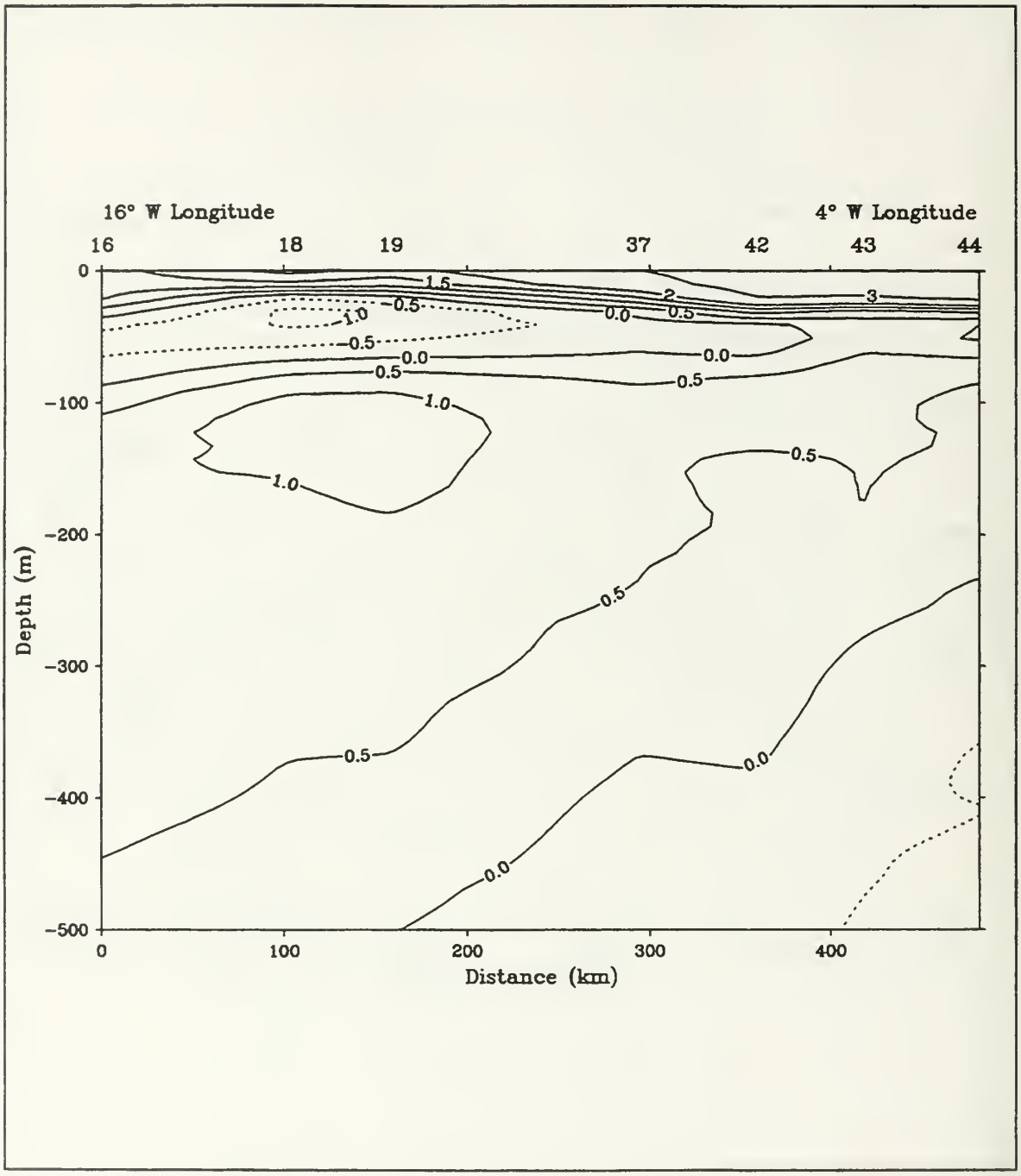

Figure 44. BARTLETT 89 temperature along Transect C (°C). This west to east section is similar in position to 1990 and exhibits the maximum expression of JMPW from 1989 data. Similar to 1990, JMPW is centered at 50 m in a shallow layer with temperature less than 0°C. This section, which is displaced to the west relative to Transect C for 1990, exhibits colder subsurface temperatures in the west due to closer proximity to the EGC and did not cross into the NAC in the east.

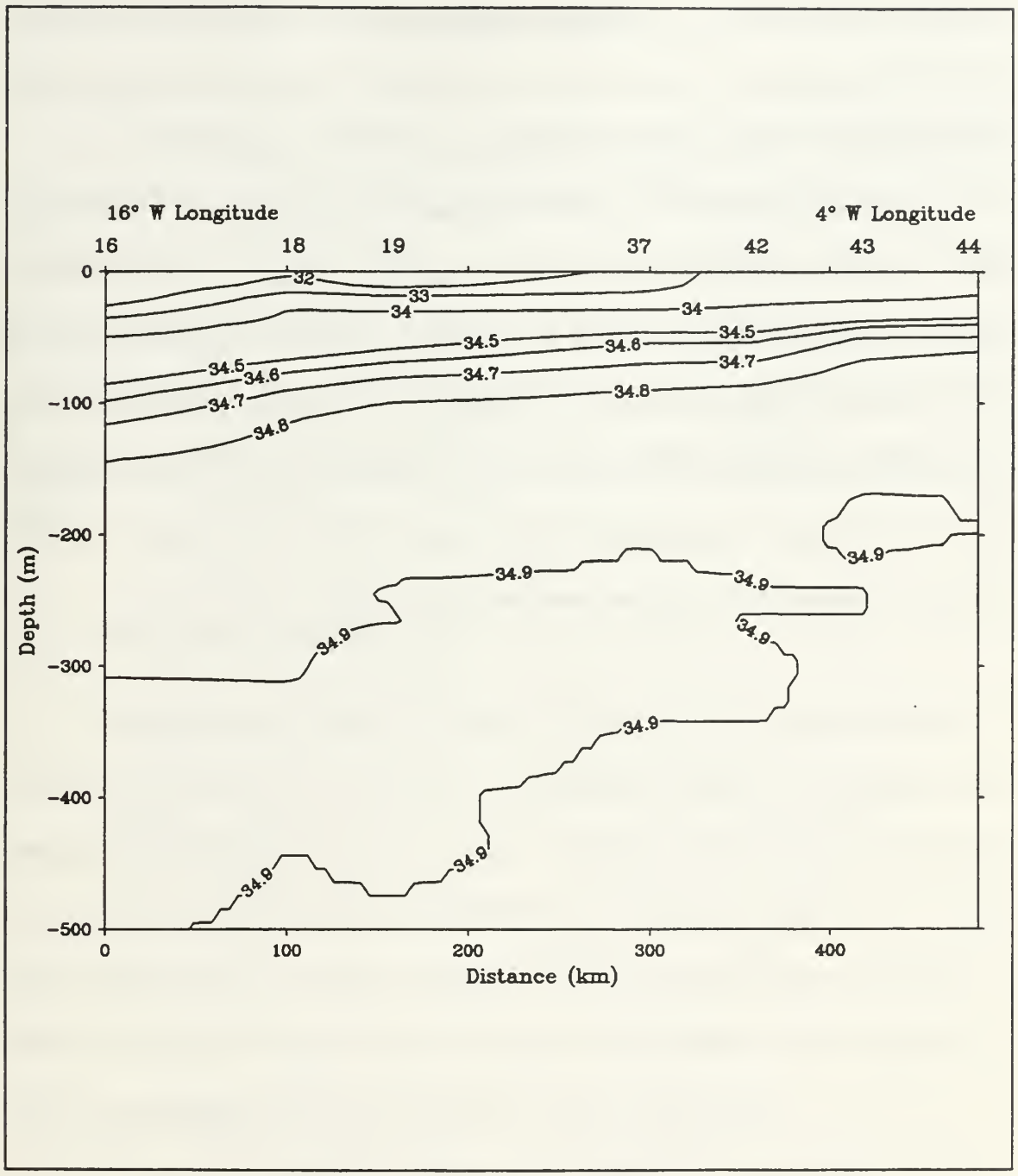

Figure 45. BARTLETT 89 salinity along Transect C (PSU). With a pattern similar to 1990, JMPW is not easily discernable from a salinity section. The isohalines do not extend east far enough to note the expected deepening as the NAC is encountered.

subsurface temperatures in the west due to closer proximity to the EGC and did not cross into the NAC in the east, as seen in Figure 44. In Figure 45, the isohalines do not extend far enough east to see the expected deepening as the NAC is encountered.

The JMPW of the JMC is typically displaced south of the warm JMAtIW of the JMC. This is a result of the position of the source water masses in which the GPW of the EGC is separated from the RAtIW by the EGPF. The GPW is located up to 60 km west of the RAtIW causing an apparent turning lag and southward displacement of the JMPW relative to the JMAtIW axis in the JMC (*Bourke et al.,* 1987). Such a portrayal is shown in Figure 1 where the cold surface portion of the JMC is south of the warm subsurface component (after *Koltermann and Lüthje,* 1989).

V. TRANSPORTS

The purpose of this Chapter is to present the results of the geostrophic analysis of transports in the upper water column during August 1990 in an effort to determine the percentage of the JMC that contributes to the meander and that portion which continues eastward as throughput. Perforce, calculations represent the baroclinic transports although various investigators have estimated that a significant portion of the total flow in the Greenland Sea region is barotropic (*Hopkins,* 1988; *Foldvik et al.,*1988; *Aagaard et al.*, 1991).

A. VOLUME TRANSPORT

The volume transport from the surface to 1000 m depth was calculated from the BARTLETT 90 baroclinic velocity field. Geostrophic velocities and transports were computed for the three vertical sections shown in Figure 46. The sections are based on sets of stations roughly normal to the dynamic height contours (Figures 8 and 9) and which represent input to the study region and output to the meander and to the GSG. In addition to the total volume transport through a section, transports were calculated for each of the predefined water masses (Table 1) evident in the section.

In Figure 46, Section 1, extending NE to SW for approximately 450 km, represents the input to the area from the EGC and GSG. Section 2 was selected as best representing water exiting the region to the south as the JMC meander while Section 3 includes water exiting the area as JMC throughput to the east to eventually complete the

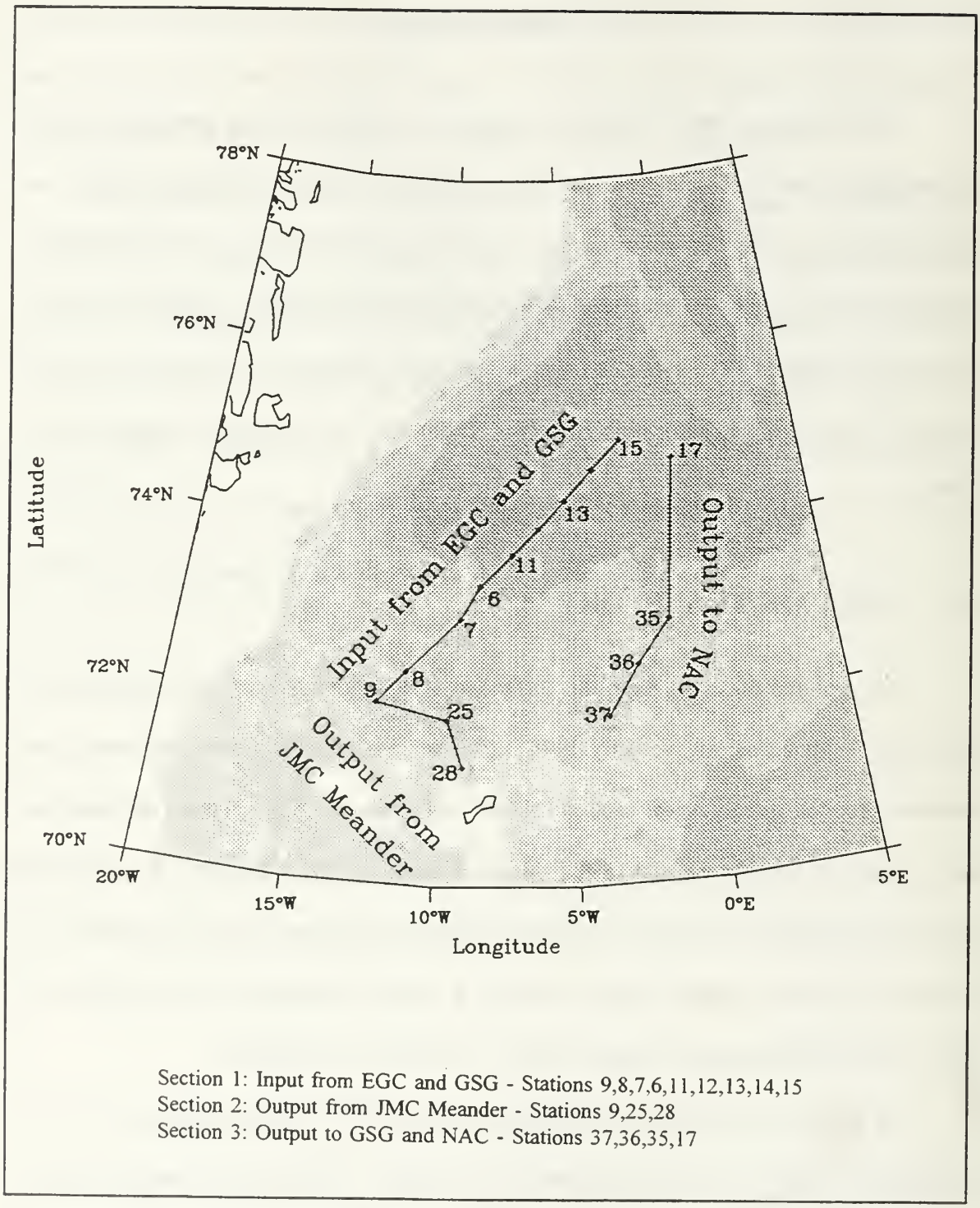

Section 1: Input from EGC and GSG - Stations 9,8,7,6,11,12,13,14,15
Section 2: Output from JMC Meander - Stations 9,25,28
Section 3: Output to GSG and NAC - Stations 37,36,35,17

Figure 46. BARTLETT 90 station sections used to determine baroclinic transports. Selections are based on sets of stations located roughly normal to dynamic height contours.

GSG or join the NAC. The vertical sections of Section 1, 2 and 3 are shown in Figures 47, 48 and 49, respectively, with the water mass types and associated transports noted on the diagrams. The sections are truncated at 500 m to give more detail in the upper layers, however, transport values to 1000 m are shown. Fresh water and heat transports will be discussed later. In the following discussion, the water masses will be grouped into two categories, surface or upper layer water and lower layer water. Surface or upper layer water extends to 100 m or less and includes GPW, JMPW, GArSW, ASW and NAtSW. Lower layer water extends from bottom of the surface layer (~ 100 m) to 1000 m and includes JMAtIW, GArIW, NArIW and GSDW. Based on the different flow patterns seen in the dynamic height contours at the surface (10 m) relative to 1000 m (Figure 8) and the contours at 100 m relative to 1000 m (Figure 9), it was felt necessary to compute upper and lower layer transports separately as well as total values.

In Figure 47, the total baroclinic volume transport into the region from the EGC and GSG is 1.45 Sv with 0.28 Sv from the surface layer (GPW + JMPW + GArSW + ASW) and 1.17 Sv from the lower layer. JMC water masses including GSDW, evident in the southern half of the section as discussed previously (see Figure 35), make up about 80% of the transport through Section 1. The warm-core eddy feature at Station 13, rotating anti-cyclonically, causes a small westward transport in the overall eastward flow. The volume transport associated with Section 2, the southward output to the JMC meander, is shown in Figure 48. The total transport is 0.39 Sv with 0.11 Sv from the surface water and 0.28 Sv from the lower layer. In Section 3, the eastward output through the region to the GSG and NAC, the total volume transport is 0.99 Sv with 0.14

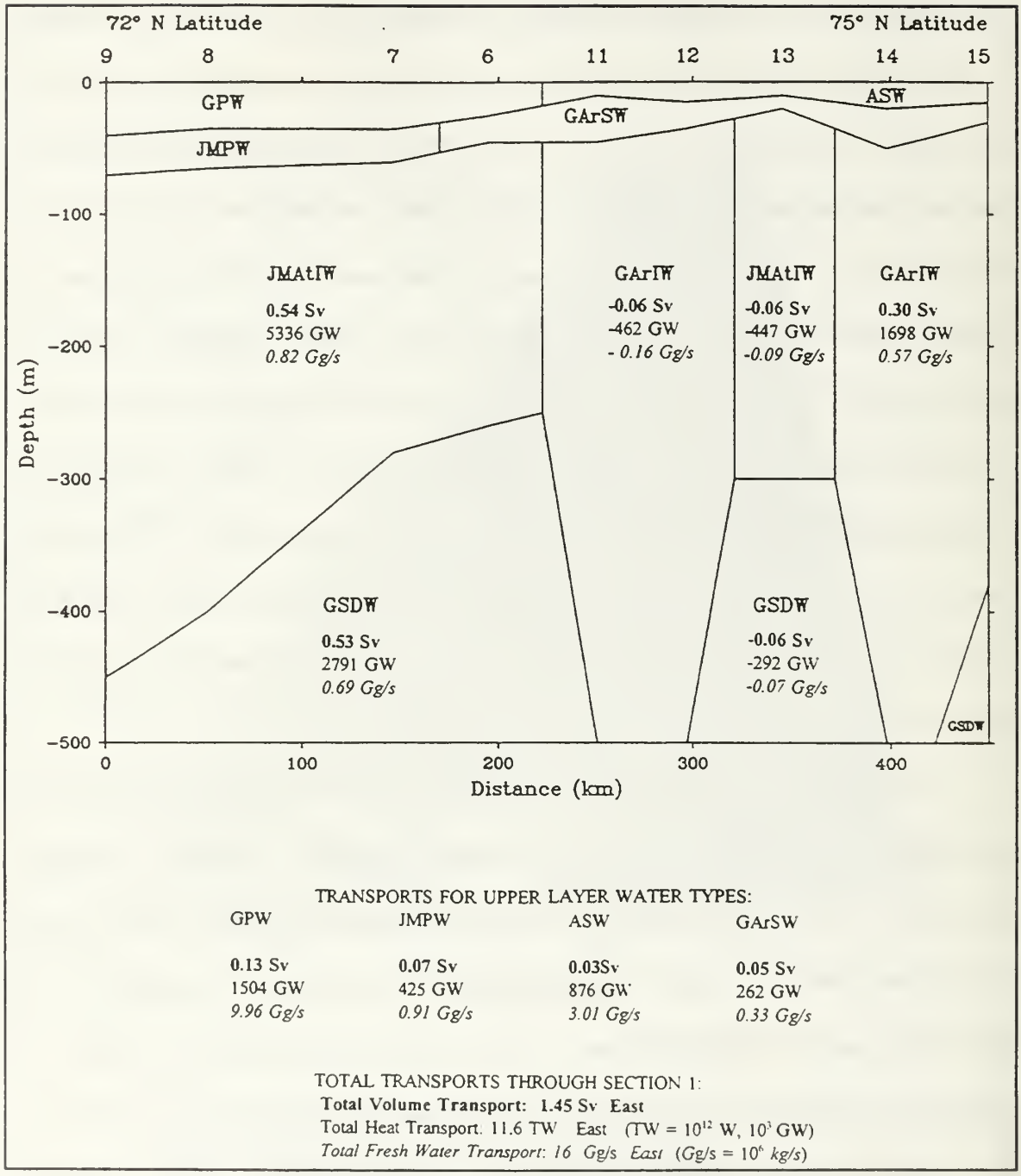

Figure 47. Baroclinic transports through Section 1 representing input from the EGC and GSG. Values for individual water mass types and for the total section are listed. Volume Transports (Sv) in bold type; Heat Transports (GW) in normal type; Fresh Water Transports (Gg/s) in italics. Positive values indicate eastward flow. GSDW transports are listed to 1000 m.

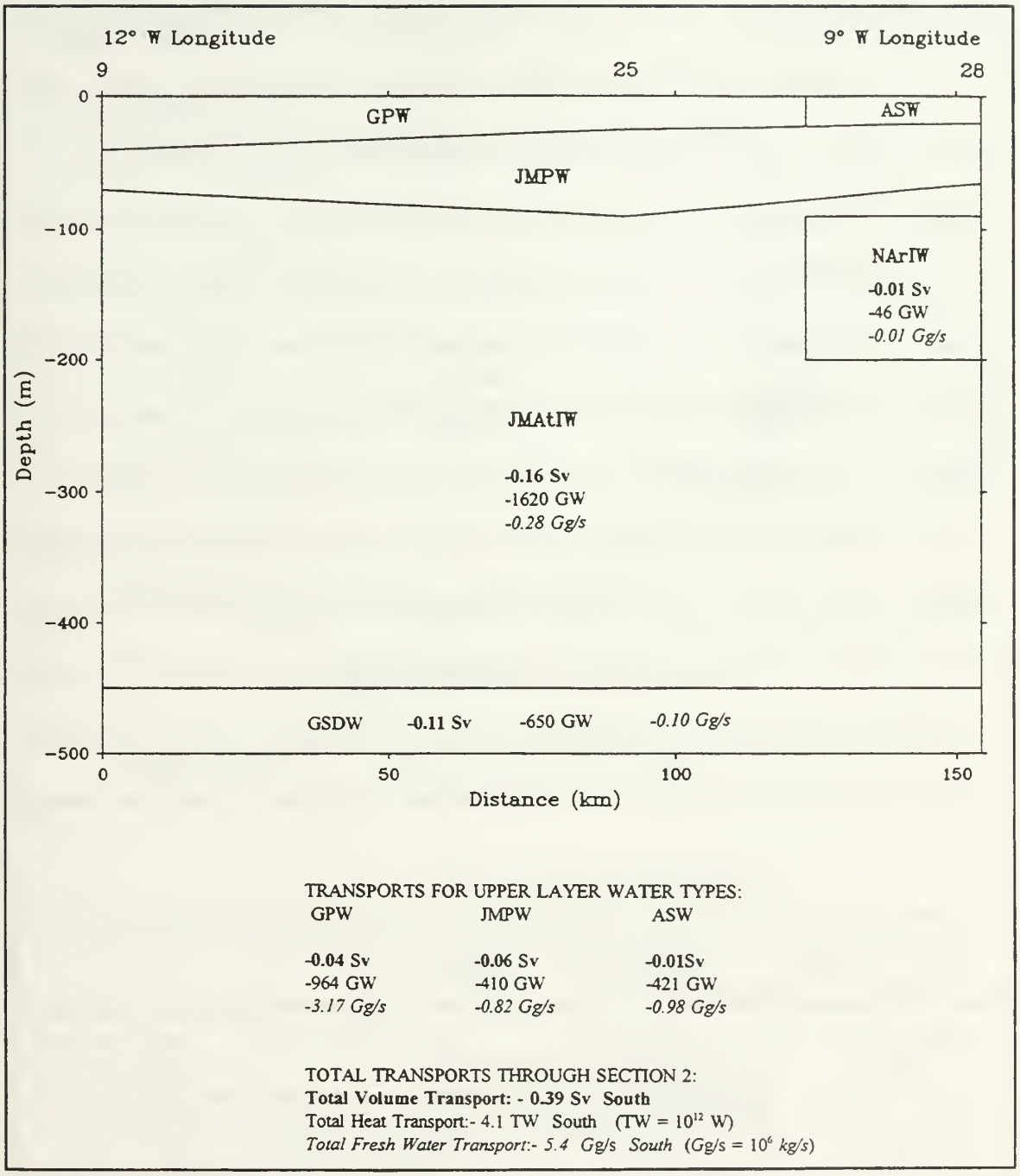

Figure 48. Baroclinic transports through Section 2 representing output of the JMC meander to the EGC. Values for individual water mass types and for the total section are listed. Volume Transports (Sv) in bold type; Heat Transports (GW) in normal type; Fresh Water Transports (Gg/s) in italics. Positive values indicate eastward flow. GSDW transports are listed to 1000 m.

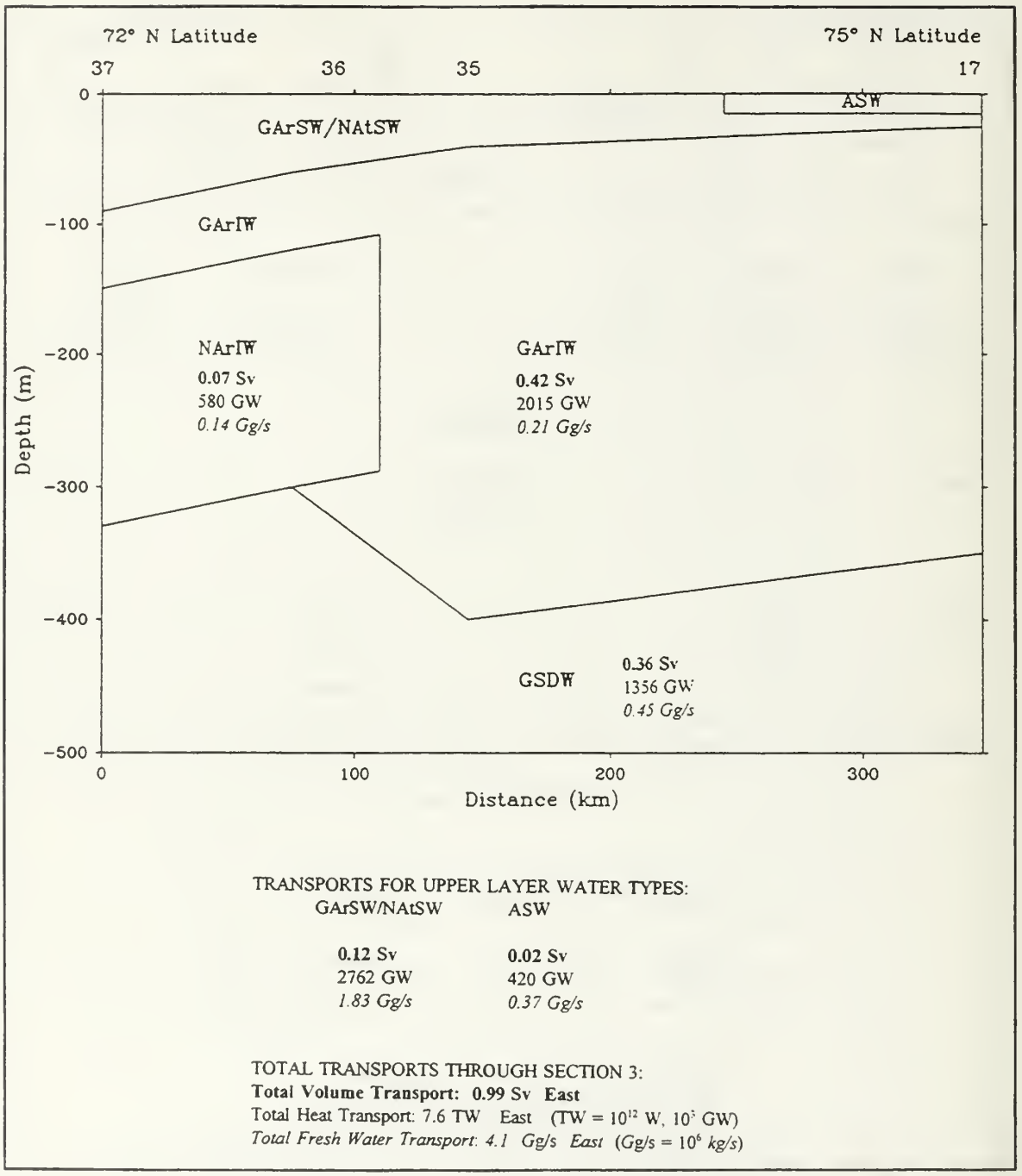

Figure 49. Baroclinic transports through Section 3 representing output of the JMC throughput to the GSG and NAC. Values for individual water mass types and for the total section are listed. Volume Transports (Sv) in bold type; Heat Transports (GW) in normal type; Fresh Water Transports (Gg/s) in italics. Positive values indicate eastward flow. GSDW transports are listed to 1000 m.

Sv from the surface and 0.85 Sv from the lower layer as seen in Figure 49. The water of NAC origin seen in Sections 2 and 3 was also noted by *Blythe* (1990).

The results of the volume transport calculations are as follows: Based on output from Sections 2 and 3, about 44% of the upper layer and 25% of the lower layer flow contributes to the JMC meander. The remainder, roughly 56% from the surface and 75% from the lower layer, continues eastward as throughput. For the total water column to 1000 m, about 28% of the input exits to the south as meander with 72% exiting eastward as throughput. Note that the input and combined output transports are not identical because the chosen sections do not form a closed system. The results, listed in Table 2, are similar to the BARTLETT 89 transports. *Blythe* (1990) estimated a total baroclinic flow of 2 Sv into the region with half of the upper layer exiting as meander and half exiting eastward. He did not specifically distinguish between upper and lower layer regimes but noted the meander dissipated below 100 m and flow became more easterly.

Depth Range	Section 1: Input EGC and GSG	Section 2: Output JMC Meander	Section 3: Output JMC Throughput
Surface Layer (0 to ~ 100 m)	0.28 Sv East	0.11 Sv South (44%)	0.14 Sv East (56%)
Lower Layer (~100 to 1000 m)	1.17 Sv East	0.28 Sv South (25%)	0.85 Sv East (75%)
Total (0 - 1000 m)	1.45 Sv East	0.39 Sv South (28%)	0.99 Sv East (72%)

Table 2. August 1990 Baroclinic Volume Transport Calculations (Sv or 10^6 m^3/s) and Associated Percentages for Three Sections Representing Input and Output for the Jan Mayen Current.

In Table 2, the percentages of meander and throughput transports in the surface and lower layers quantify the relationships seen in the dynamic height patterns discussed in the previous chapter. There it was shown that roughly half of the surface layer contributed to the meander (Figure 8) with the meander becoming much less prominent in the lower layer (Figure 9).

It is interesting to note that the volume of JMAtIW present in the 1989 study region was about twice the amount in 1990; roughly 14,000 km^3 in 1989 and 7,000 km^3 in 1990. This is a notable change, probably of interannual time scale.

The geostrophic velocities associated with Section 1 for 1990 are shown in Figure 50. The higher upper-layer flows are centered at Station 6 with near-surface speeds of 3 cm/s slowing to 1 cm/s at about 300 m. The division between meander and throughput occurs near Station 11. For identical stations in 1989, Figure 51 shows similar speeds, centered about 100 km south of the 1990 position, encompassing a wider area and extending to nearly 500 m, perhaps corresponding to the greater volume of JMAtIW present in 1989. The velocities for Sections 2 and 3 (not presented) are on the order of 1 - 2 cm/s near the surface with values less than 1 cm/s below 50 m.

The baroclinic velocities and volume transports determined for 1990 appear to be reasonable when compared to other studies, though there is a scarcity of information in the JMC region. *Bourke et al.* (1988) estimated 3.1 Sv for the baroclinic transport of the EGC. *Foldvik et al.* (1988) estimated the net southward volume transport by the EGC at 79°N above 700 m to be 3 Sv with mean speeds of 10 - 30 cm/s based on year-long current meter measurements. At 71° N, the baroclinic volume transports between

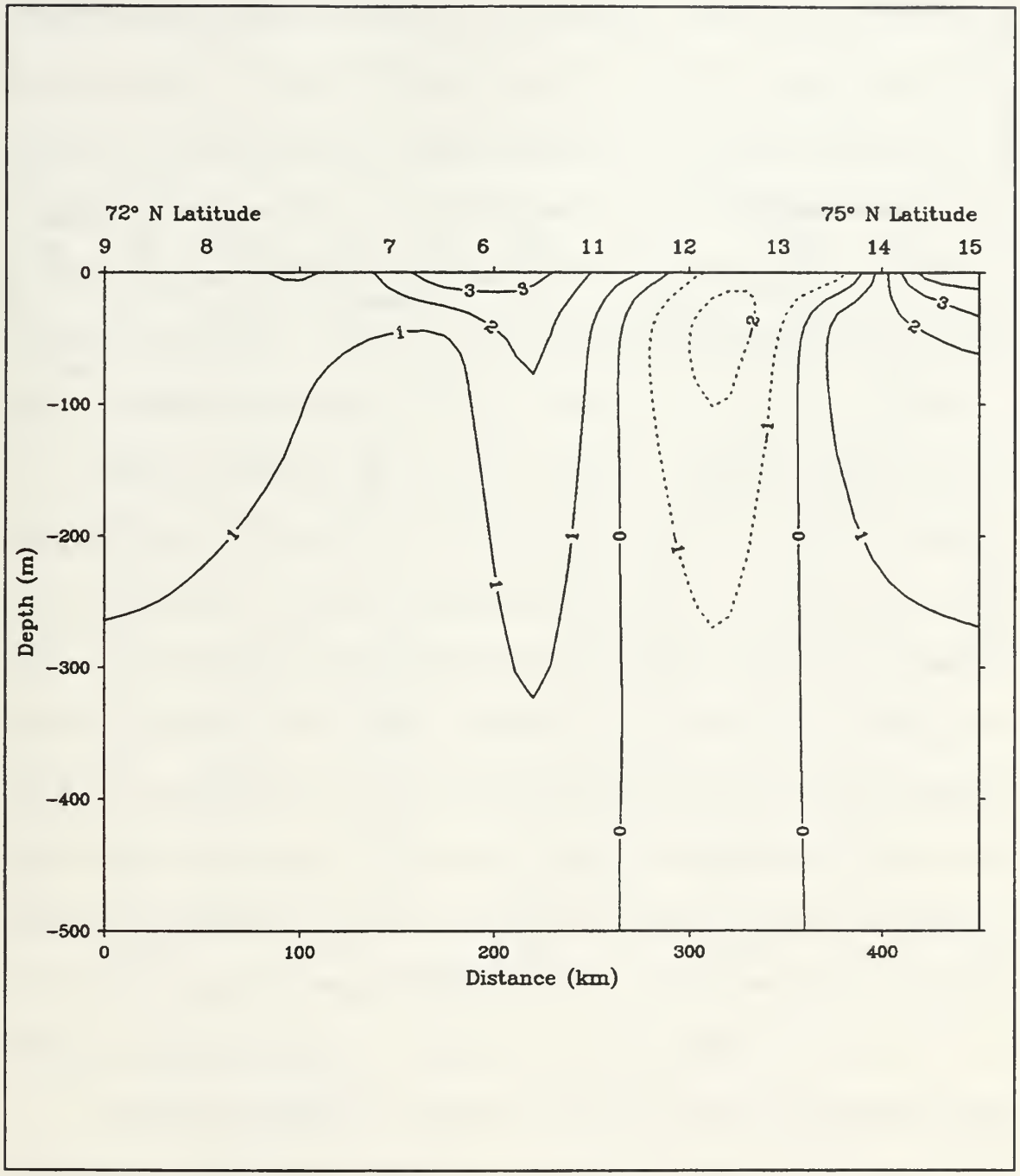

Figure 50. BARTLETT 90 geostrophic velocities (cm/s) along Section 1. Positive values indicate southeasterly flow. The area of northwesterly flow at Station 13 is associated with an eddy.

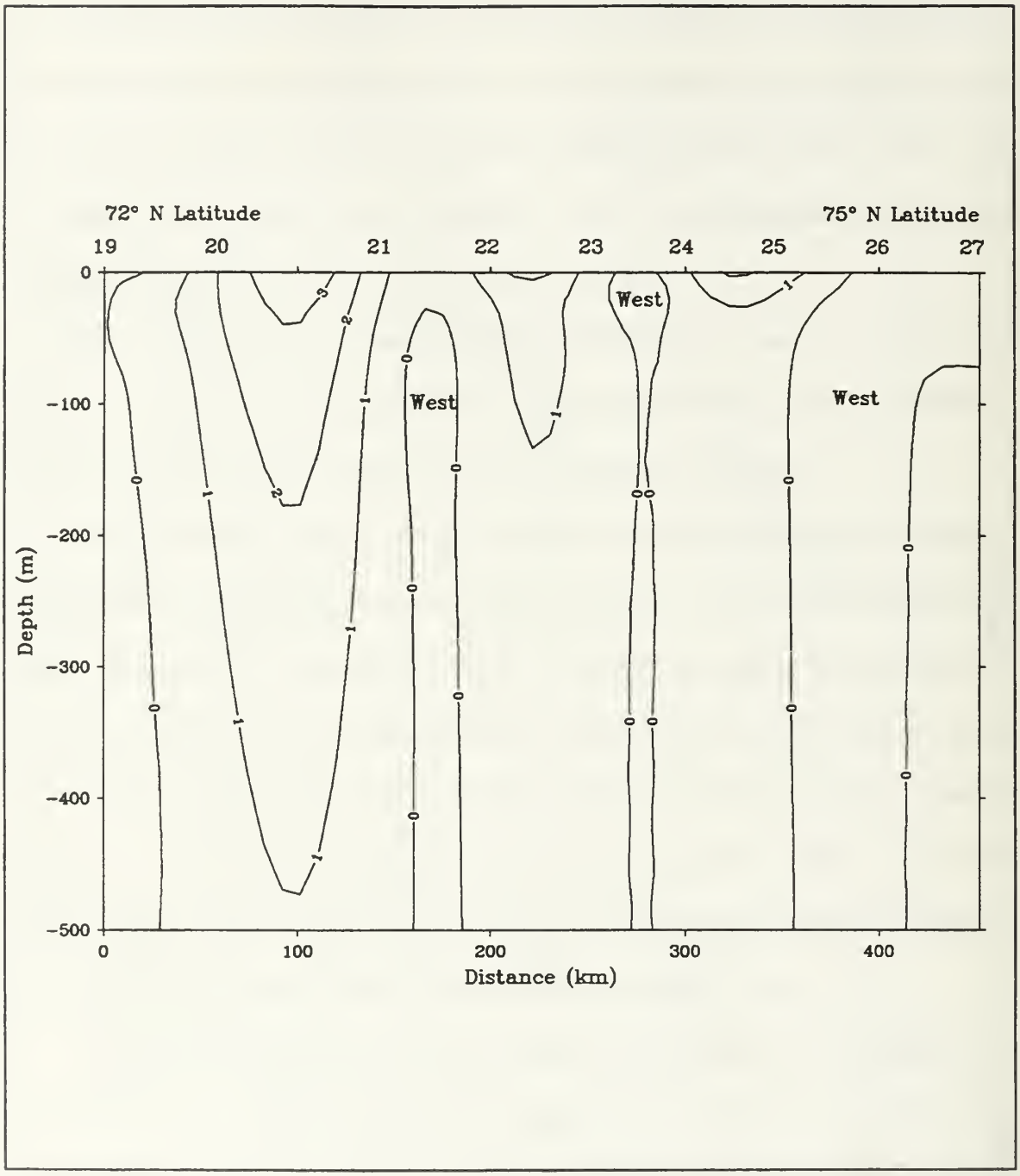

Figure 51. BARTLETT 89 geostrophic velocities (cm/s) along a section of stations most closely matched to BARTLETT 90 Section 1. Positive values indicate eastward flow.

Greenland and Jan Mayen averaged 2.3 Sv southward from 1987 to 1991 with a maximum value of 3 Sv in 1990 (*Mortensen et al.,* 1992). *Aagaard et al.* (1991) estimated year-long mean current meter velocities at 73°N, 8°W to be from 6 cm/s at 80 m depth to 5.4 cm/s at 2570 m. The slight change in speed with depth is indicative of the barotropic nature of the flow. Thus the net total southward transport of the EGC is estimated to be of order 3 - 4 Sv at 75°N with ~ 1 Sv exiting eastward as JMC throughput and 2 - 3 Sv transported south at 71°N.

Lagrangian drifting SOFAR floats, analyzed by *McCarren* (1991), yield an additional measure of the total flow and the complicated trajectory of the JMC. However, since the BARTLETT baroclinic measurements and the float measurements were not carried out simultaneously at the same location, the difference between the flows are not an accurate measure of the barotropic component. One particular float, MZ86, had the best signal strength and was tracked for the longest period of time. Launched in the West Spitsbergen Current in April 1989 (Figure 5), Float MZ86 was acoustically tracked until August 1990 following a course shown in Figure 52. Initially ballasted to drift at 200 m and allowed to creep to a maximum depth of 500 m, the float was transported by three different current regimes shown on Figure 52 as Legs 1, 2, and 3.

In September 1989, MZ86 was tracked on Leg 1 moving south through the center of the Boreas Basin with an average speed of 17 cm/s. In mid-October 1989, the float approached the Greenland continental shelf at about 77°N (Leg 2) with increased speeds averaging 28 cm/s at approximately 400 m depth. The baroclinic flow at this depth in September 1984 was found to be less than 2 cm/s (*Bourke et al.,* 1987). From late

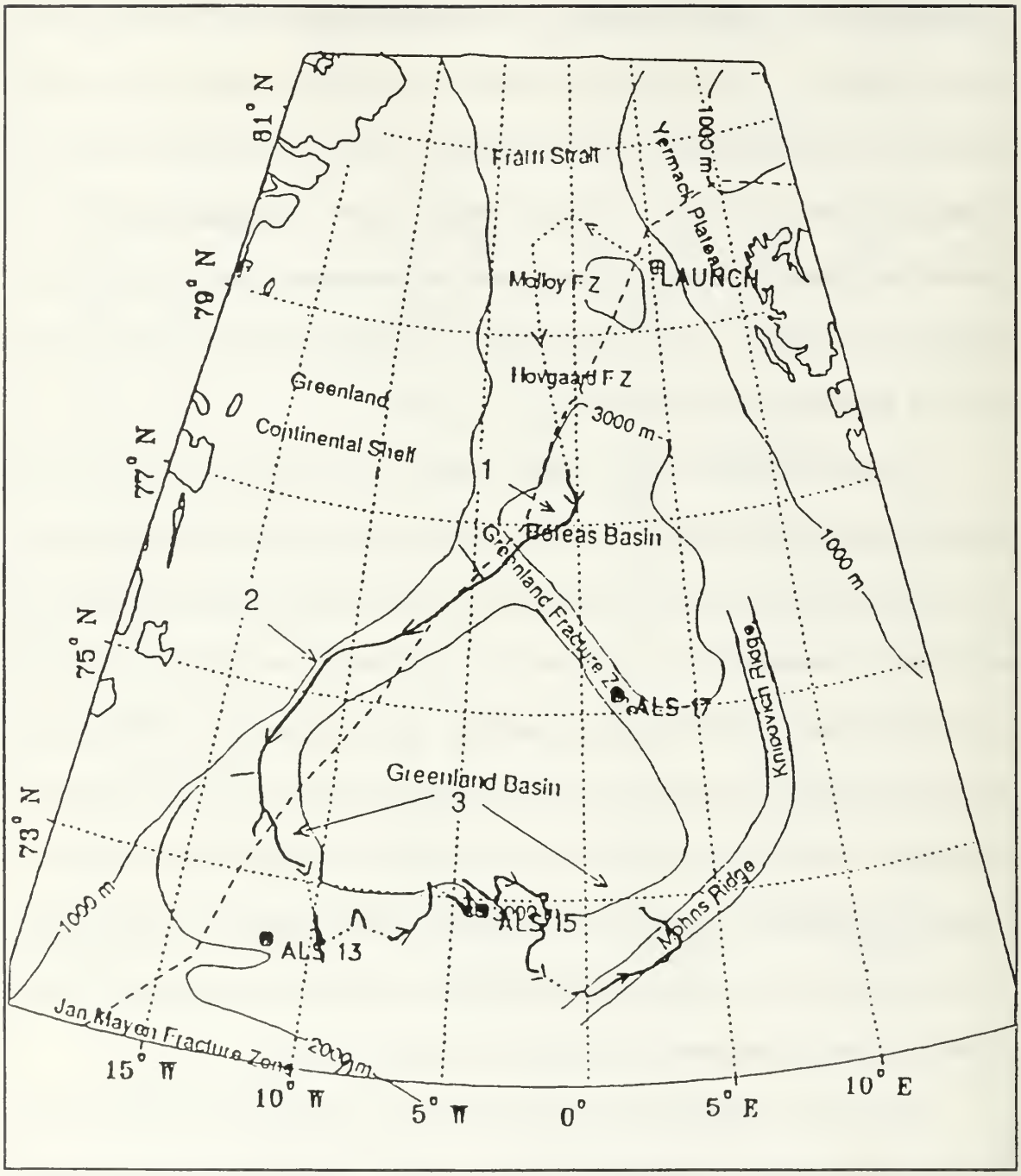

Figure 52. Trajectory of float MZ86. The float was transported by 3 current regimes shown as Legs 1, 2 and 3. Leg 1: MZ86 averaged speeds of 17 cm/s. Leg 2: MZ86 increased speed to an average of 28 cm/s. Leg 3: After turning eastward, MZ86 slowed to 3 to 5 cm/s (from *McCarren,* 1991).

October 1989 to August 1990, MZ86 was tracked making a slow turn to the east near 74°N and meandering across the southern margin of the Greenland Basin (Leg 3) at an average speed of 3 - 5 cm/s. During Leg 3, MZ86 was embedded in JMAtIW and exhibited maximum velocities of 20 cm/s or more. The float was captured in various eddy-like features along the course, eventually turning northeast at 72.5°N apparently to merge with the NAC.

In another drifter study, *Poulain et al.* (1996) analyzed the trajectories of 107 satellite-tracked drifters drogued to 15 m from June 1991 to August 1993. The majority of drifters were in the eastern regions of the Nordic Seas so that the East Greenland Current and Greenland Basin were not well sampled due to ice coverage and deployment strategy; however, the few drifters deployed in the vicinity of the JMC do give evidence of the surface meander at about 73°N.

A recent, state-of-the-art modeling study of the circulation of the Nordic Seas and Arctic Ocean yields additional information on the total flow field in the JMC region. The vector-parallel model used for the simulations, described in detail by *Parsons* (1995), is based on the Semtner-Chervin General Circulation Model (GCM) with a free-surface and modifications for the Nordic and Arctic regions, such as an improved equation of state for colder temperatures. The high resolution simulation model achieves 1/6° horizontal resolution (~ 18 km in latitude) in 30 vertical levels. The vertical layers vary in thickness, from 20 m near the surface to 200 m at depths beyond 700 m. High-frequency forcing is provided by monthly temperature and salinity fields over unsmoothed topography from *Levitus* (1994) data and 3-day period winds from the European Center for Medium Range

Weather Forecasting (ECMWF).

Model results of the annual mean velocity during 1992 in the JMC region were generously provided by *W. Maslowski (personal communication,* 1996). These results are indicative of the long term mean velocity field (ice is not included) with seasonality averaged out; however, small interannual variability in the mean picture should be anticipated. The model circulation patterns for the near-surface (0 - 45 m) and mid-depth (180 - 440 m) layers (not shown) are generally similar to the 1989 and 1990 BARTLETT summer results. The model output shows the JMC as partly an anticyclonic meander in the seaward portion of the EGC, somewhat more pronounced in the near-surface layer. Total flow speeds from the model in the upper layer vary from ~ 5 cm/s as the JMC throughput progresses eastward to ~ 1 cm /s nearer the NAC. Values from 3 - 4 cm/s occur in the JMC meander region. Similar to the 1990 surface layer transports (Table 2), it appears about 50% of the JMC flow contributes to the meander with 50% exiting to the east as throughput. In the mid-depth layer, the throughput velocities are similar to the upper layer while the meander speeds are slower at ~ 1 - 2 cm/s. The model results indicate about 60% of the JMC exits eastward with 40% exiting as meander in the mid-depth layer. By comparison, the August 1990 lower layer results (Table 2) indicate 75% of the JMC is throughput with 25% as meander. Considering that the 1990 results are based on summer baroclinic transports in a single layer from 100 to 1000 m, these apparent differences are not unreasonable. As previously stated, *Blythe* (1990) estimated that half of the JMC upper layer exited as meander and half as throughput during September 1989.

B. FRESH WATER AND HEAT TRANSPORTS

As discussed by *Blythe* (1990), the fresh water budget is of importance to vertical circulation at high latitude centers of convection such as the GSG. The liquid fresh water transport into the BARTLETT 90 survey region was calculated for the three sections shown in Figure 46 from the baroclinic flow field using a reference salinity for the Nordic Seas of 34.93 (after *Aagaard and Carmack,* 1989). Approximately 16 x 10^6 kg/s of fresh water enters the region eastward through Section 1 (Figure 47) while 5.4 x 10^6 kg/s exits to the south in the JMC meander (Figure 48). Another 4.1 x 10^6 kg/s exits eastward to the GSG and NAC through Section 3 (Figure 49) leaving 6.5 x10^6 kg/s to accumulate in the survey area. As expected, the large majority of fresh water transport is associated with the upper layer water masses. Thus, about 33% of the input fresh water transport exits to the south via the JMC meander, another 26% exits to the east, and 41% remains in the study region. For 1989, *Blythe* (1990) determined that about half of the input fresh water exited south via the meander with one third retained in the survey area.

A rough comparison can be made between the total fresh water available in the EGC and the portion which becomes involved in the JMC. *Aagaard and Carmack* (1989) estimated that annually 3950 km^3 of fresh water as liquid and ice flows southward from the Arctic Ocean in the EGC. Thus, using the BARTLETT 90 transports stated above, about 347 km^3 (~ 9%) of fresh water annually is input to the JMC from the EGC with about 170 km^3 (~ 4%) of the total annually available quantity of fresh water in the EGC involved in the JMC meander and 205 km^3 (~ 5%) retained in the study region. This

compares to 389 km^3 (~ 10%) of the yearly quantity contributing to the meander in 1989, over twice the amount in 1990, with 290 km^3 (~ 7%) remaining in the survey area (*Blythe,* 1990). It is important to note that caution must be used when comparing results between BARTLETT 90 and 89 data due to the differences in station sections. For instance, the BARTLETT 89 section representing input to the region was approximately 100 km west of the 1990 position.

Calculations for the heat transport through the region using a reference temperature of -1.8°C are again based on the input and output values shown in Figures 47, 48, and 49. For the 1990 data, an overall net loss rate of 0.1×10^{12} W results which can be considered essentially zero relative to the size of the area. Therefore, an advective heat balance seemed to exist at the time of the survey which was also found in the 1989 data.

VI. CONCLUSIONS

This study reports on the analysis of a hydrographic survey conducted in the vicinity of the Jan Mayen Current (JMC) in August 1990 aboard the USNS BARTLETT. The findings are compared to a similar survey performed in September 1989, analyzed by *Blythe* (1990), to verify phenomena and demonstrate interannual changes.

In the 1990 summer, as in 1989, the JMC contains both a portion of the East Greenland Current (EGC) flowing eastward to close the Greenland Sea Gyre (GSG) and an anticyclonic meander in the EGC flow north of Jan Mayen. Centered at about 73°N, the current is associated with two water masses: Jan Mayen Polar Water (JMPW) and Jan Mayen Atlantic Intermediate Water (JMAtIW). Below the seasonal surface layer, a subsurface layer of cold, moderately saline JMPW (modified Greenland Polar Water) is typically found at ~ 50 m depth. The warm, saline JMAtIW (modified Return Atlantic Intermediate Water) occurs in a layer between 50 to 400 m, typically at ~ 100 m, and is displaced north, about 100 km, of the JMPW layer due to the more easterly position of the Return Atlantic Intermediate Water before the turn of the southward-flowing East Greenland Current to the east. The course of the JMC clearly responds to underlying topographic features indicating the dominant barotropic nature of the flow, though its contribution was not quantitatively determined in this study.

The surface waters were warmer by 1 - 3°C over the study area and fresher by 1 - 2 PSU in the meander region in August 1990 compared to September 1989. This is likely a seasonal response as September typically exhibits cooler temperatures than mid-

summer with a lesser rate of inflow of fresh water to the GSG (*Pawlowicz*, 1995). As expected, the subsurface minimum temperature, Tmin, which is associated with the JMPW layer in the JMC, was colder by ~ 0.5°C and shallower by up to 25 m in the JMC region during August 1990 compared to September 1989 as expected due to the additional insolation and mixing in September. In addition to seasonal effects, *Budéus et al.* (1993) attribute the colder temperatures in the Tmin layer in the GSG during 1990 to a lack of deep convection during winter 1989-1990. JMAtIW, distinguishable by a temperature maximum, Tmax, occupied roughly half the volume in August 1990 that it encompassed in 1989. Baroclinic velocities for summers 1990 and 1989 are similar with typical near-surface speeds of 3 cm/s slowing to 1 cm/s at depth. Circulation patterns, based on dynamic heights, showed greater variability over the study region in 1990 compared to 1989 when there was a notable lack of mesoscale eddy features.

Baroclinic calculations for both years indicate that the meander portion of the JMC is concentrated in the upper waters (< 100 m). In August 1990, approximately 44% of the flow in the upper layer of the JMC contributes to the meander with 56% continuing eastward as throughput to the GSG and Norwegian Atlantic Current (NAC). In the lower layer (~ 100 to 1000 m), about 25% of the JMC flow remains with the meander and 75% exits to the east. The total input flow to the JMC from the EGC is 1.45 Sv with 0.28 Sv from the surface layer and 1.17 Sv from the lower layer. For September 1989, *Blythe* (1990) estimated a total baroclinic flow of 2 Sv into the region with half of the upper layer exiting as meander and half continuing eastward, while noting that the meander dissipates below 100 m with flow becoming more easterly. Additionally, based on

August 1990 fresh water transports, it is estimated that ~ 9% of the fresh water annually available from the EGC is input to the JMC with about half of this amount returning to the EGC via the meander.

While this study is based on baroclinic determinations, the barotropic nature of the JMC, responding to the bathymetric influence of the Jan Mayen Fracture Zone, is evidenced by the trajectories of subsurface drifters and a high resolution model of the total mean velocity field. That the Jan Mayen Current is partly an anticyclonic meander in the seaward side of the EGC, particularly in the upper layer, is clear from both the 1990 and 1989 summer studies. The classical view of the JMC exiting eastward from the EGC solely to form the southern limb of the GSG is no longer valid.

summer with a lesser rate of inflow of fresh water to the GSG (*Pawlowicz*, 1995). As expected, the subsurface minimum temperature, Tmin, which is associated with the JMPW layer in the JMC, was colder by ~ 0.5°C and shallower by up to 25 m in the JMC region during August 1990 compared to September 1989 as expected due to the additional insolation and mixing in September. In addition to seasonal effects, *Budéus et al.* (1993) attribute the colder temperatures in the Tmin layer in the GSG during 1990 to a lack of deep convection during winter 1989-1990. JMAtIW, distinguishable by a temperature maximum, Tmax, occupied roughly half the volume in August 1990 that it encompassed in 1989. Baroclinic velocities for summers 1990 and 1989 are similar with typical near-surface speeds of 3 cm/s slowing to 1 cm/s at depth. Circulation patterns, based on dynamic heights, showed greater variability over the study region in 1990 compared to 1989 when there was a notable lack of mesoscale eddy features.

Baroclinic calculations for both years indicate that the meander portion of the JMC is concentrated in the upper waters (< 100 m). In August 1990, approximately 44% of the flow in the upper layer of the JMC contributes to the meander with 56% continuing eastward as throughput to the GSG and Norwegian Atlantic Current (NAC). In the lower layer (~ 100 to 1000 m), about 25% of the JMC flow remains with the meander and 75% exits to the east. The total input flow to the JMC from the EGC is 1.45 Sv with 0.28 Sv from the surface layer and 1.17 Sv from the lower layer. For September 1989, *Blythe* (1990) estimated a total baroclinic flow of 2 Sv into the region with half of the upper layer exiting as meander and half continuing eastward, while noting that the meander dissipates below 100 m with flow becoming more easterly. Additionally, based on

August 1990 fresh water transports, it is estimated that ~ 9% of the fresh water annually available from the EGC is input to the JMC with about half of this amount returning to the EGC via the meander.

While this study is based on baroclinic determinations, the barotropic nature of the JMC, responding to the bathymetric influence of the Jan Mayen Fracture Zone, is evidenced by the trajectories of subsurface drifters and a high resolution model of the total mean velocity field. That the Jan Mayen Current is partly an anticyclonic meander in the seaward side of the EGC, particularly in the upper layer, is clear from both the 1990 and 1989 summer studies. The classical view of the JMC exiting eastward from the EGC solely to form the southern limb of the GSG is no longer valid.

APPENDIX A. METHODS

A. INSTRUMENTATION AND METHODS

The BARTLETT 90 data set consists of conductivity, temperature, and pressure measurements collected using a Neil Brown Instrument Systems Mark III CTD. The unit was calibrated before and after the cruise at the NPS calibration facility and by water samples taken with a rosette sampler. The CTD was fastened to a standard instrument cage supplied by the BARTLETT which included a 12-bottle rosette sampler. The package was lowered at a nearly constant rate of 60 m/min modulated by the roll of the ship. The data acquisition program recorded 8616 records per cast evenly spaced over the depth range selected prior to lowering. Thus, for a 1000 m cast, an average of 8.6 observations per meter were collected.

Water samples, approximately 12 per cast, were collected on each up-cast with Niskin bottles. The samples, used for salinity measurements, were distributed uniformly over the depth span on nearly all lowerings. The samples were stored in Kimex bottles, a high-alumina borosilicate glass, with Nalgene caps over polyethylene "thimble" closures which tightly seal both the inner bottle neck and bottle rim. The Kimex bottles were specifically chosen based on tests at Scripps Institute of Oceanography which have shown that seawater samples stored in this type of bottle had no detectable salinity change after six months storage (*D. Muus, personal communication*, 1990). The water sample salinities were measured in the NPS calibration laboratory four months after the cruise

using an AGE Instruments salinometer referred to Standard Water Batch P112.

B. DATA PROCESSING AND ACCURACY

Data were transferred to tape for calibration coefficient application and editing on the NPS Mainframe computer. By block averaging, the original 8.6 observations per meter were compressed to depth spacings of 1.0 m centered closely on the integral depths. The data from the deep lowerings (1000 - 3000 m) were block averaged to 2 meter spacings and further averaged to 50 meter spacing for salinity corrections. The pre-cruise and post-cruise temperature and pressure calibrations resulted in correction coefficients that were acceptably similar and their means were applied to the data. The conductivities were initially corrected in this way, later to be refined by comparison with salinity samples taken with the rosette sampler. A complication arose in this process because of a small change in the conductivity calibration which occurred as a result of the CTD hitting the bottom at Station 23. No spare conductivity cell was available so the data were treated in two parts, the "pre-crash" data supported by the pre-cruise calibration and bottle salinities prior to the crash and the "post-crash" data, supported again by bottles and the post-cruise calibration. Fortunately, no noticeable effect of the crash on instrument stability was detected (*Paquette et al.*, 1991).

The salinity calibration data set was relatively poor in quality owing to poorly functioning Niskin bottles. As a result, the 50 meter salinity averages were more accurate than individual bottle salinities, and they were used instead. It was also necessary to subtract 0.007 PSU from the bottle-based salinity calibration to bring the deepwater CTD

average salinities into agreement with the deepwater bottle samples of HÅKON MOSBY 1989 at the GSP inter-calibration station. It was later determined the 0.007 PSU discrepancy resulted from a -9.2 dbar pressure sensor hysteresis error on CTD down-casts and some fraction of +9.2 dbar error when stopped for bottle tripping on the up-cast. Further details of the editing process is documented in the BARTLETT 90 data report (*Paquette et al.*, 1991). The final accuracy of the measurements was as follows: temperature, ± 0.0015°C; salinity, ± 0.005 PSU (practical salinity units); pressure, ± 3 dbar.

APPENDIX B. ADDITIONAL FIGURES

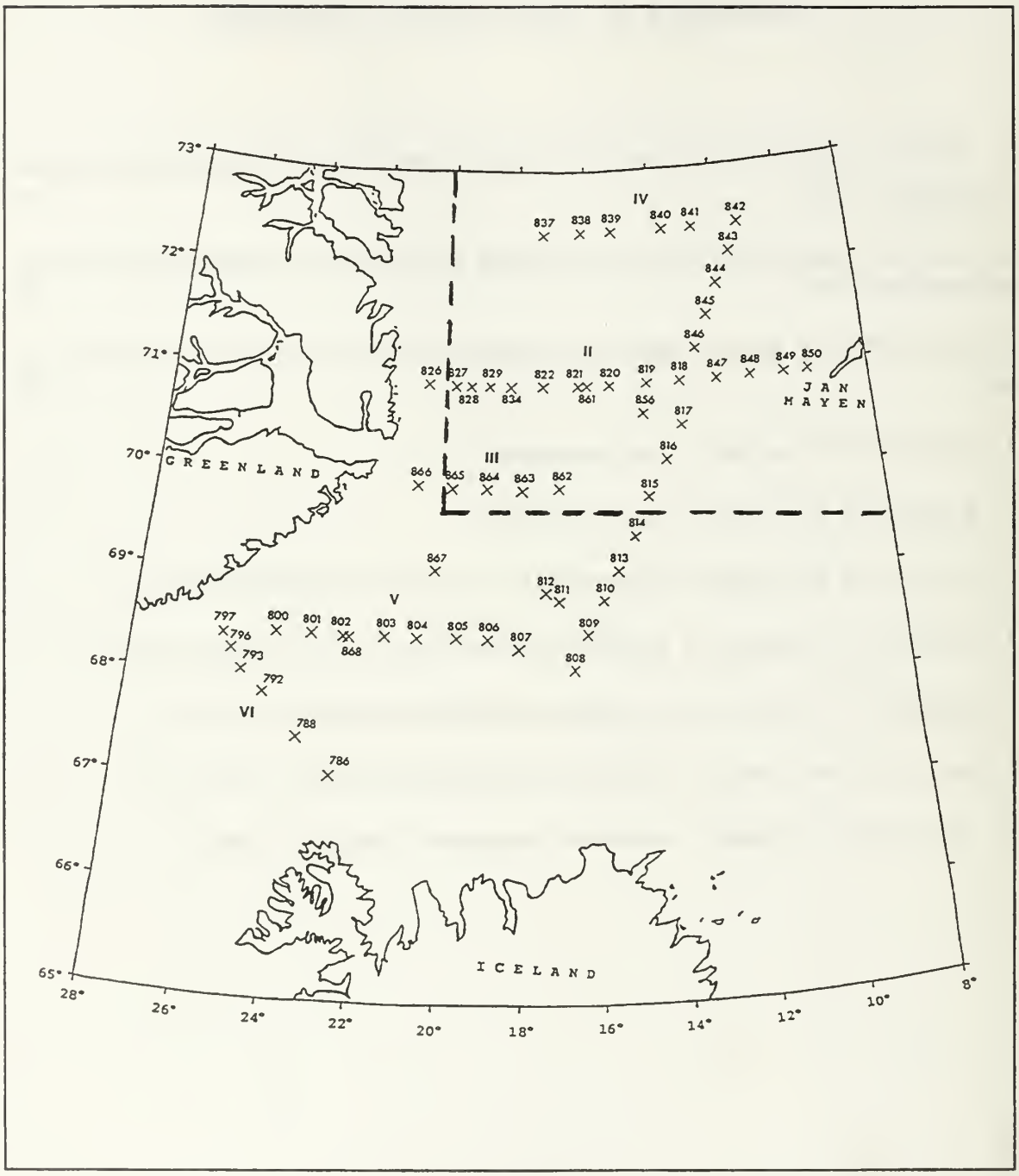

Appendix B, Figure 1. BJARNI SÆMUNDSSON station positions during the joint Danish/Icelandic cruise of September 1990. CTD data from stations located in the upper right corner (inside dashed line) have been combined with BARTLETT 90 data in horizontal views (from *Mortensen et al.*, 1991).

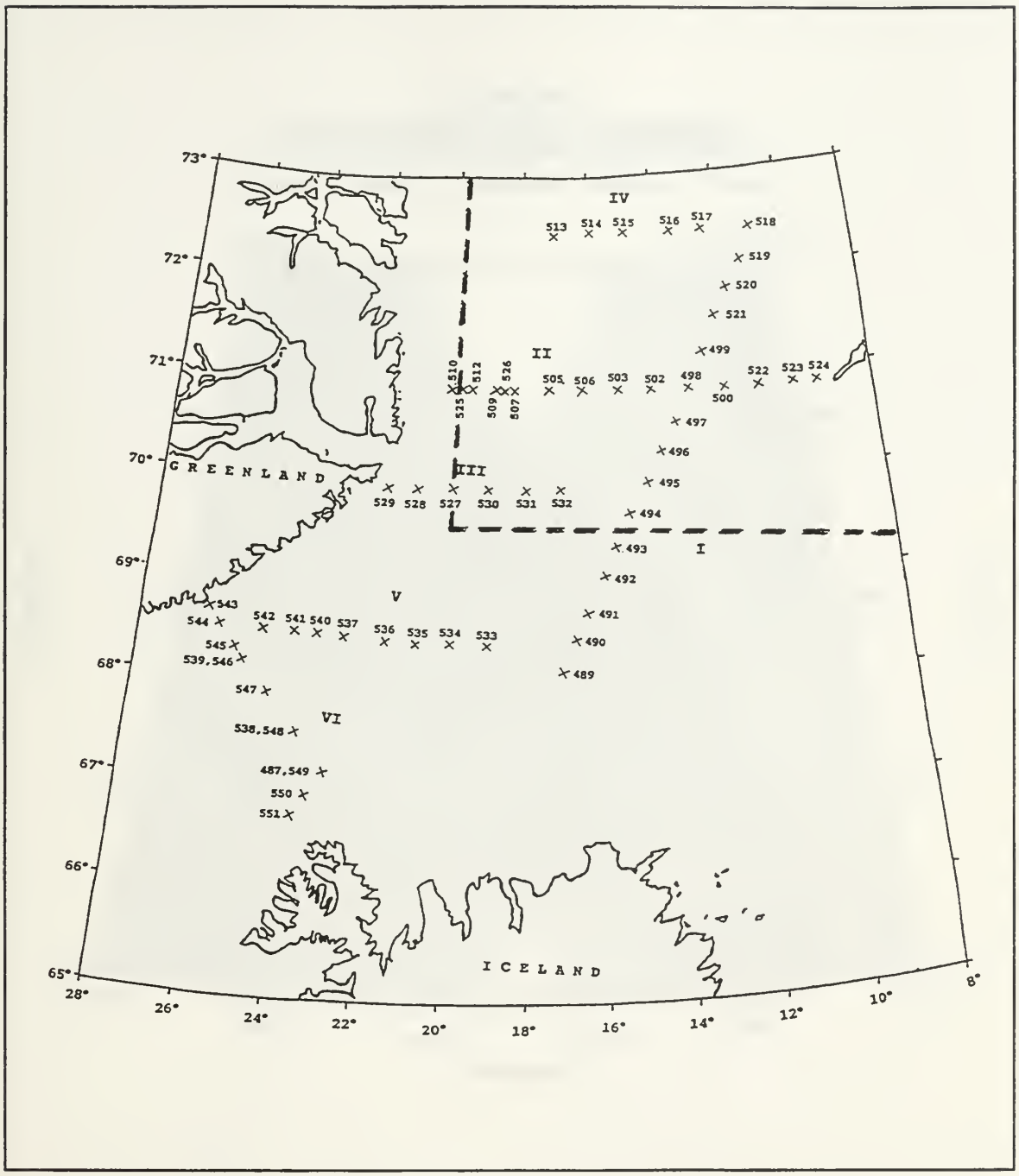

Appendix B, Figure 2. BJARNI SÆMUNDSSON station positions during the joint Danish/Icelandic cruise of September 1989. CTD data from stations located in the upper right corner (inside dashed line) have been combined with BARTLETT 89 data in horizontal views (from *Buch et al.,* 1991).

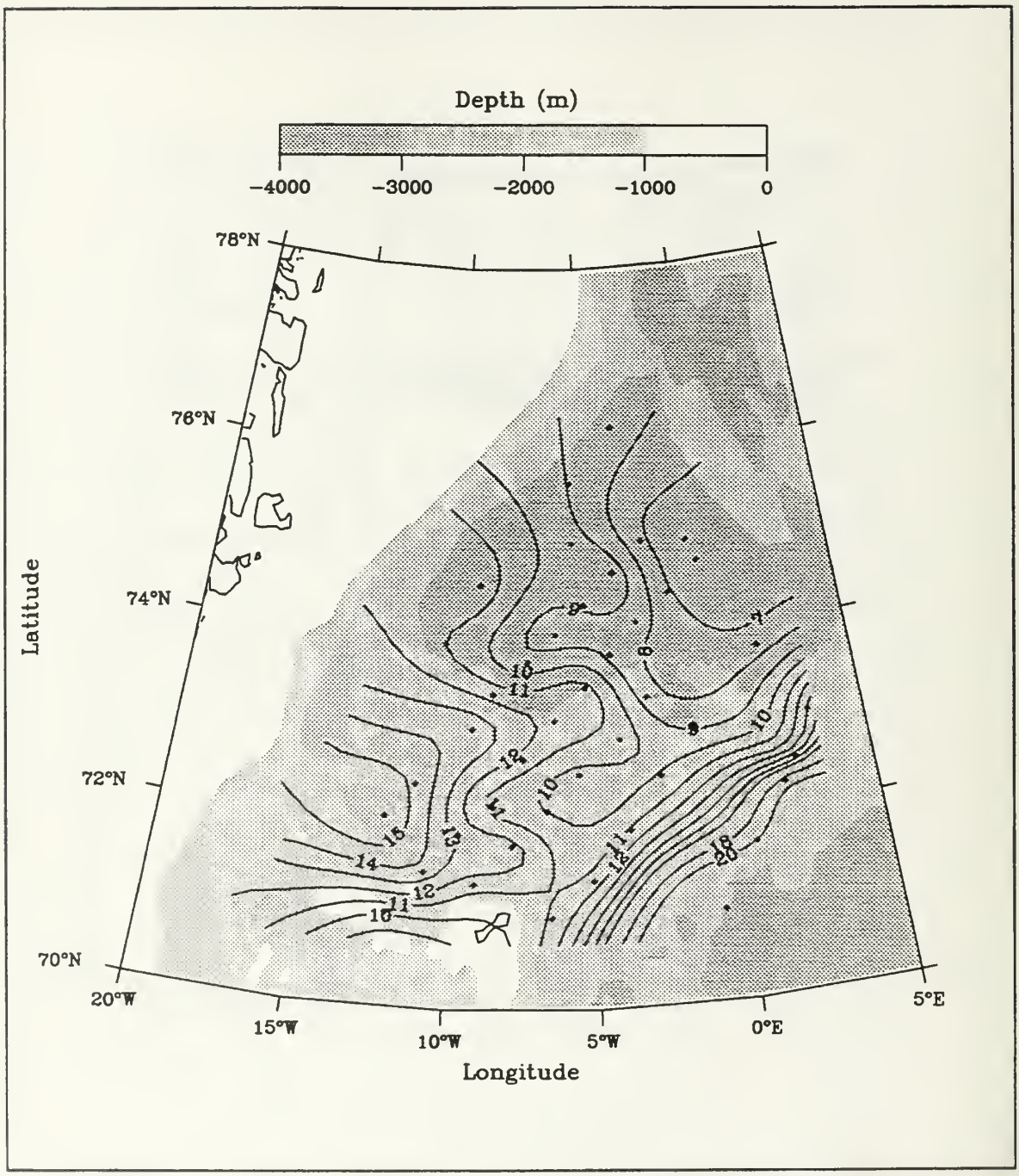

Appendix B, Figure 3. BARTLETT 90 dynamic height at the surface (10 m) referenced to 1000 dbar (dyn cm). The BJARNI SÆMUNDSSON 90 data has not been combined with BARTLETT data. Comparison with Figure 8 allows the reader to assess any distortions caused by combining the two data sets.

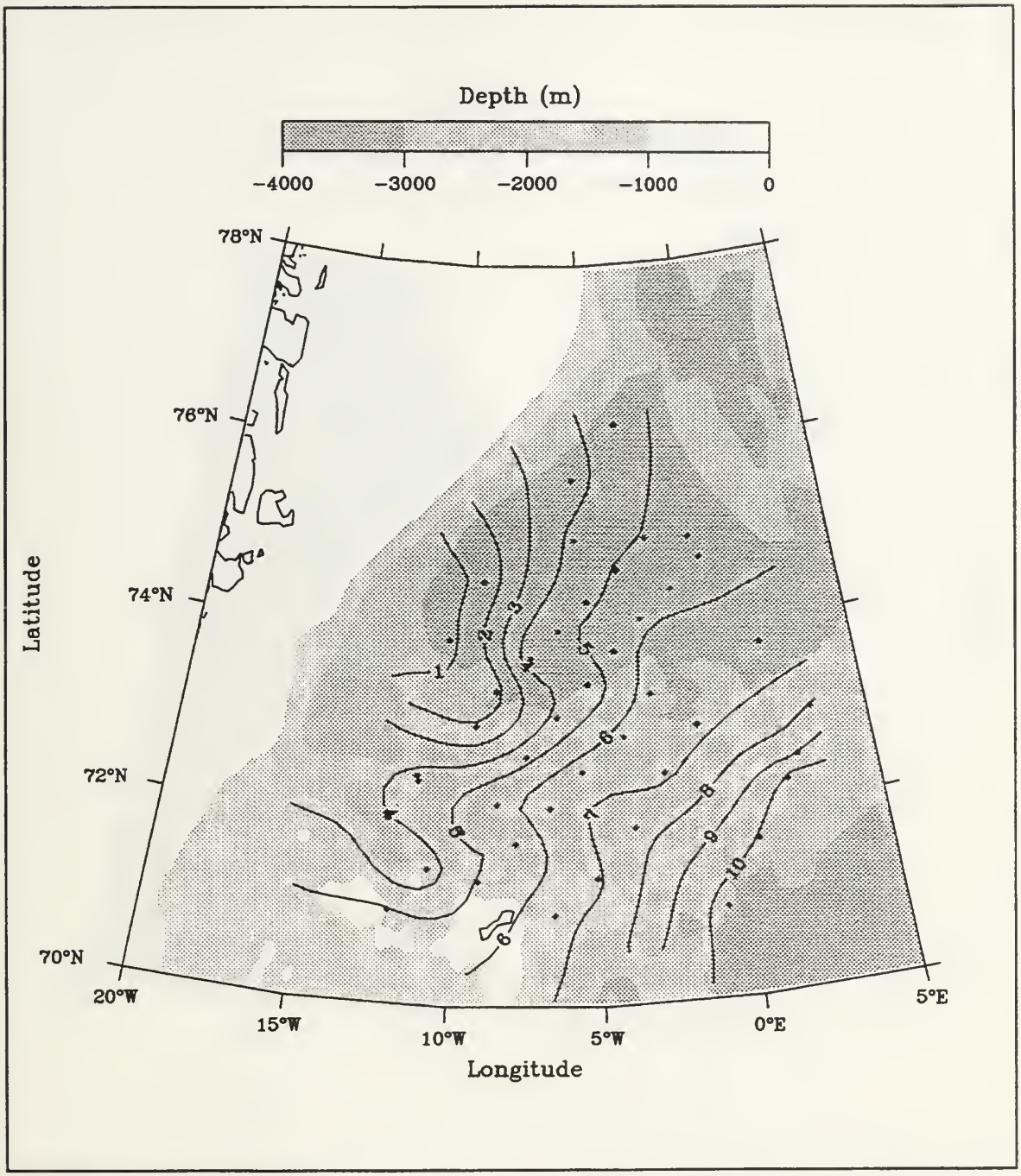

Appendix B, Figure 4. BARTLETT 90 surface (10 m) temperature (°C). The BJARNI SÆMUNDSSON 90 data has not been combined with BARTLETT data. Comparison with Figure 12 allows the reader to assess any distortions caused by combining the two data sets.

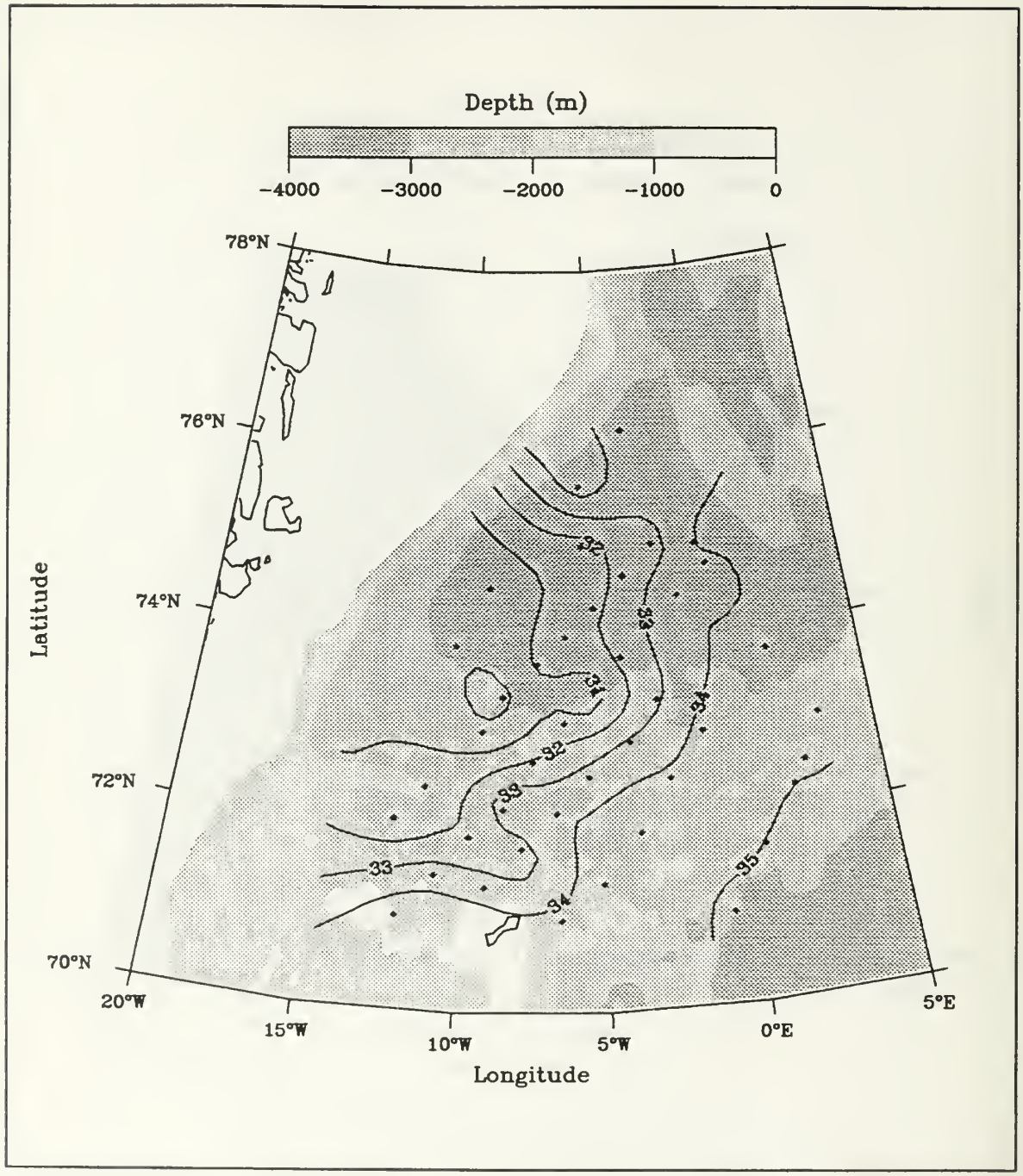

Appendix B, Figure 5. BARTLETT 90 surface (10 m) salinity (PSU). The BJARNI SÆMUNDSSON 90 data has not been combined with BARTLETT data. Comparison with Figure 13 allows the reader to assess any distortions caused by combining the two data sets.

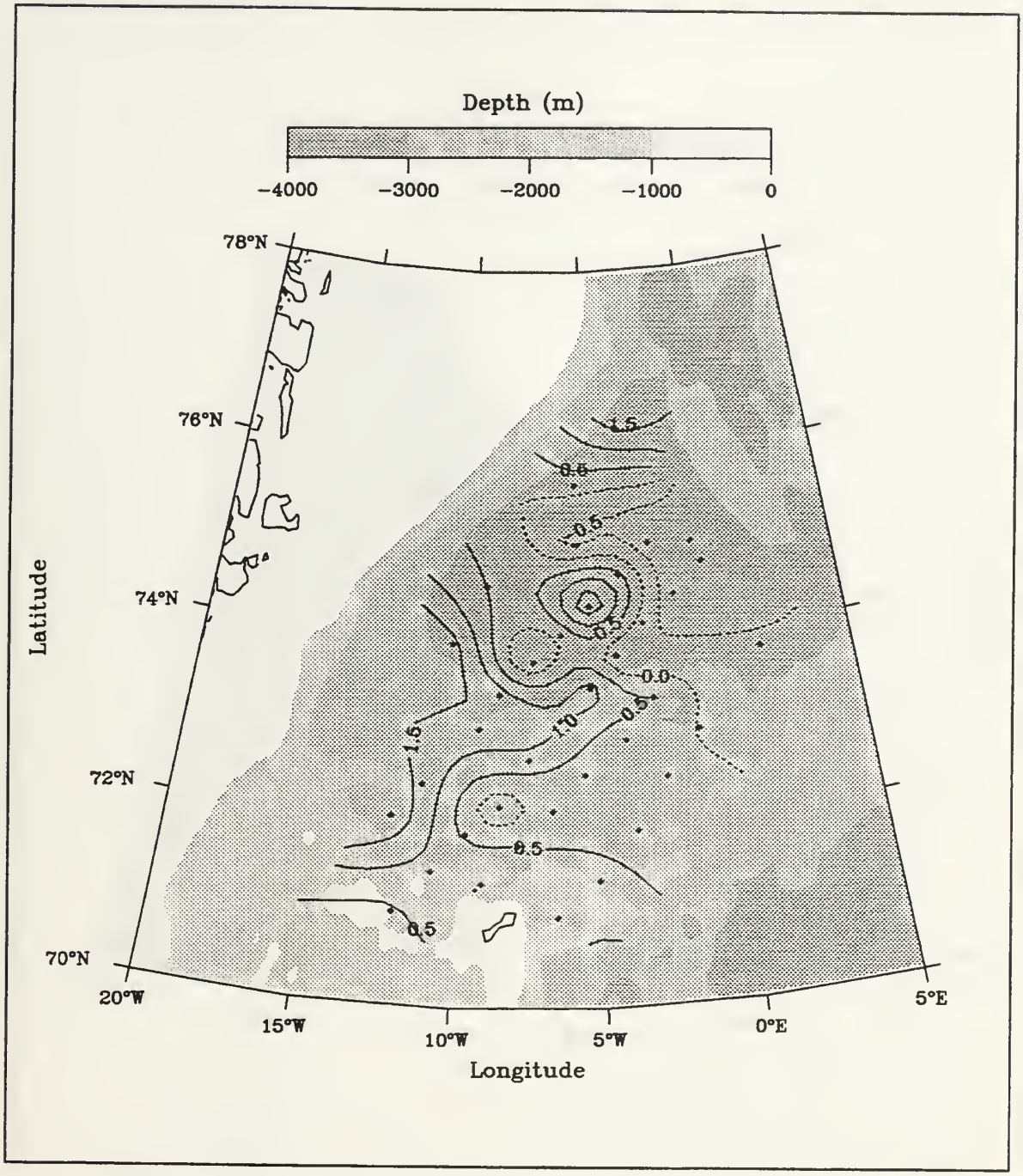

Appendix B, Figure 6. BARTLETT 90 contours of intermediate temperature maximum (Tmax) (°C). The BJARNI SÆMUNDSSON 90 data has not been combined with BARTLETT data. Comparison with Figure 16 allows the reader to assess any distortions caused by combining the two data sets.

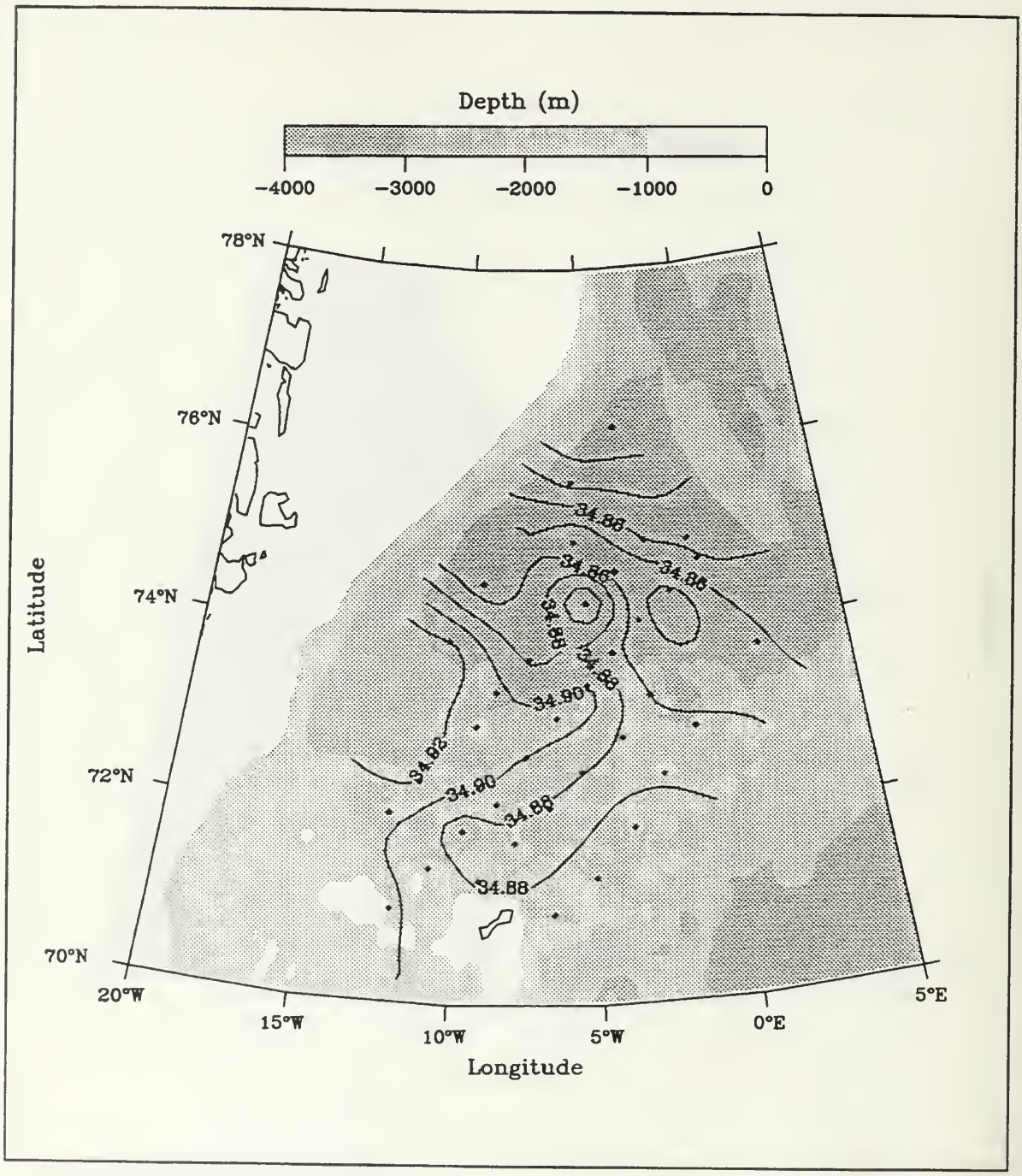

Appendix B, Figure 7. BARTLETT 90 salinity at intermediate temperature maximum (Tmax) (PSU). The BJARNI SÆMUNDSSON 90 data has not been combined with BARTLETT data. Comparison with Figure 17 allows the reader to assess any distortions caused by combining the two data sets.

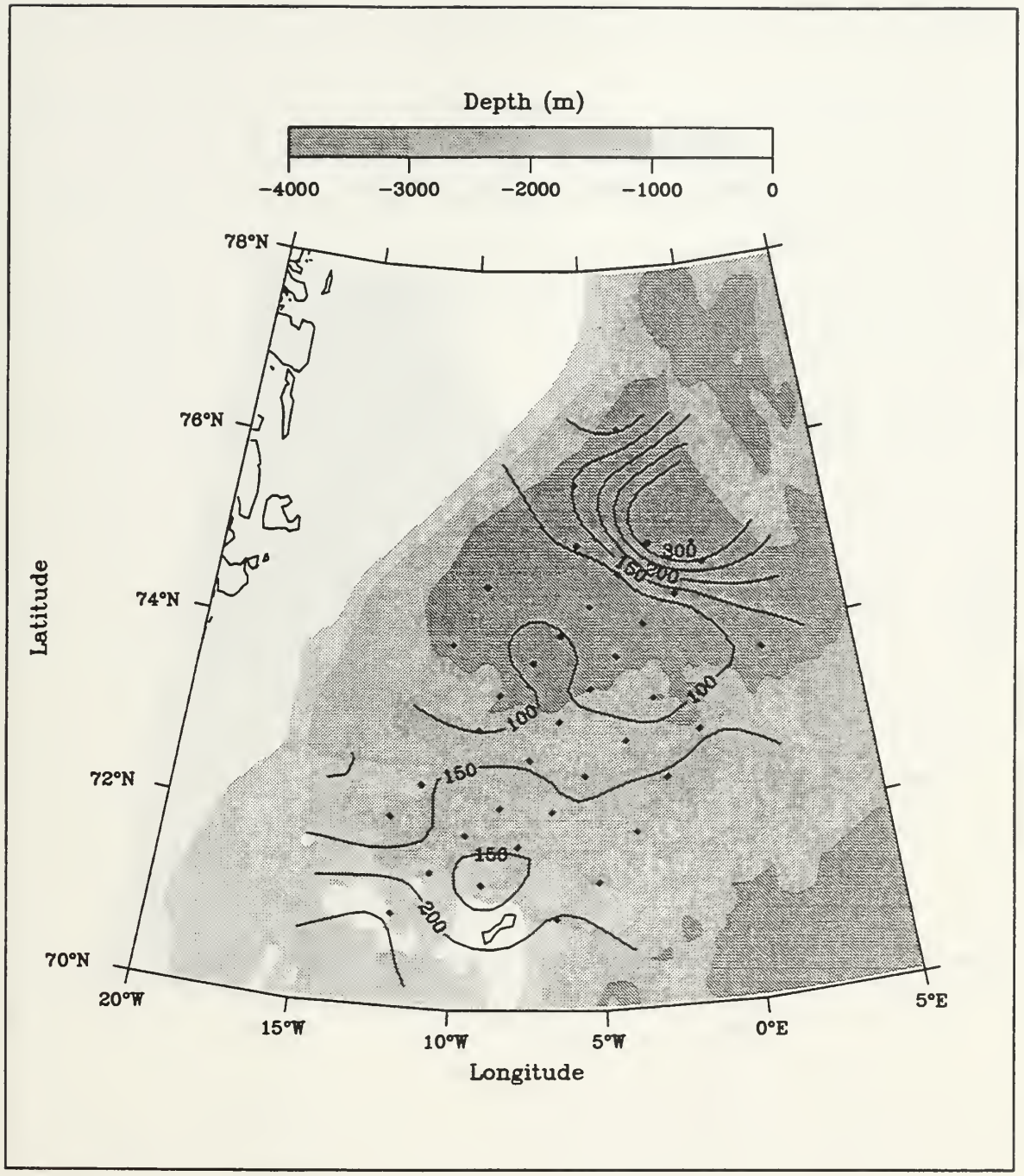

Appendix B, Figure 8. BARTLETT 90 depth of intermediate temperature maximum (Tmax) (m). The BJARNI SÆMUNDSSON 90 data has not been combined with BARTLETT data. Comparison with Figure 18 allows the reader to assess any distortions caused by combining the two data sets.

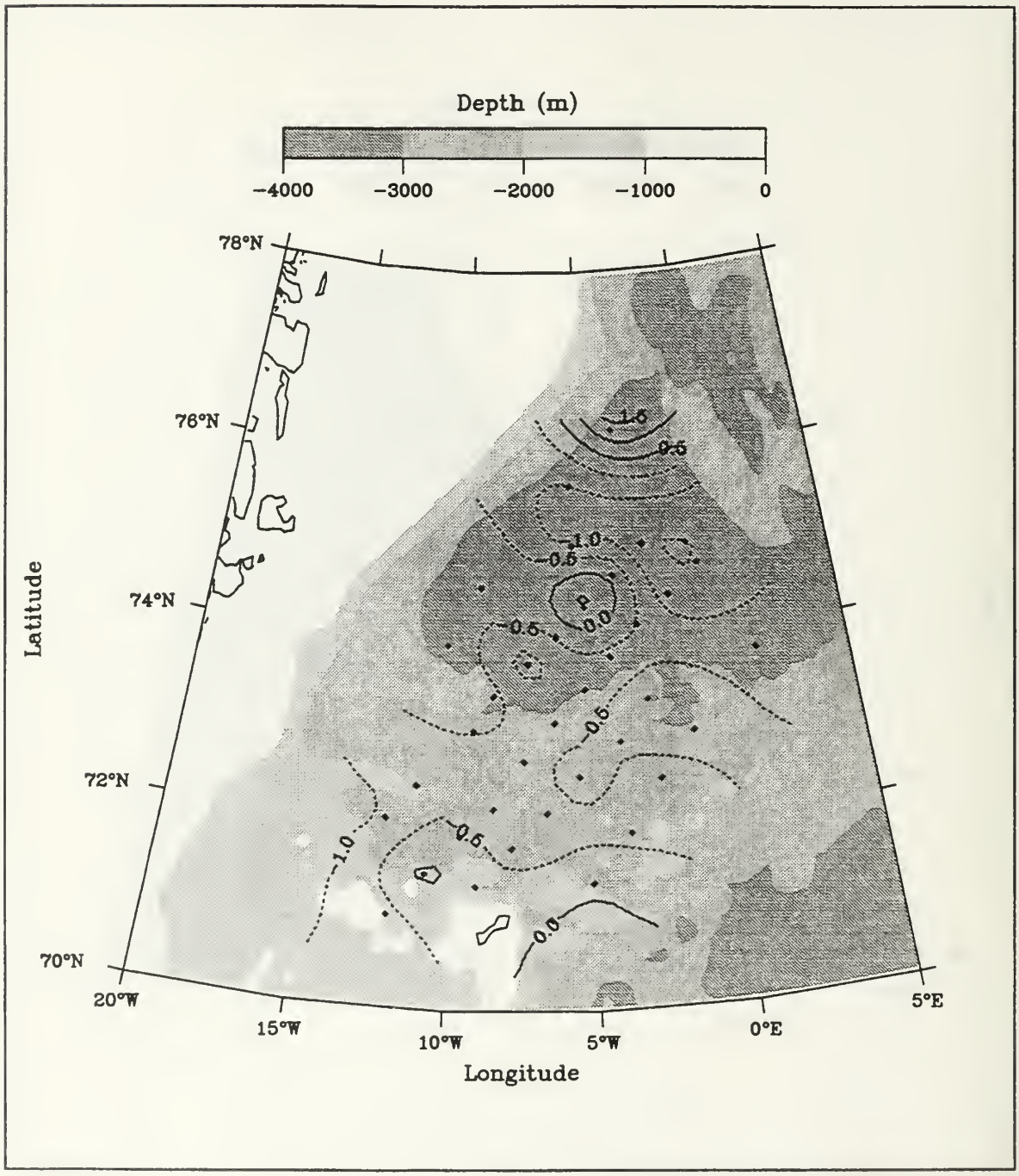

Appendix B, Figure 9. BARTLETT 90 contours of subsurface temperature minimum (Tmin) (°C). The BJARNI SÆMUNDSSON 90 data has not been combined with BARTLETT data. Comparison with Figure 38 allows the reader to assess any distortions caused by combining the two data sets.

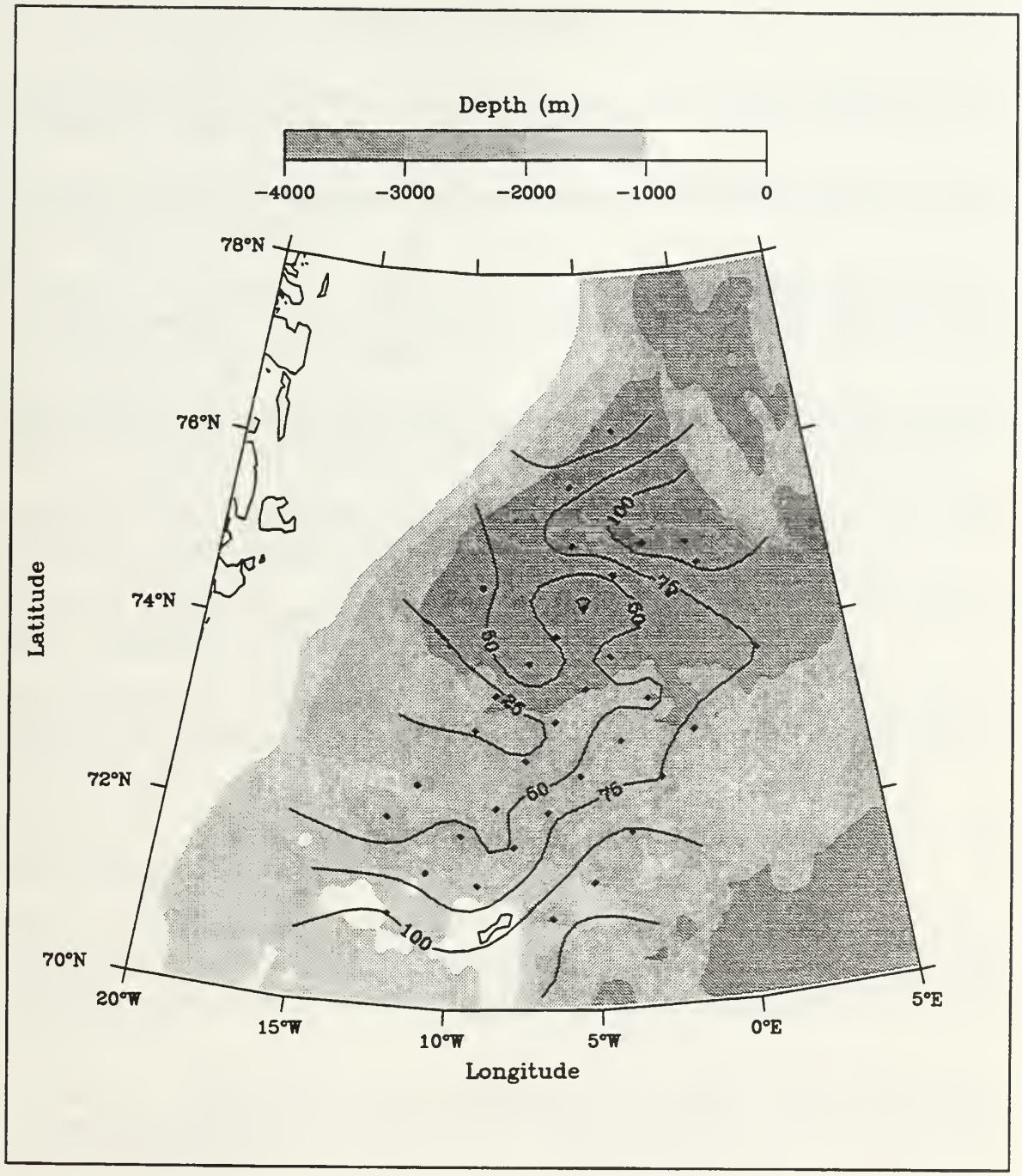

Appendix B, Figure 10. BARTLETT 90 depth of subsurface temperature minimum (Tmin) (m). The BJARNI SÆMUNDSSON 90 data has not been combined with BARTLETT data. Comparison with Figure 39 allows the reader to assess any distortions caused by combining the two data sets.

LIST OF REFERENCES

Aagaard, K., and E. C. Carmack, The role of sea ice and other fresh water in the Arctic circulation, *J. Geophys. Res., 94,* 14,485-14,498, 1989.

Aagaard, K., and L. K. Coachman, The East Greenland Current north of Denmark Strait, part I, *Arctic, 21,*181-200, 1968.

Aagaard, K., E. Fahrbach, J. Meincke, and J. H. Swift, Saline outflow from the Arctic Ocean: Its circulation to the deep waters of the Greenland, Norwegian, and Iceland Seas, *J. Geophys. Res., 96,* 20,433-20,441, 1991.

Blythe, R. F., The Jan Mayen Current and the Deep Waters of the Greenland Basin, Master's Thesis, Naval Postgraduate School, Monterey, California, September, 1990.

Bourke, R. H., J. L. Newton, R. G. Paquette, and M. D. Tunicliffe, Circulation and water masses of the east Greenland shelf, *J. Geophys. Res., 92,* 6729-6740, 1987.

Bourke, R. H., R. G. Paquette, and R. F. Blythe, The Jan Mayen Current of the Greenland Sea, *J. Geophys. Res., 97,* 7241-7250, 1992.

Bourke, R. H., R. G. Paquette, R. F. Blythe, and M. D. Stone, On the deep and bottom waters of the Greenland Sea from summer 1989 and 1990 data, *J. Geophys. Res., 98,* 4629-4638, 1993.

Bourke, R. H., A. M. Weigel, and R. G. Paquette, The westward turning branch of the West Spitsbergen Current, *J. Geophys. Res., 93,* 14,065-14,077, 1988.

Buch, E., J. Mortensen, S. S. Kristmannsson, and S. Aa. Malmberg, Density Distribution, Geopotential Anomaly Fields and Geostrophic Profiles in the western Iceland Sea, 1989., GSP Int. Rep. no. 42, Royal Danish Adm. of Navigation and Hydrography and Mar. Res. Inst. Rvík., 1991.

Budéus, G., A. Maul, and G. Krause, Variability in the Greenland Sea as revealed by a repeated high spatial resolution conductivity-temperature-depth survey, *J. Geophys. Res., 98,* 9985-10,000, 1993.

Carmack, E. C., On the Hydrography of the Greenland Sea, Doctoral Dissertation, University of Washington, Seattle, Washington, 1972.

Carmack, E. C., and K. Aagaard, On the deep water of the Greenland Sea, *Deep-Sea Res., 20,* 687-715, 1973.

Dietrich, G., *Atlas of the Hydrography of the Northern North Atlantic,* Conceil International Pour L'Exploration de la Mer, Service Hydrographic, Copenhagen, 1969.

Foldvik, A., K. Aagaard, and T. Tørresen, On the velocity field of the East Greenland Current, *Deep-Sea Res., 35,* 1335-1354, 1988.

Gladfelter, W. H., Oceanography of the Greenland Sea, USS ATKA (AGB-3) survey, summer 1962, *Manuscr. Rep. 0-64-63,* Mar. Sci. Dep., U.S. Naval Oceanographic Office, Washington, D.C., February, 1964.

Gloersen, P., W. J. Campbell, D. J. Cavalieri, J. C. Comiso, C. L. Parkinson, and H. J. Zwally, Arctic and Antarctic Sea Ice, 1978-1987: Satellite passive-microwave observations and analysis, *NASA Rep. SP-511,* Scientific and Technical Information Program, National Aeronautics and Space Administration, Washington, D.C., 1992.

Gross, M. G., *Oceanography A View of the Earth,* Prentice-Hall, Inc., 497pp., 1977.

GSP Group, A venture toward improved understanding of the ocean's role in climate, *Eos Trans. AGU, 71(24),* 750-755, 1990.

Hopkins, T. S., THE GIN SEA Review of Physical Oceanography and Literature from 1972, *SACLANTCEN Rep. SR-124,* Undersea Research Centre, Supreme Allied Command Atlantic, 1988.

Johannessen, O. M., Brief overview of the physical oceanography, in *The Nordic Seas,* edited by B. G. Hurdle, pp. 103-128, Springer-Verlag, New York, 1986.

Jónsson, S., The structure of the large and mesoscale circulation in the Nordic Seas, with special reference to the Fram Strait, Doctoral Dissertation, University of Bergen, Bergen Norway, 1989.

Koltermann, K. P., and H. Lüthje, *Hydrographic Atlas of the Greenland and Northern Norwegian Seas (1979-1987),* Deutsches Hydrographisches Institut Nr. 2328, Hamburg, Germany, 1989.

Levitus, S., R. Burgett, and T. Boyer, World Ocean Atlas, 1994: Volume 3, Salinity, *NOAA Atlas NESDIS 3,* NOAA, Washington, D.C., 1994.

Levitus, S., and T. Boyer, World Ocean Atlas, 1994: Volume 4, Temperature, *NOAA Atlas NESDIS 3,* NOAA, Washington, D.C., 1994.

McCarren, D. H., Analysis of Drifting SOFAR Buoys in the Greenland Sea, 1989-1990, Master's Thesis, Naval Postgraduate School, Monterey, California, December, 1991.

Maslowski, W., personal communication, 1991.

Meincke, J., Introduction, Nordic Seas Symposium, sponsored by the Deutche Forschungsgemeinschaft and the U S National Science Foundation, Hamburg, Germany, 1995.

Meincke, J., S. Jónsson, and J. H. Swift, Variability of convective conditions in the Greenland Sea, *ICES Mar. Sci. Symp., 195,* 32-39, 1992.

Mortensen, J., personal communication, 1991.

Mortensen, J., E. Buch, J. W. Nielsen, S. S. Kristmannsson, and S. Aa. Malmberg, Density Distribution, Geopotential Anomaly Fields and Geostrophic Velocity Profiles in the western Iceland Sea, 1990., GSP Int. Rep.no. 43. Royal Danish Adm. of Navigation and Hydrography and Mar. Res. Inst. Rvík., 1991.

Mortensen, J., E. Buch, J. W. Nielsen, S. S. Kristmannsson, and S. Aa. Malmberg, Density Distribution, Geopotential Anomaly Fields and Geostrophic Velocity Profiles in the western Iceland Sea, 1990., GSP Int. Rep.no. 51. Royal Danish Adm. of Navigation and Hydrography and Mar. Res. Inst. Rvík., 1992.

Muus, D., personal communication, 1990.

Paquette, R. G., R. H. Bourke, J. F. Newton, and W. F. Perdue, The East Greenland Polar Front in autumn, *J. Geophys. Res., 90,* 4866-4882, 1985.

Paquette, R. G., R. H. Bourke, and M. D. Stone, Data Report, USNS BARTLETT cruise to the Greenland Sea in August 1990, *Technical Rep. NPS-OC-92-001,* Naval Postgraduate School, Monterey, California, 1991.

Parsons, R. A., On the Barents Sea Polar Front in summer and the interpretations of the associated regional oceanography using an Arctic Ocean general circulation model, Doctoral Dissertation, Naval Postgraduate School, Monterey, California, September, 1995.

Pawlowicz, R., A note on seasonal cycles of temperature and salinity in the upper waters of the Greenland Gyre from historical data, *J. Geophys. Res., 100,* 4715-4726, 1995.

Poulain, P. M., A. Warn-Varnas, and P. P. Niiler, Near-surface circulation of the Nordic Seas as measured by Lagrangian drifters, *J. Geophys. Res., 100,* 18,237-18,258, 1996.

Richez, C., J. C. Gascard, and C. Rouault, Recirculation of Atlantic water in the Greenland Sea, Paper presented at the Nordic Seas Symposium, sponsored by the Deutche Forschungsgemeinschaft and the U S National Science Foundation, Hamburg, Germany, 1995.

Rudels, B., D. Quadfasel, H. Friedrich, and M. N. Houssais, Greenland Sea convection in the winter of 1987-1988, *J. Geophys. Res., 94,* 3223-3227, 1989.

van Aken, H. M., G. Budéus, and M. Hähnel, The anatomy of the Arctic Frontal Zone in the Greenland Sea, *J. Geophys. Res., 100,* 15,999-16,014, 1995.

van Aken, H. M., D. Quadfasel, and A. Warpakowski, The Arctic Front in the Greenland Sea during February 1989: Hydrographic and biological observations, *J. Geophys. Res., 96,* 4739-4750, 1991.

INITIAL DISTRIBUTION LIST

		No. Copies
1.	Defense Technical Information Center 8725 John J. Kingman Road., Ste 0944 Ft. Belvoir, VA 22060-6218	2
2.	Dudley Knox Library Naval Postgraduate School 411 Dyer Rd. Monterey, California 93943-5101	2
3.	Chairman (Code OC) Department of Oceanography Naval Postgraduate School Monterey, California 93943-5100	1
4.	Chairman (Code Mr) Department of Meteorology Naval Postgraduate School Monterey, California 93943-5100	1
5.	Robert H. Bourke (OC/Bf) Department of Oceanography Naval Postgraduate School Monterey, California 93943-5100	2
6.	Robert G. Paquette (OC/Pa) Department of Oceanography Naval Postgraduate School Monterey, California 93943-5100	1
7.	Ken L. Davidson (MR/Ds) Department of Meteorology Naval Postgraduate School Monterey, California 93943-5100	1
8.	Chairman Department of Oceanography U. S. Naval Academy Annapolis, Maryland 21402	1

9. Chief of Naval Research — 1
Attn: High Latitude Program (Code 322)
800 N. Quincy Street
Arlington, Virginia 22217

10. Commander — 1
Naval Oceanography Command
Stennis Space Center
Bay St. Louis, Mississippi 39522-5000

11. Commanding Officer — 1
Naval Oceanographic Office
Stennis Space center
Bay St. Louis, Mississippi 39522-5001

12. Commanding Officer — 1
Naval Polar Oceanography Center,
Suitland
Washington, D. C. 20373

13. Director — 1
Attn: Technical Information Division
Naval Research Laboratory
Washington, D. C. 20375

14. Oceanographer of the Navy (N-096) — 1
Naval Observatory
34th and Massachusetts Avenue NW
Washington, D. C. 20390

15. Cold Regions Research and Engineering Laboratory — 1
Attn: Library
U. S. Army Corps of Engineers
Hanover, New Hampshire 03755-1290

16. Applied Physics Laboratory — 1
Attn: Library
University of Washington
1013 Northeast 40th Street
Seattle, Washington 98105

17. Library 1
Woods Hole Oceanographic Institute
Woods Hole, Massachusetts 02543

18. Dr. J. H. Swift 1
Scripps Institution of Oceanography
La Jolla, California 92093

19. Library 1
Graduate School of Oceanography
Narragansett Bay Campus
University of Rhode Island
Narragansett, Rhode Island 02882

20. Library 1
School of Oceanography
Oregon State University
Corvallis, Oregon 97331

21. Library 1
Scott Polar Research Institute
University of Cambridge
Cambridge, England
CB2 1ER

22. Library 1
Institute of Polar Studies
103 Mendenhall
125 South Oval Mall
Columbus, Ohio 43210

23. Library 1
Institute of Marine Science
University of Alaska
Fairbanks, Alaska 99701

24. Library 1
Department of Oceanography
University of British Columbia
Vancouver, British Columbia
Canada
B2Y 4A2

25. Library 1
Bedford Institute of Oceanography
P. O. Box 1006
Dartmouth, Nova Scotia
Canada
B2Y 4A2

26. Library 1
Department of Oceanography
Dalhousie University
Halifax, Nova Scotia
Canada
B3H 4J1

27. National Snow and Ice Data Center 1
Cooperative Institute for Research
in Environmental Sciences
Boulder, Colorado 80309

28. Dr. E. Carmack 1
Institute of Ocean Sciences
P. O. Box 6000
Sidney, British Columbia
Canada
V8L 4B2

29. Dr. D. Quadfasel 1
Institut fur Meereskinde
Universitat Hamburg
Troplowitzstrasse 7
22146 Hamburg
Germany

30. Dr. J. Meincke 1
Institut fur Meereskinde
Universitat Hamburg
Troplowitzstrasse 7
22529 Hamburg
Germany

31. Dr. K. Aagaard 1
Applied Physics Laboratory
University of Washington, HN-10
1013 Northeast 40th Street
Seattle, Washington 98195

32. Dr. T. O. Manley 1
Department of Geology
Middlebury College
Middlebury, Vermont 05753

33. Dr. A. Foldvik 1
Geophysical Institute
University of Bergen
Allegaten 70
5007 Bergen
Norway

34. Dr. S. Jónsson 1
Marine Research Institute
P. O. Box 875
602 Akureyri
Iceland

35. Dr. T. S. Hopkins 1
4146 Jordan Road
Campus Box 8202
North Carolina State University
Raleigh, North Carolina 27695

36. Dr. E. Fahrbach 1
Alfred Wegener Institute for
Polar and Marine Research
Postfach 120161
27515 Bremerhaven
Germany

37. Dr. G. Budéus 1
Alfred Wegener Institute for
Polar and Marine Research
Columbusstrasse
27568 Bremerhaven
Germany

38. Dr. B. Rudels 1
Institut fur Meereskinde
Universitat Hamburg
Troplowitzstrasse 7
22529 Hamburg
Germany

39. Dr. E. Buch 1
Royal Danish Administration of
Navigation and Hydrography
Overgaden o. Vandet 62B
1023 Copenhagen K
Denmark

40. Dr. J. Mortensen 1
University of Copenhagen
Geophysical Department
Haraldsgade 6
2200 Copenhagen N
Denmark

41. Dr. S. Aa. Malmberg 1
Institute for Marine Research
P. O. Box 1390
Skulagata 4
121 Reykjavik
Iceland

42. Dr. J. C. Gascard 1
Laboratoire d'Oceanographie Dynamique
et de Climatologie
Universite Pierre et Marie Curie
Paris 6, Paris
France

43. Dr. R. Muench 1
Earth and Space Research
1910 Fairview E., #102
Seattle, Washington 98102-3699

44. Dr. M. van Aken 1
Netherlands Institute for Sea Research
P. O. Box 59
1790 Ab den Burg/Telex
The Netherlands

45. Marla Stone (OC/So) 3
Department of Oceanography
Naval Postgraduate School
Monterey, California 93943-5100